THE EFFECTS OF SURFACE INSTABILITIES ON LAMINAR FILM CONDENSATION

22

Joseph Gerstmann

Peter Griffith

September 30, 1965

Technical Report No. 5050-36

Contract No. NSF GP-2402

Department of
Mechanical Engineering

Massachusetts Institute
of Technology

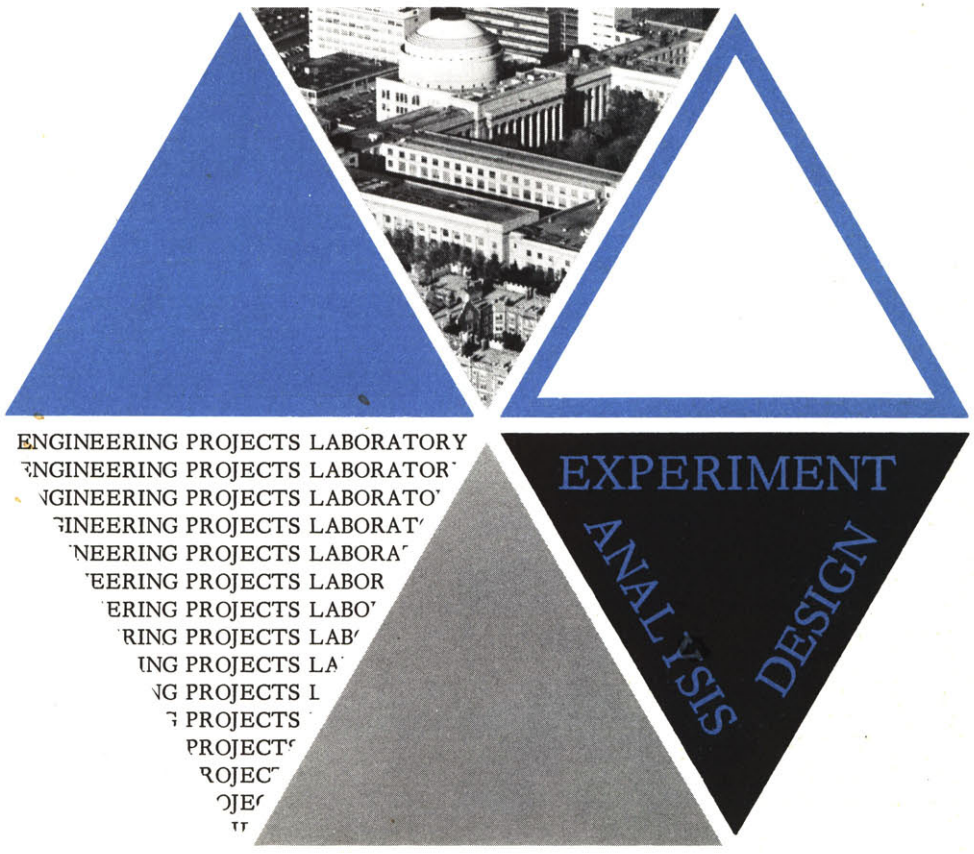

TECHNICAL REPORT No. 5050-36

THE EFFECTS OF SURFACE INSTABILITIES ON LAMINAR FILM CONDENSATION

by

Joseph Gerstmann

Peter Griffith

Sponsored by the National Science Foundation
Contract No. NSF GP-2402
DSR Project No. 5050

September 30, 1965

Department of Mechanical Engineering
Massachusetts Institute of Technology
Cambridge 39, Massachusetts

ABSTRACT

Heat transfer rates for laminar film condensation of Freon-113 were measured on the underside of horizontal surfaces, inclined surfaces, and vertical surfaces. Several distinct regimes of flow were observed. On the underside of horizontal surfaces, the interface is best described as a fully established Taylor Instability. At slight angles of inclination there are three regimes of flow. Near the leading edge, the interface is smooth and waveless. Next there is a region of developing waves which are best described as longitudinal ridges. As the ridges grow in amplitude, drops are formed at the crests and subsequently fall from the surface. Beyond the point at which drops first fall, a third regime exists which can be considered to be a fully established state, independent of distance from the leading edge of the surface. At moderate angles of inclination and up to the vertical, "roll waves" appear a short distance from the leading edge.

An analysis is presented which considers the surface waves to be fully established flows, resulting from bounded instabilities. It is shown that the shape of the interface can be determined without investigating the stability of the unperturbed film. The analysis results in an equation for the shape of the interface which is used to determine the average reciprocal film thickness, hence the heat transfer coefficient. The results of the analysis are valid for condensation on the underside of horizontal surfaces and slightly inclined surfaces.

The wavelengths predicted by the analysis are in fair agreement with the experimentally observed wavelengths. The observed heat transfer rates agree quite well with the theory.

ACKNOWLEDGEMENT

This research was performed at the Heat Transfer Laboratory of the Massachusetts Institute of Technology and was Supported by the National Science Foundation under Contract No. NSF GP-2402. Much of the numerical work was performed at the Computation Center at the Massachusetts Institute of Technology. Support was provided for one of the authors (J. Gerstmann) as an N. S. F. Fellow.

TABLE OF CONTENTS

LIST OF FIGURES

NOMENCLATURE

C_p	specific heat
g	acceleration of gravity
h	heat transfer coefficient; enthalpy
h_{fg}	latent heat of vaporization
h'_{fg}	change in specific enthalpy in transformation of vapor into subcooled liquid
k	thermal conductivity
L	characteristic length
Nu	Nusselt number
p	pressure
Q/A	heat transfer rate
r	radial length coordinate
R^*	radius at which interface has zero slope
R_1, R_2	radii of curvature
T	temperature
T_{wall}	wall temperature
ΔT	temperature difference
ΔT_{avg}	interface temperature minus average wall temperature
ΔT_{io}	temperature rise of coolant from inlet to outlet
v	velocity
x, y, z	length coordinates

Greek Letters

Γ	flow rate per unit width
δ	film thickness
δ_{MAX}	maximum film thickness
δ_o	minimum film thickness
η	reduced film thickness,
θ	angle of inclination
λ	wavelength
μ	viscosity
ρ	density
ρ_v	vapor density
σ	surface tension
T	dimensionless temperature difference Eq. 3-10 Pg 44
ψ	perturbation film thickness
ω	coolant flow rate

CHAPTER I

INTRODUCTION

1.1 Background

The prediction of heat transfer rates in film condensation had its start in the work of Nusselt[1]*, who determined the velocity profile and film thickness for a steady laminar film falling under the action of gravity. He assumed that the motion of the film was dominated by viscosity and that the film thickness was a monotonic function of the distance from the leading edge. These two basic assumptions are not independent. If the film thickness varies monotonically, then one can show that, for laminar flow, momentum fluxes may be neglected with but small error. If, on the other hand, the film is wavelike, then momentum fluxes become important. The laminar, monotonic state is in fact always unstable, and the surface of the film can appear wavelike. Fortunately, in condensing systems, the waves increase heat transfer rates only by about 20%, while the effect on average film thickness is still less. Perhaps for this reason, later investigators retained Nusselt's assumption of a monotonic film.

Using Nusselt's model, Bromley[2] and Rohsenow[3] obtained the non-linear temperature variation in the film, and showed that the non-

* Numbers in parentheses refer to references at end of the thesis.

linear effect was small for fluids with large latent heats, and at small temperature differences. Sparrow and Gregg[4] treated the film as a boundary layer and took into account momentum fluxes and showed that they were small at large Prandtl numbers. However, their assumption of steady flow precluded wavelike effects. Other investigators[5, 6, 7] included the effects of vapor shear and turbulent flow.

The effects of waves on heat and mass transfer began to receive attention in the 1940's. Hanratty and Hershman[8] present an extensive survey of the literature in this area. The waves which form on condensing films have been termed "roll waves" by Hanratty and Hershmann as they are similar in form to the long waves observed in water runways which are characterized by wave crests which steepen and roll over on themselves. They are observed in flows down slightly inclined surfaces, vertical surfaces, and even on the undersides of inclined surfaces. Kapitza[9] was the first to attempt to predict the amplitude of the waves and thus their effect on heat transfer. Using a shallow water approximation and a modified integral form of the differential equations, he obtained expressions for the Reynolds number ($4\Gamma/\mu$) at which a smooth laminar film would become unstable, the wavelength of the disturbances, and (by taking into account the second-order terms in his linearized analysis), the amplitude of the waves when the disturbances had become "fully developed". He predicted sinusoidal waves whose amplitude was . 46 times the

average film thickness which in turn was 7% less than the thickness predicted by Nusselt. However, neither the form of the waves nor their effect on film thickness agree well with experiment. Later, Dukler and Bergelin[10] made Capacitometer measurements of average film thickness and wave profile. Their results show that the average film thickness agrees very well with Nusselt's prediction at (length) Reynolds numbers up to 1000. They fail to note, however, that it is the average of the reciprocal film thickness that is of importance for the determination of heat transfer rates.

Brooke Benjamin[11] appears to be the first one to show that films are unstable at all Reynolds numbers and inclinations, although at small Reynolds numbers the growth rates and wave numbers are extremely small. He notes that, at a Reynolds number of about 20, the growth rate of disturbances begins to increase rapidly, which may explain why many experimenters have found what appears to be a "transition Reynolds number". In 1961 Hanratty and Hershman used a shallow water approximation and an integral form of the differential equations which were linearized to obtain a dispersion relation which was linear in wave velocity and quartic in wave number. By assuming that the wave numbers were real, they obtained a neutral stability curve of wavelength as a function of (film thickness) Reynolds number. They found good agreement between wave number, wave velocity, and Reynolds number at transition from the smooth film to the wave state. Their results also agreed well with those of Brooke

Benjamin and Binnie [12].

It should be emphasized that, except for Kapitza's work, all investigations have dealt with roll waves at or near "transition". In fact, as the waves grow, they change from the essentially two-dimensional waves moving downstream into steep, jagged, rolling crests which are much unlike the analytical model. Furthermore, all analyses to date have assumed the disturbances to be spatially periodic and temporally increasing, the so-called "absolute instability". In fact, in the experiments which have been performed and in the systems encountered in practice, the wave states are of the spatially increasing, temporally periodic form, the so-called convective instability. The most likely reason for assumption of an absolute instability is that the dispersion relation is quadratic in wave velocity, and quartic in wave number. Thus, with a convective instability one must solve for the complex roots of a quartic algebraic equation, while for an absolute instability, one need solve only a quadratic. Gaster [13] and Watson [14] have shown that, for hydrodynamic instabilities, either choice gives identical results for the neutral curve, and that there are simple relationships valid in the vicinity of the neutral curve whereby one may obtain the behavior under one type of instability from knowledge of the behavior under the other. However, if the wave state is far from the neutral curve, the two types of instability are essentially different. It appears, therefore, that, if any further progress is to

be made in the field of roll waves, they must be considered as convective, not absolute, instabilities.

1.2 Absolute-Convective Instabilities

The statement that the Nusselt analysis is accurate to within 20% is true only for condensation on near-vertical surfaces. For condensation on the underside of inclined surfaces, the agreement becomes worse, until for condensation on the underside of horizontal surfaces there is no agreement whatsoever. At this angle a smooth film is absolutely unstable. The surface of the film forms pendent drops which grow and depart from the surface. This type of instability has become known as the Taylor instability [15]. The earliest attempt at predicting heat transfer rates under the above conditions was made by Popov [16] in 1951. He considered the surface to be covered by spherical drops separated by areas of uniformly thick film. Vapor condensed on the film and the condensate flowed radially into the drops. His experimental data exhibited considerable scatter, possibly because of non-condensable gases. Both his theory and his experimental data give considerably lower heat transfer coefficients than those of Gerstmann [17]. In 1960 Berenson [18] considered a similar problem, that of film boiling on the upper side of a horizontal surface. He assumed the boiling surface to be covered with hemispherical bubbles separated by areas of uniform film. The bubble spacing was determined by the Taylor wave

length, while the bubble sizes were determined from various experimental observations. He proposed that the mechanism of vapor removal was by radial laminar flow into the bubbles and showed that the momentum fluxes in the vapor could be neglected in comparison to viscous shear. Except for the boundary condition on velocity at the liquid-vapor interface, Berenson's analysis is equally valid for film condensation on the underside of a horizontal surface. Although his analysis agrees well with boiling data, the agreement is poor for condensation.

When the surface is inclined slightly off horizontal, the drops all run downstream and become elongated until they can be more aptly described as longitudinal ridges (See Figure 10). Pg. 24 In the crests of the ridges the direction of flow is downstream, while in the troughs between the ridges the flow is predominantly transverse. The ridges grow as they progress downstream and drops form at the crests and periodically fall. Were it linear, this motion would be classed as a combination absolute-convective instability, however, as it is actually non-linear, it remains unclassified. To the author's knowledge, no work has been reported on this type of flow.

1.3 Scope of This Investigation

In the present study we will confine the bulk of our attention to the two types of flow encountered with horizontal and slightly inclined surfaces. These represent an extreme departure from the wave-

less Nusselt state, and have received a minimum of attention in the past. We have stated that the phenomena under consideration are fundamentally instabilities. Previous investigators have analyzed similar phenomena such as film boiling by examining the stability of the unperturbed state and have used the results of the stability analysis, notably the wavelength, to formulate a model representing the ultimate results of the instability. For example, Berenson used the wavelength of the Taylor instability as the characteristic dimension of the vapor bubbles formed at the liquid-vapor interface in film boiling. The implication of this method is that a small perturbation analysis is still valid when the perturbations are no longer small.

In cases where the ultimate state of an unstable system is very much different from its state when the perturbations are still small, the above procedure will not apply. Normally such is the case when the instability is highly non-linear and a linearized stability analysis is valid only for small perturbations. Furthermore, because of the high degree of non-linearity, analysis of the non-linear effects is apt to be quite difficult.

In this study we shall show that the problem can be approached from a different point of view. Instead of examining the unstable behavior of an initially unperturbed system, if the instabilities are bounded, the ultimate state of the unstable system may be considered as a stable state. The characteristics of this pseudo-stable system may then be

determined by an ordinary equilibrium type analysis. For example, instead of considering the Taylor Instability as an instability per se, it may be regarded as a system of standing waves whose amplitudes vary periodically in time. The only information required to perform the analysis is a qualitative description of the phenomenon, i. e. whether the interface is steady or periodic in time, and whether the interface takes the form of drops, ridges, standing or travelling waves, etc. Of course, if this qualitative description is not available from a stability analysis, then it must be obtained from an experimental observation. The experimentally obtained information may be in the form of a photograph or even a visual observation. The important point is that the only information necessary to perform this analysis is of a qualitative, not quantitative, nature. The advantage of this technique is that, if the flow remains laminar, the ultimate state of an unstable system is completely described without the necessity of following the course of the instability throughout all of its stages.

CHAPTER II

EXPERIMENTAL PROGRAM

2.1 Experimental Objectives

The experimental program had a twofold purpose. First, as the analysis would require knowledge of the final state of the interface, it would be necessary to make experimental observations of the nature of the various regimes and of their extent. Also, from visual and photographic observations, we could check the geometrical consistency of the analysis. Second, the experiment should yield reliable heat transfer data for the various regimes.

2.2 Design Considerations

The main design considerations were as follows:

1. The condensing surface must be unobstructed visually.
2. The test section must be rotatable about a horizontal axis.
3. Determination of the heat transfer coefficient would require measurement of surface temperature, vapor temperature, average, or preferably local, heat flux.
4. Measures for eliminating non-condensable gases must be provided.
5. The boundaries of the condensing surface must not interfere

with the phenomena occurring on the surface.

6. It would be advisable to test fluids with widely differing properties as a further check on the validity of any analysis.

2.3 Choice of Fluids

In addition to having widely differing properties, the test fluids should have low toxicity, not too high a boiling point, reasonably well established properties, and, of course, should not react with the rest of the apparatus. Freon-113, a refrigerant, appeared to be well suited, although some precautions would have to be taken with the choice of materials since it is also a solvent. Since its vapor is heavier than air, the problems of non-condensable gases could be minimized with proper venting.

Water appeared to be suitable as a second fluid, as in terms of the dimensionless temperature difference suggested in (17), it differs from Freon-113 by three orders of magnitude, the heat transfer coefficient would be about 10 times greater than that of Freon-113, and it is also of practical importance as a heat exchange fluid.

2.4 Description of the Apparatus

There were several basic decisions to be made in the design of the apparatus. First, there was the choice of local or average heat flux measurements. In order to make local heat flux measurements, the

temperature profile within the test surface would have to be measured. For the measurements to be at all accurate, a temperature difference of at least two or three degrees would have to exist between the cooling surface and the condensing surface at the minimum heat flux (Freon-113 at about $10^{\circ}F$ temperature difference). This would result in a temperature difference of 100 - $150^{\circ}F$ at the maximum heat flux (water at about $50^{\circ}F$ temperature difference). Also a material which would yield so large a temperature gradient would make measurement of the surface temperature difficult. It was decided, therefore, to determine the heat flux by a heat balance on the coolant flow. The other major decision was whether to insulate all surfaces of the test section but the test surface, or to expose only the test surface to vapor and take into account any heat losses through uninsulated surfaces. Although it was quite difficult to insulate the test section properly, especially at the edges of the test section, this course was taken as it was felt that it was far better to eliminate losses than to correct for them in the reduction of data.

The test section was made of pure copper bar and measured 18" x 6" x 2". 24 half-inch diameter holes were drilled along the six inch length 1/4" beneath the top surface to provide passage for the coolant flow. 1/2" deep cross-overs were milled between the passages to connect them in series (See Figure 1). The cross-over between the 11th and 12th passage was blocked off and replaced with an insulated by-pass of 1/4" copper

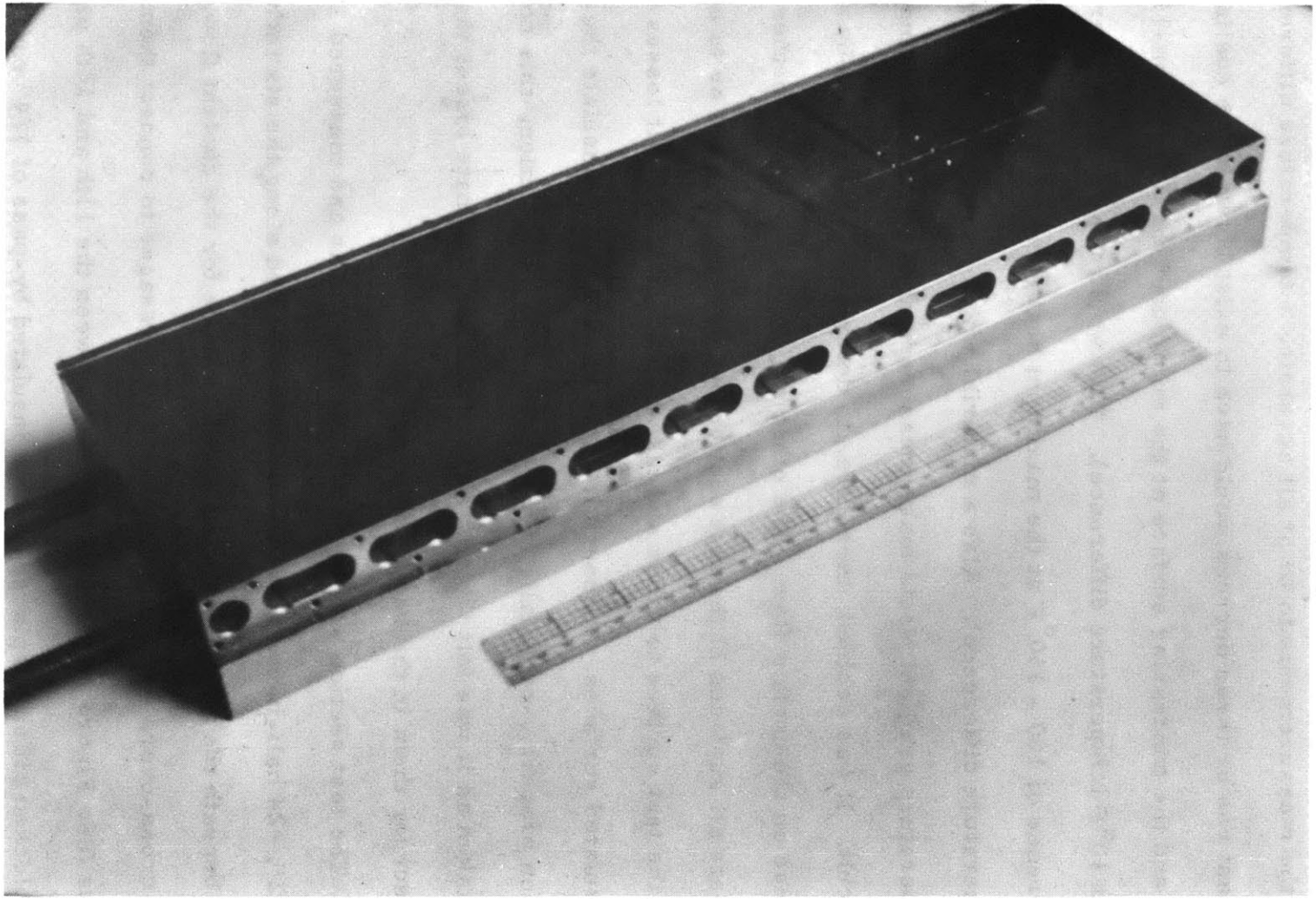

Figure 1: Copper Test Section With
Cover Plate Removed

tubing in which a thermocouple measured the coolant temperature at that point. Two teflon gaskets and brass cover plates sealed the ends of the coolant passages. Four 1/16" diameter thermocouple holes were drilled to within a nominal distance of 1/16" from the test surface. They were spaced 3/4", 6", 12" and 17 1/4" from the leading edge of the test section. Although the nominal distance from the test surface was 1/16", the actual measured distances were 1/16", 1/8", 3/32", and 1/16". #28 A. W. G. copper constantan thermocouples were installed in these holes and sealed with melted paraffin. Extreme care was taken to make the thermocouple junctions as small as possible (less than 1/16" diameter).

The test section was bolted to a 16" x 16" x 1" Bakelite cover plate at the leading edge. All piping and wiring passed through the cover plate and was suitably sealed. A ten-junction copper-constantan thermopile was installed between the coolant inlet and outlet in addition to thermocouples between the coolant inlet and the by-pass, and between the by-pass and the coolant outlet. A thermocouple above the test section was used to measure the vapor temperature and to serve as reference for the thermocouples near the test surface. All thermocouple wells were filled and sealed with paraffin.

The insulation for the test section was made of polyurethane foam, Ecco-foam FPH, having a thermal conductivity of 0.015 BTU/ft-hr-^{o}F., and was molded in place to a thickness of 2". As the foam was not resistant to Freon-113, it was necessary to protect it with a coating. Samples

of Ecco-coat EC-200, an epoxy resin, did not appear to be affected by either Freon-113 vapor or steam, so about 20 coats were applied to the foam. Calculation of heat losses through the insulation (Appendix A) show that they do not exceed 1%.

A 30" x 18" x 18" Dexion frame surrounding the test section was bolted to the Bakelite cover plate. The condensing chamber was a 24" x 12" x 12" pyrex jar supported by the Dexion frame and sealed to the cover plate with a neoprene gasket. Immersion heaters to boil the test fluid lay on the bottom of the pyrex jar. Supported by the Dexion frame, the entire apparatus could be rotated to any desired angle (See Figure 2). The apparatus was contained in a large, temperature controlled, glass-windowed box maintained at saturation temperature.

About half of the vapor produced in the test section was vented to a reflux condenser located above the constant temperature box. The condensate from this condenser was returned to the test chamber. A small amount of the vented vapor was allowed to pass through the reflux condenser to a second condenser vented to the atmosphere, where the condensate was removed from the system. In this manner the vapor was continually stripped of non-condensable gases. Furthermore, the pressure drop through the exterior condenser system caused the test chamber to become slightly pressurized, thus protecting against air leaking into the system.

The coolant used for all the tests was water which was circulated

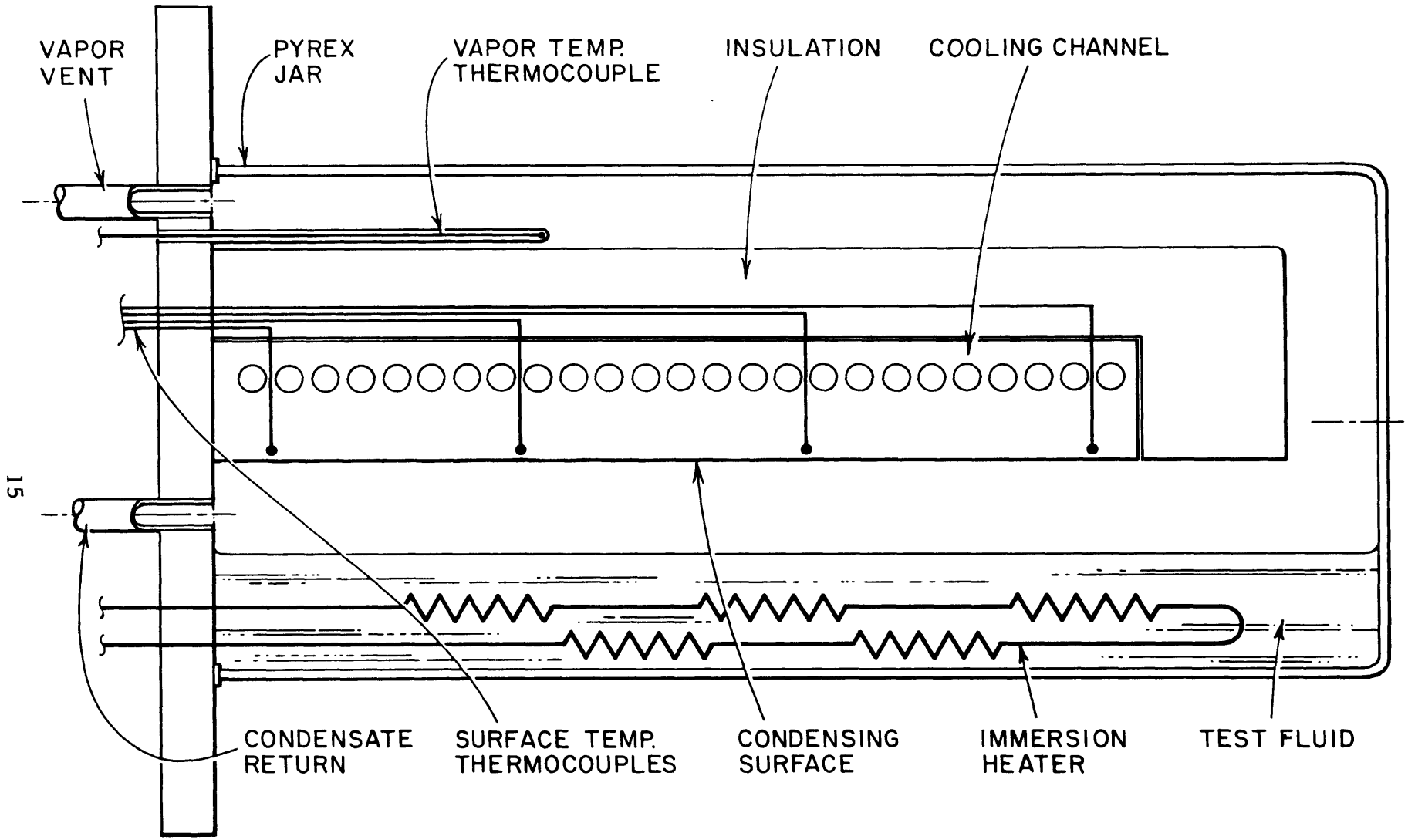

FIGURE 2. EXPERIMENTAL APPARATUS.

through the system from a 40 gallon reservoir. The tests were started with the water at 32°F, and it was allowed increase in temperature during the tests at the rate of one degree every three to ten minutes. The water flow rate was measured by a Brooks Rotameter, calibrated to ±1%. All piping external to the test section was of 3/4" I. D. rubber hose. The thermocouples were switched with a Leeds and Northrup thermocouple switch and the emf measured with a Rubicon potentiometer reading to within 1/2 μv. A photograph of the entire apparatus is shown in Figure 3, and schematic in Figure 4.

2.5 Experimental Procedures

Before any test data was taken, the test fluid was boiled in the condensing chamber, and the vapor was condensed in the external condensers to remove non-condensable gases. In the meantime, the apparatus was brought up to saturation temperature in the constant temperature box. After about an hour of de-gassing, the coolant reservoir was filled with water and ice which was allowed to come to equilibrium before the water was circulated through the system. As the water circulation was started, the power to the boilers, controlled with a Variac, was increased so that the residual vented vapor was condensed at a constant rate.

The jacket of the secondary condenser was made of transparent lucite so that the vapor-air interface could be observed. The power to

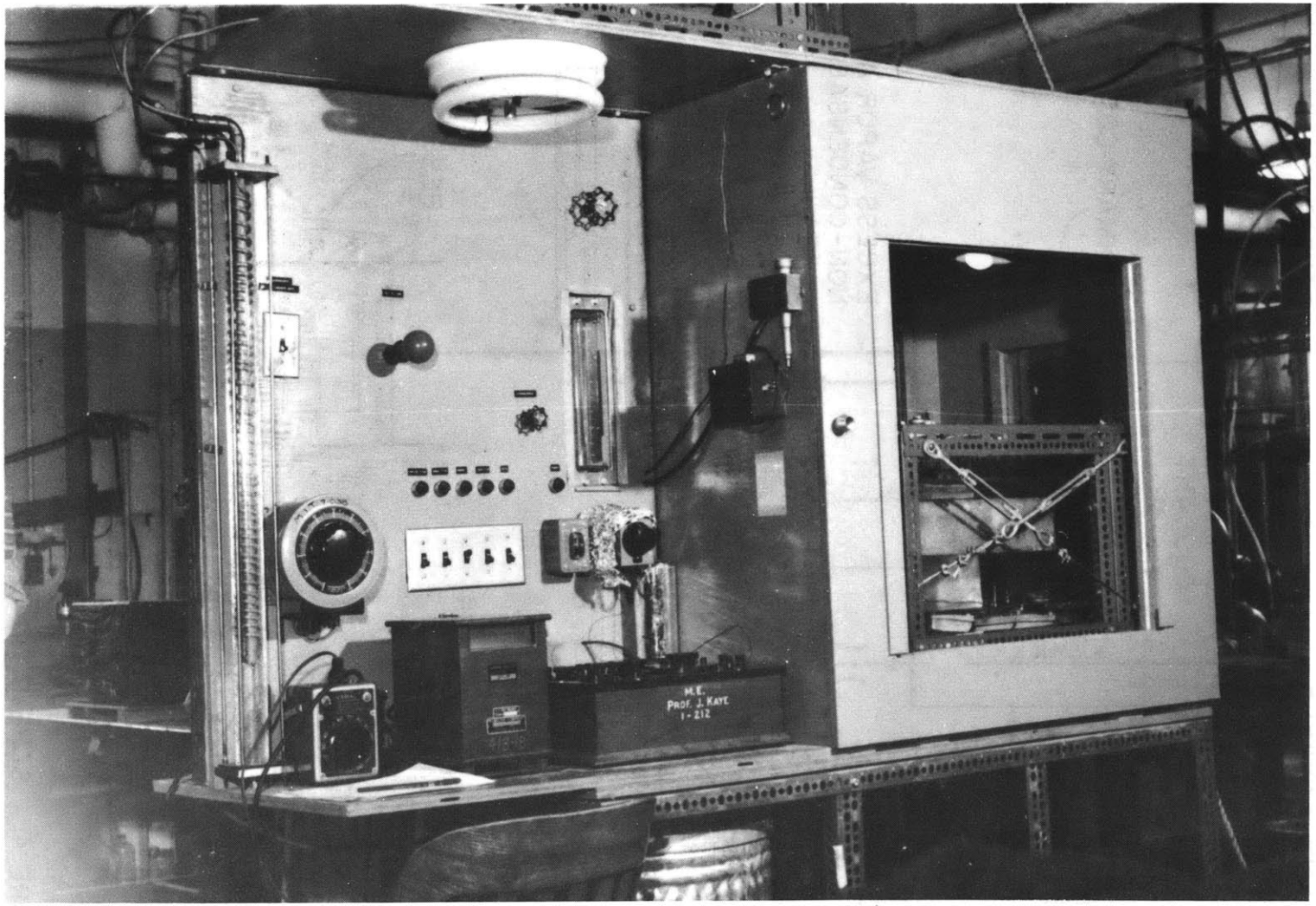

Figure 3: Overall View of System. Primary condenser is out of picture above the apparatus.

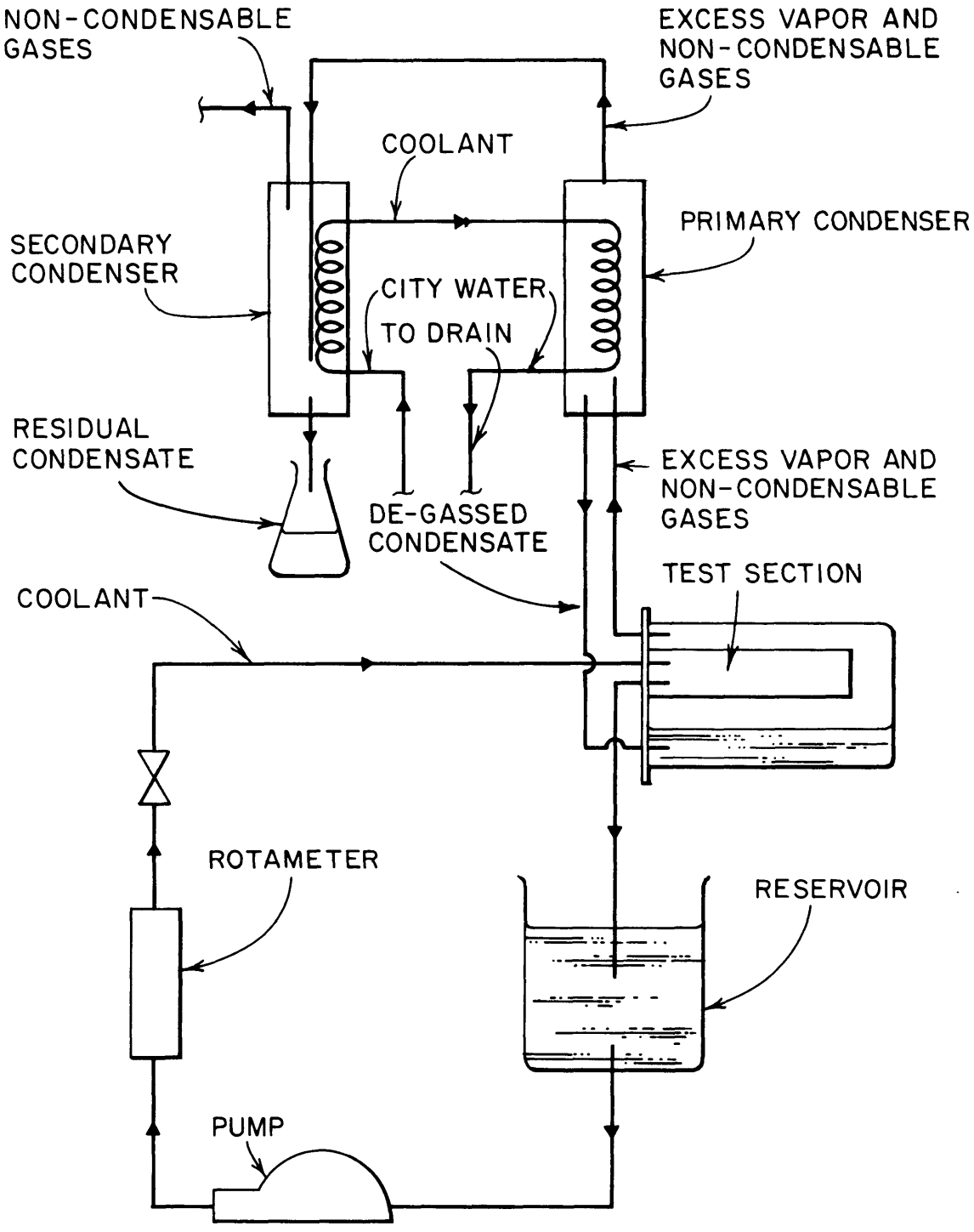

FIGURE 4. SCHEMATIC OF EXPERIMENTAL APPARATUS.

the boilers and the rate of coolant flow in the external condensers was adjusted so that vapor-air interface was maintained just beyond the inlet to the secondary condenser. This assured that there would be a minimum of diffusion of air into the primary condenser with the least expenditure of the test fluid.

Before any data were recorded, the instruments were checked to make sure that the system had reached a quasi-steady state. The following measurements were recorded:

Coolant temperature.

Vapor temperature.

Surface temperature at 3/4", 6", 12", and 17 1/4". These are denoted as T. C. #1, T. C. #2, T. C. #3 and T. C. #4 respectively in Appendix B*.

Coolant temperature rise from inlet to outlet (ΔT_{io} in Appendix B).

Coolant temperature rise from inlet to middle of test section. (Q(0-9)).

Coolant temperature rise from middle of test section to outlet. (Q(9-18)).

Coolant flow rate. (Flow)

The method of data reduction is presented in Appendix C.

---

*In several tests only T. C. #1 and T. C. #4 were recorded so that less time would elapse between the surface temperature measurements and the heat flux measurements. Comparison shows that these two temperatures are sufficient to obtain an accurate average. The reference junction for these thermocouples was at vapor temperature, so that the above measurements are actually the difference in temperature between the vapor and the test surface.

2.6 Experimental Results

Extensive tests were made with Freon-113 condensing on the underside of horizontal surfaces and surfaces inclined up to 5°. Also data were recorded for condensation at angles of 7 1/2°, 11 1/2°, 21°, 62 1/2°, and 90° from the horizontal to show the transition from horizontally dominated to vertically dominated condensation. The data included measurements of heat transfer rate, surface temperature, vapor temperature, and angle of inclination, in addition to photographic measurements of pertinent geometric variables.

The attempts to obtain data on the condensation of steam were unsuccessful. Unfortunately, the epoxy coating covering the insulation failed after about a half hour of exposure to steam. The mode of failure was a softening and subsequent rupturing of the epoxy coating followed by a release of gases by the foam insulation. The steam vented from the test chamber smelled strongly of the solvent used in the preparation of the epoxy, which was supposed to evaporate upon curing of the epoxy. Evidently, when the insulation was coated, insufficient time elapsed between the application of the coats to allow complete curing and solvent evaporation. Thus, although the outer coats were cured, the base coats never cured completely and the exposure to 212° temperatures caused the evaporation of the solvents with the resultant bubbling and rupture of the coating. Consequently, this work deals only with the results of experi-

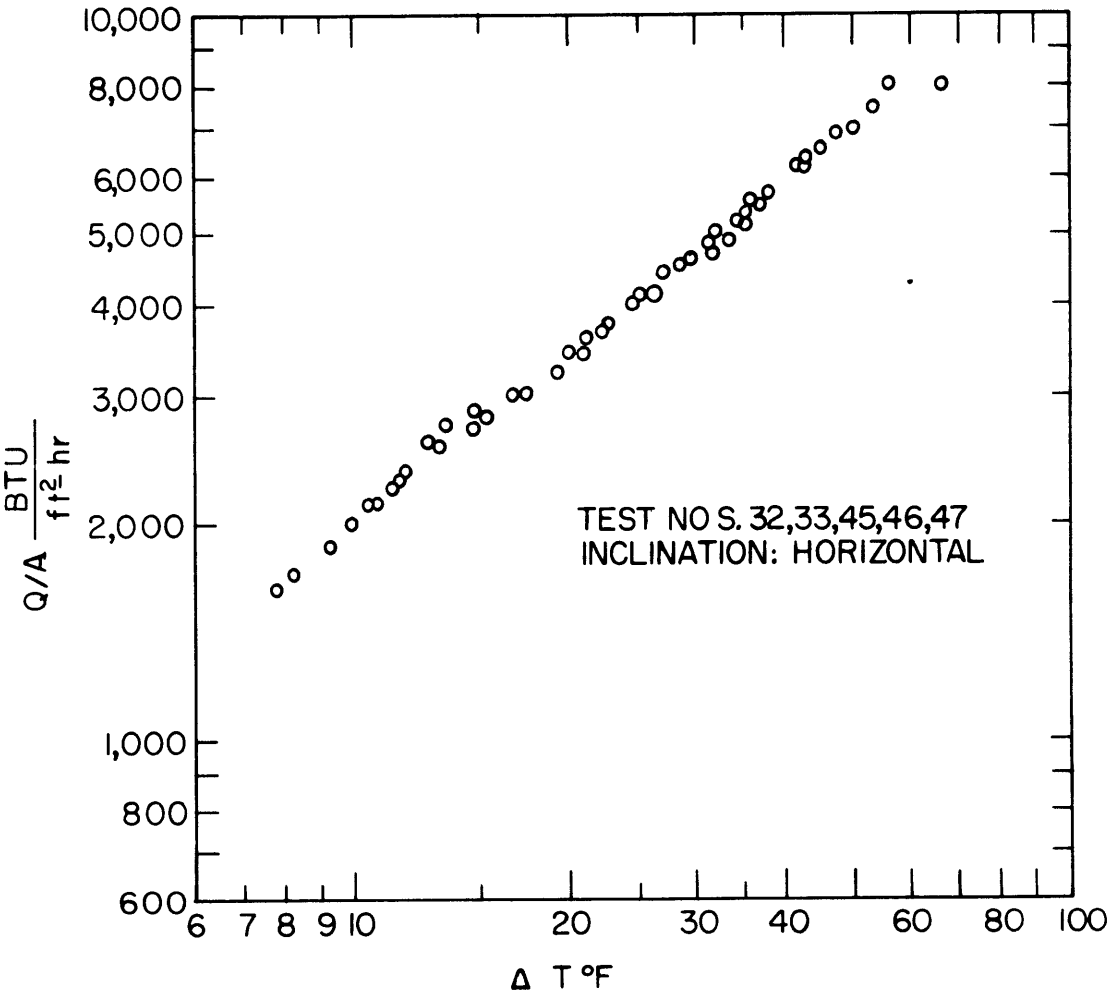

FIGURE 5: HEAT TRANSFER RATE VERSUS TEMPERATURE DIFFERENCE

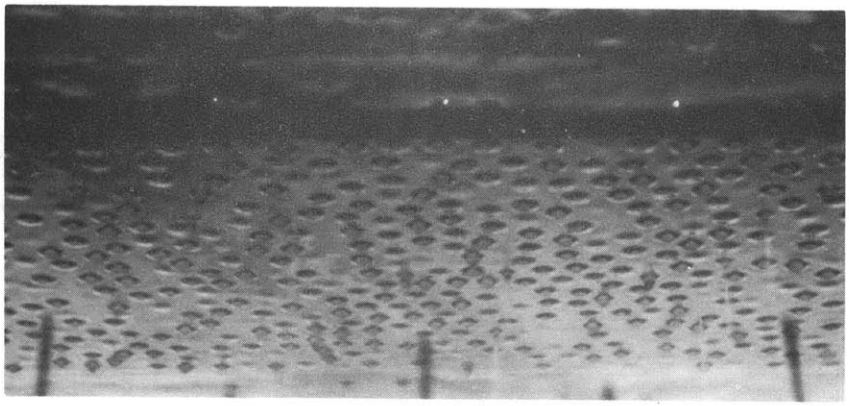

$Q/A = 2800$ BTU/ft^2-hr

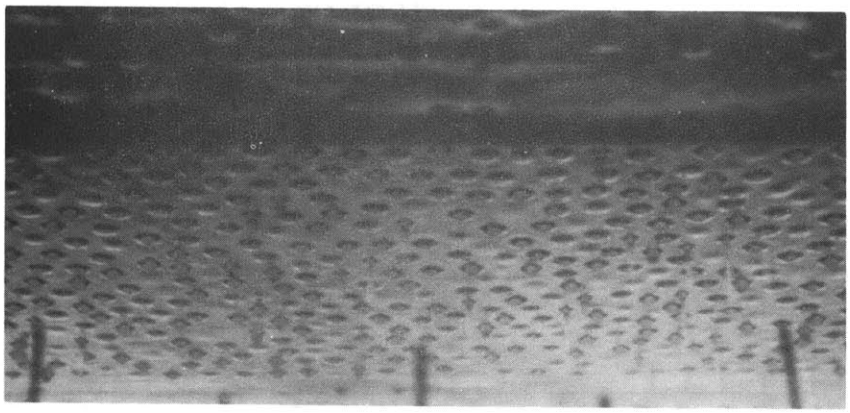

$Q/A = 6300$ BTU/ft^2-hr

Figure 6: Condensation on a Horizontal Surface

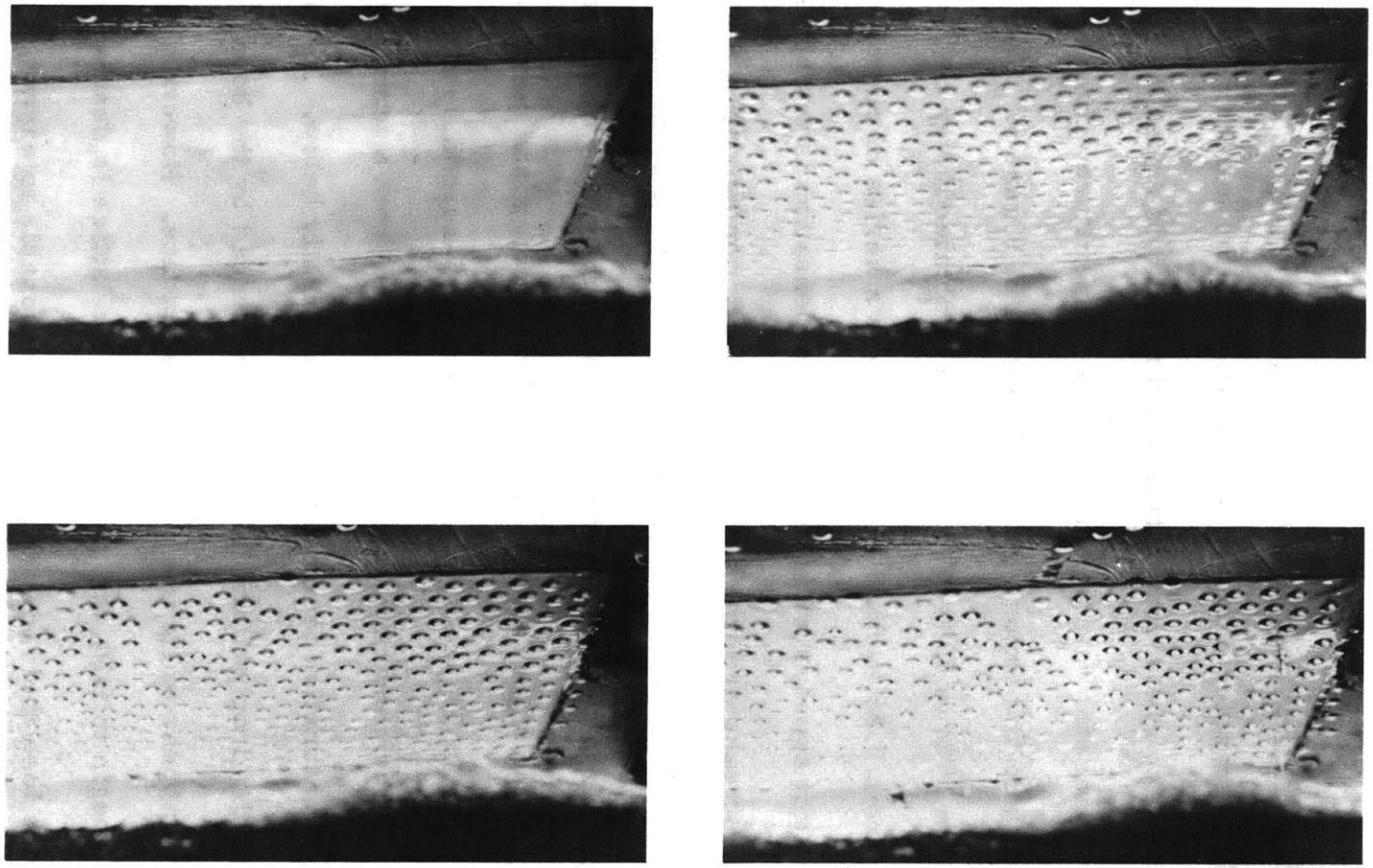

Figure 7: Stages in the Growth of the Taylor Instability

ments using Freon-113.

2.6.1 Horizontal Surfaces

The heat transfer data for condensation on the underside of a horizontal surface are shown in tables 2 through 6 of Appendix B, and a plot of heat transfer rate versus average temperature difference between the surface and vapor (ΔT_{avg}) is shown in Figure 5. Heat transfer rates from 1640 to 8030 BTU/ft^2-hr were obtained over temperature differences from 7.85 to 56.5^{o}F. Figure 6 is a series of photographs of the surface as it appears when horizontal condensation is taking place. The vertical streaks are markings on the Pyrex condensing chamber used to correct for parallax. The photographs show a somewhat random drop spacing, although some instances of uniformity may be observed, particularly at the higher heat fluxes. These photographs may be compared with those in Figure 7 which represent a 15-second sequence which occurred when the condensing surface was cooled from a temperature slightly above saturation temperature to one slightly below. In these photographs, the drop pattern is strongly influenced by the boundaries, and the drops appear to lie in a close-packed lattice. However, as soon as the drops begin to fall, the symmetry of the lattice is destroyed and the boundaries lose their influence. It is reasonable to expect, therefore, that, under steady operating conditions, the influence of the boundaries is negligible beyond one wavelength from the boundary.

Referring again to Figure 6, it is seen that there is a larger drop density at high heat flux than at low heat flux. This is due to the fact that the frequency of drop departure is much lower at low heat flux, thus the drops have a greater chance to coalexce. At high heat fluxes, above about 4000 BTU/ft^2-hr, there is a minimum of coalescence, and the average drop density is about 6.5 drops per square inch. Even though the plate was horizontal, the drops were not stationary, but meandered about due to the disturbances of neighboring drops. Slow motion pictures of the interface show that a new drop begins to grow at the same location that a fallen drop has just vacated.

2.6.2 Inclined Surfaces

The heat transfer data for condensation on the underside of slightly inclined surfaces are shown in Tables 7 through 15 of Appendix B and plots of heat transfer rate versus temperature difference for angles of 2 3/4 and 5^o are given in Figures 8 and 9. Heat transfer rates from 1075 to 7480 BTU/ft^2-hr at temperature differences from 6.3 to 71.5^{o}F were obtained. Photographs of the interface at 4^o and 5^o are shown in Figure 10. (Note that the liquid surface at the bottom of the pictures is a horizontal reference.) It is seen that at the high heat fluxes the drops superimposed upon the ridges are more pronounced than at low fluxes, and at low fluxes there are fewer drops than at high fluxes. Also the point

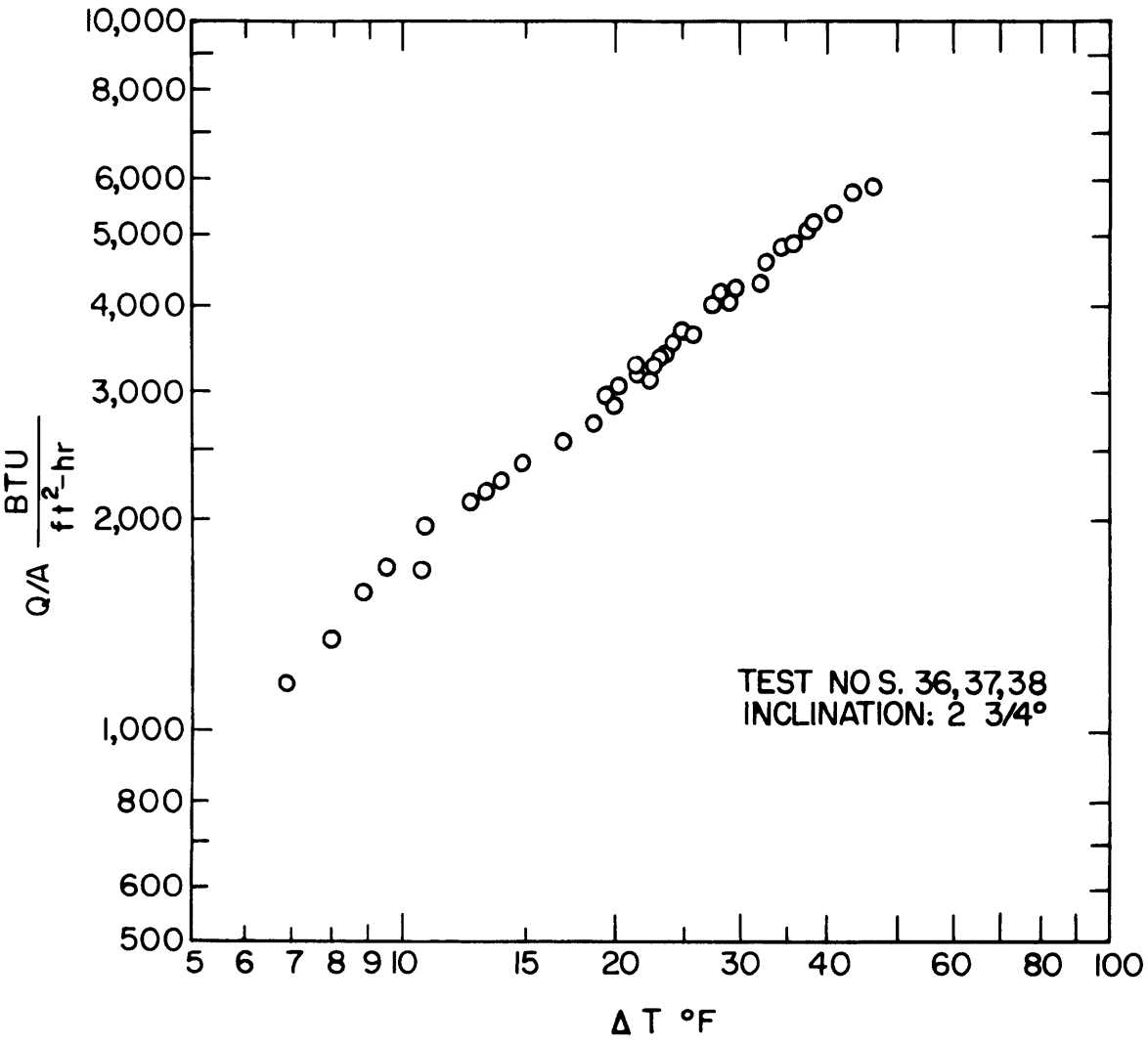

FIGURE 8. HEAT TRANSFER RATE VERSUS TEMPERATURE DIFFERENCE

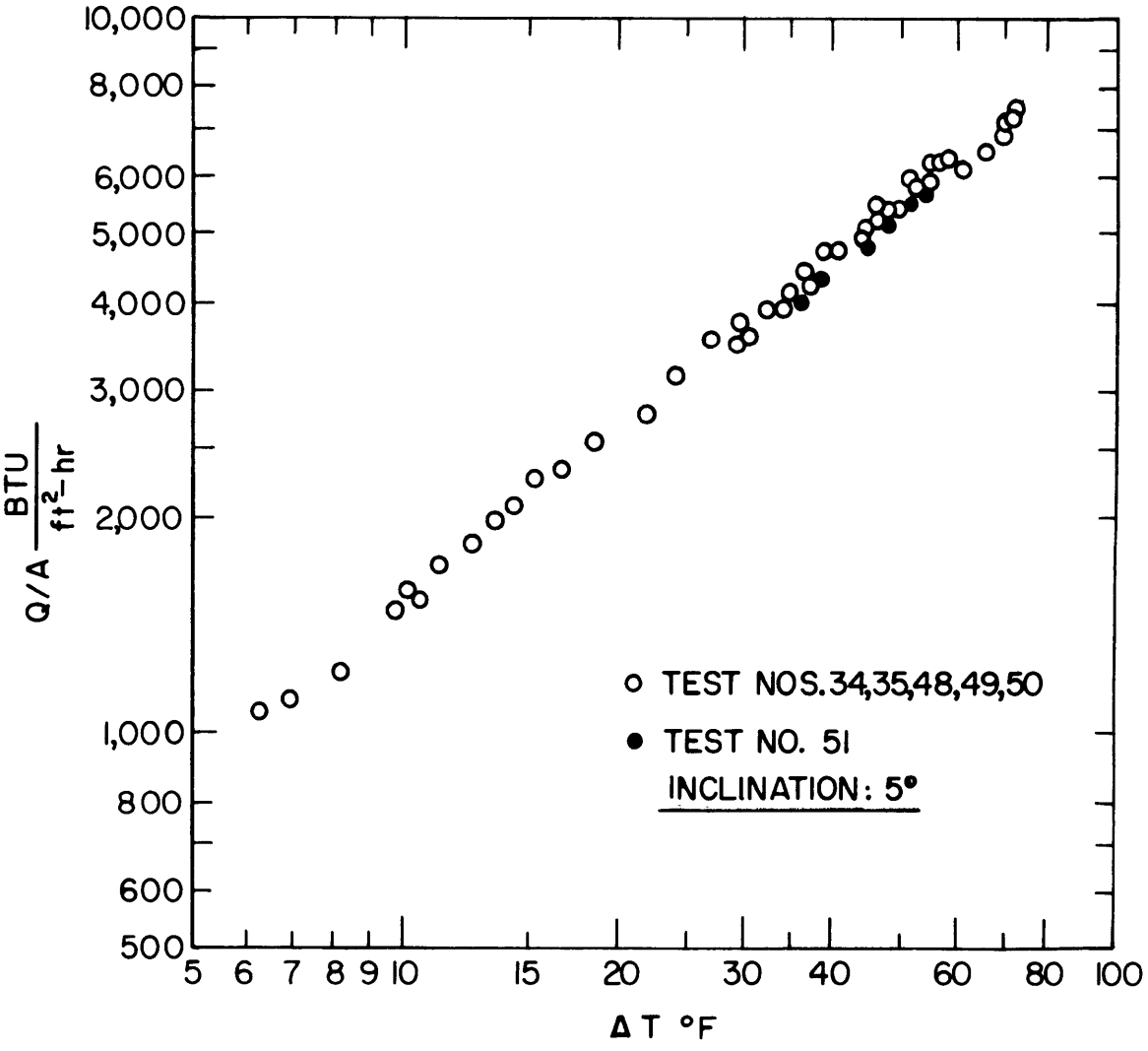

FIGURE 9. HEAT TRANSFER RATE VERSUS TEMPERATURE DIFFERENCE

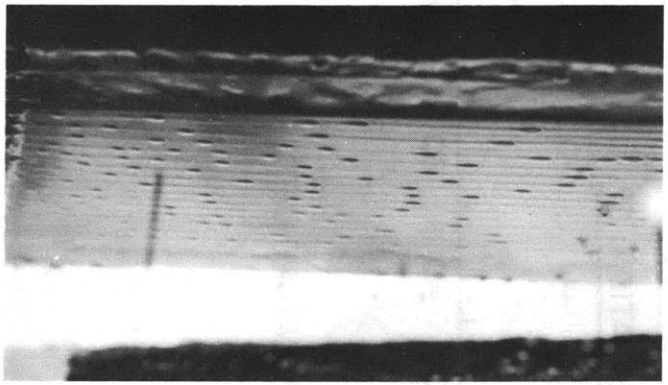

4°; Q/A = 760 BTU/ft^2-hr

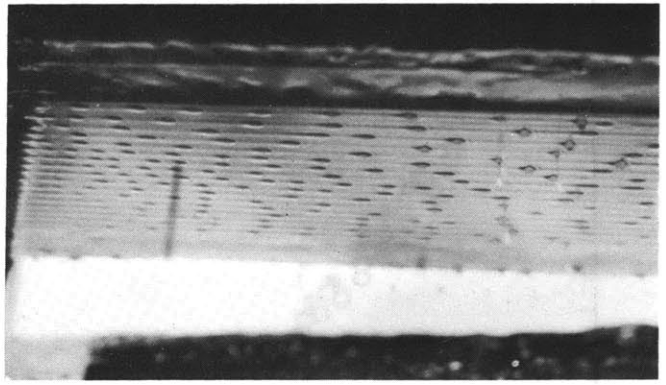

4°; Q/A = 1450 BTU/ft^2-hr

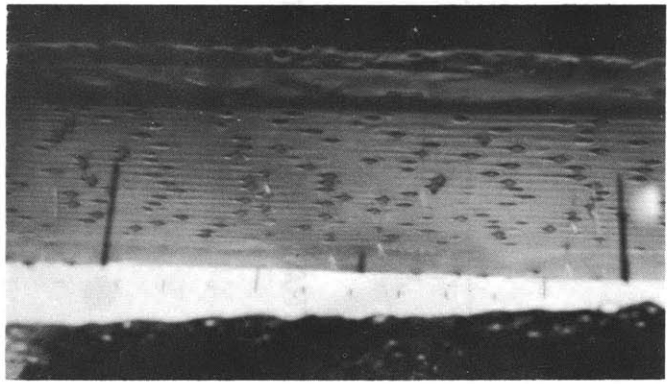

4°; Q/A = 4600 BTU/ft^2-hr

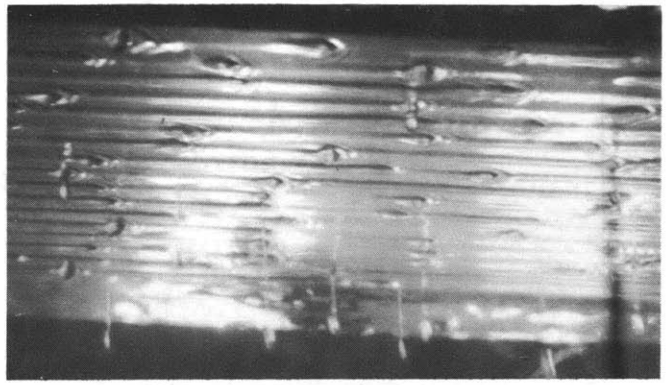

5°; Q/A = 3900 BTU/ft^2-hr

Figure 10: Condensation on an Inclined Surface

at which drops first fall from the surface moves downstream as the heat flux is reduced. Examination of the last photograph in Figure 10 shows that in front of each drop there is a small bow wave of very short wavelength.

At all angles at which ridges were observed, 17 ridges were counted across the six inch portion of the test surface. A transient test was run to see whether the number of ridges formed initially was the same as in the steady state. The test surface was brought to just above saturation temperature, and then the pressure in the condensing chamber was raised slightly until ridges formed. The pressure was then dropped so that the condensate film began to evaporate from the surface, the thicker ridges remaining. In this manner the ridges were "frozen" so that they could be counted. During the transient, adjacent ridges would occasionally merge, or a single ridge might separate into two ridges. However, the junction or the fork would always move downstream. Thus the number of ridges was always determined by events at the leading edge of the plate. In these tests 17 and sometimes 18 ridges were counted, making the wavelength most often obtained 6/17, or 0.353".

2.6.3 Surfaces at Larger Inclinations

In addition to the tests run at angles up to 5^{o}, data were taken at angles of 7 1/2, 11 1/2, 21, 62 1/2, and 90^{o}. The heat transfer data from these tests are given in Tables 16 through 22 of Appendix B. The

results are plotted in Figure 11, and it is seen that increasing the angle of inclination decreases the heat transfer rate up to an angle of about 11°, where further increases in angle lead to increased heat transfer rates. Some views of the condensing surface at angles of 9, 13 and 19 1/2° are shown in Figures 12, 13 and 14 .

In Figure 12 it is seen that at low heat flux the interface is quite similar to that at small angles. As the heat flux in increased, however, the interface looks quite different. Although not visible in the photograph, the leading edge of the plate appears to be quite smooth, then drops form and become more and more elongated as they move down the plate, until they are best described as ridges. These ridges are more sinuous than at smaller inclinations and interfere with one another to such an extent that neighboring ridges sometimes collide. Figure 13 further illustrates this point.

In Figure 14, (19 1/2°) it is evident that the interface is now of an essentially different form. The disturbances may no longer be described as drops. After an initially smooth starting length, transverse wave crests appear which are soon distorted into jagged wave fronts. The jaggedness increases until near the end of the plate, the originally transverse waves are now no longer identifiable as such, and may be considered as longitudinally oriented.

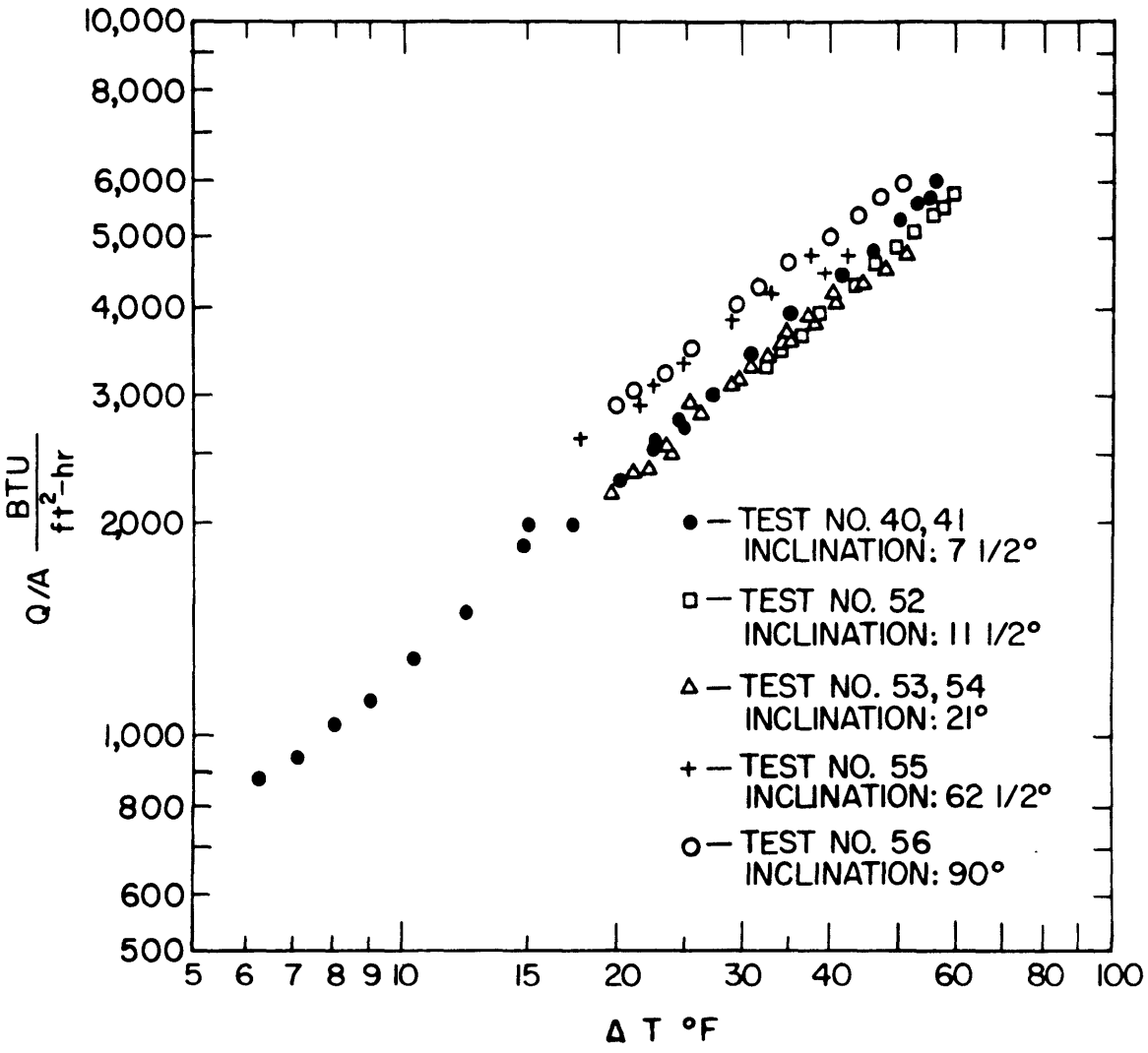

FIGURE 11. HEAT TRANSFER RATE VERSUS TEMPERATURE DIFFERENCE

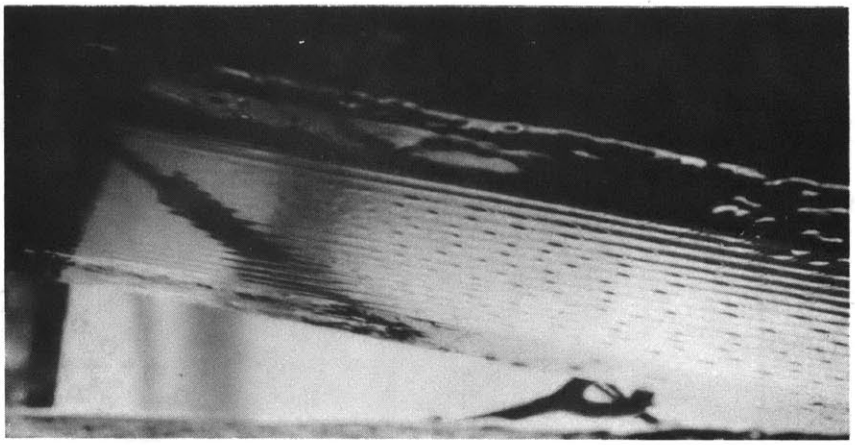

Q/A = 650 BTU/ft^2-hr

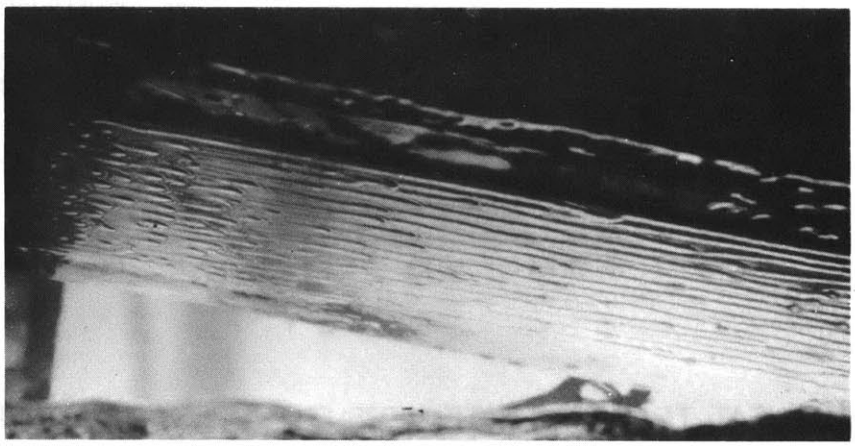

Q/A = 3900 BTU/ft^2-hr

Figure 12: Film Condensation at 9° Inclination

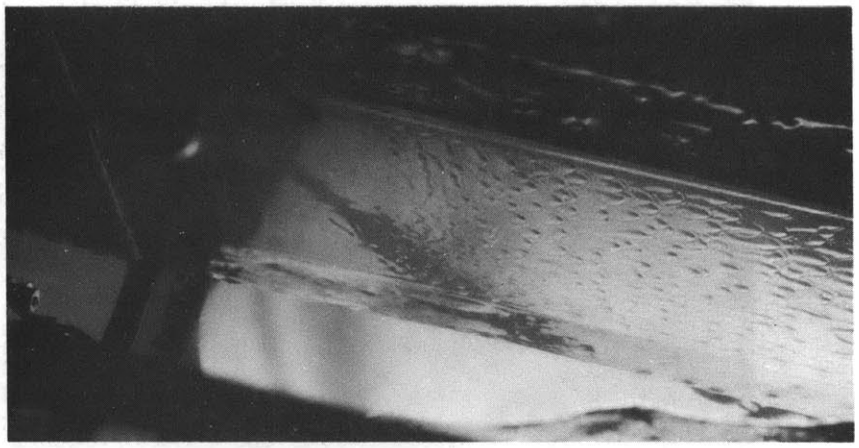

Q/A = 2000 BTU/ft^2-hr

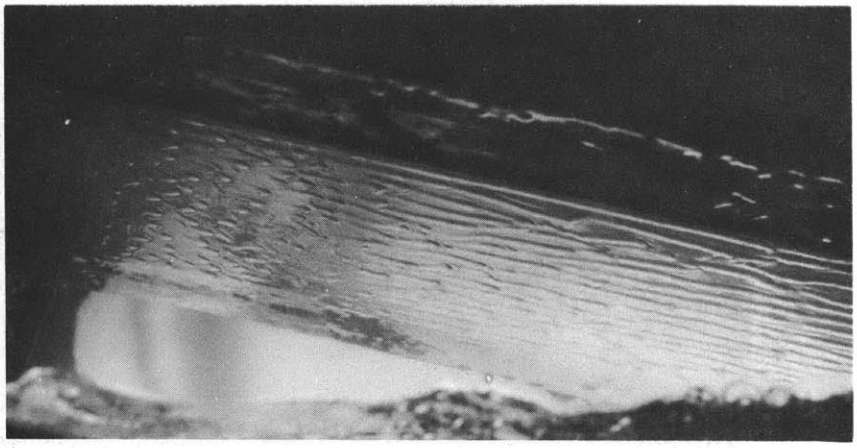

Q/A = 4500 BTU/ft^2-hr

Figure 13: Film Condensation at 13^o Inclination

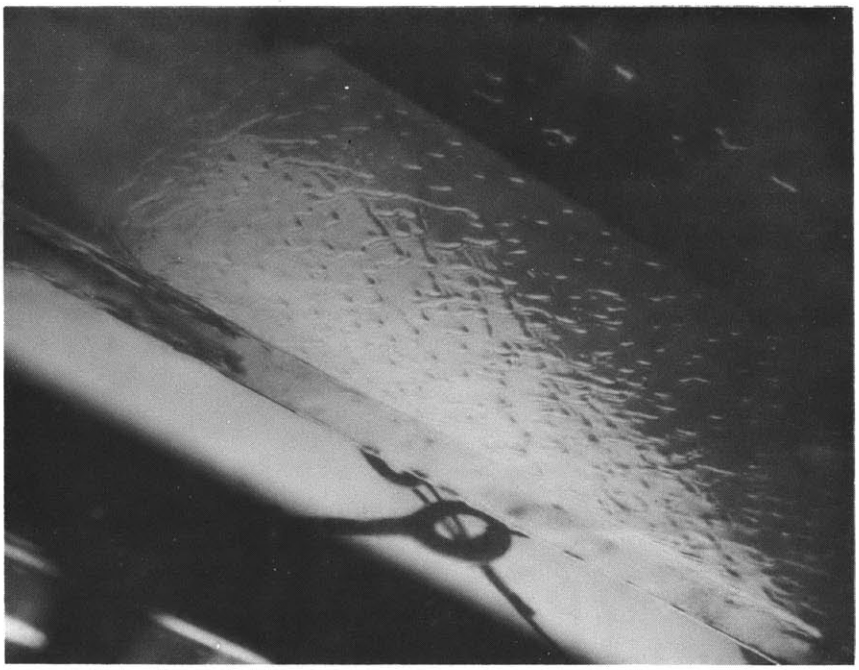

Q/A = 2100 BTU/ft^2-hr

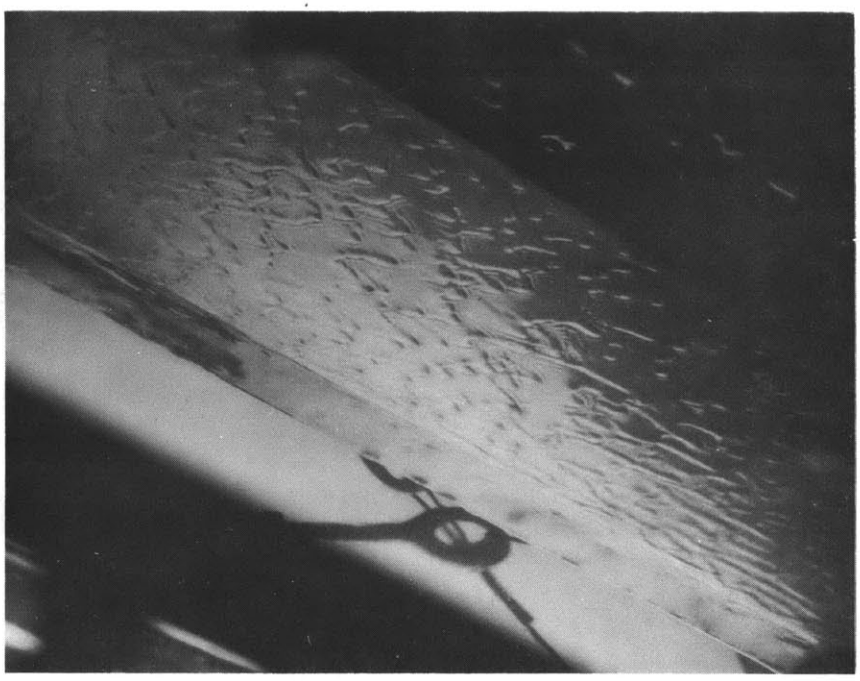

Q/A = 3800 BTU/ft^2-hr

Figure 14: Film Condensation at 19 1/2^o Inclination

At angles greater than 20°, the form of the interface is essentially unchanged even up to vertical surfaces.

2.6.4 Regimes of Flow

In the experiments described above, we may classify the flow as four basically different types. First there is the situation which obtains when the condensing surface is horizontal; here there is no preferred direction to the flow nor any characteristic dimension impressed upon the flow by the system. That is, dimensions of the condensing plate do not affect the hydrodynamics, thus the state of the film does not depend upon the distance from a particular boundary. Here the flow is dominated by the presence of pendent drops, and the flow is essentially radial into the drops.

Second there are the states of flow which are determined by the angle of inclination and the distance from the leading edge of the plate. These may be classified into three groups. The first is the glassy, smooth flow which exists near the leading edge of the plate, where the disturbances are of extremely small amplitude. The second is the developing wave state where the disturbances are of appreciable amplitude but there is no rupture of the interface (i. e. no drops have fallen from the surface.) Third there is the state which exists beyond the point at which the interface has first ruptured, where it is reasonable to expect that the flow is now independent of the distance from the leading edge, although there may

be a periodic dependence on the longitudinal direction. Although the lines of demarkation between all of the classes but the last are quite hazy, a qualitative separation is possible.

The most difficult distinction is between the horizontal, drop dominated flow, and the inclined, ridge-type flow. For even when the surface is slightly tilted, and the drops run in one direction and become slightly elongated, one does not observe a significant difference in the heat transfer rate, nor can one say that the interface is ridge-like. However, we can say with some degree of definiteness that at 1^{o} the surface is still drop-like, while at 4^{o}, the disturbances must be called ridges rather than drops.

The remaining three regimes are mapped in Figure 15 for angles of $2\ 3/4^{o}$, 5^{o}, and $7\ 1/2^{o}$. It is seen that in all cases the transition points move downstream with increasing angle and decreasing heat flux.

2.7 Non-Condensable Gases

In all investigations of this type, the question arises as to whether the tests were free of the effects of non-condensable gases. Rather elaborate precautions are always necessary to rid a system of these detrimental effects. As was mentioned in the section on experimental procedures, care was always taken to see that the Freon-air interface was kept in the secondary condenser, so that the primary reflux condenser would contain only pure Freon plus traces of non-condensables in the process of being removed from the system. In this manner, the condensate returning to the test chamber would be kept free of any dissolved gases. The effectiveness of this system was checked by allowing the

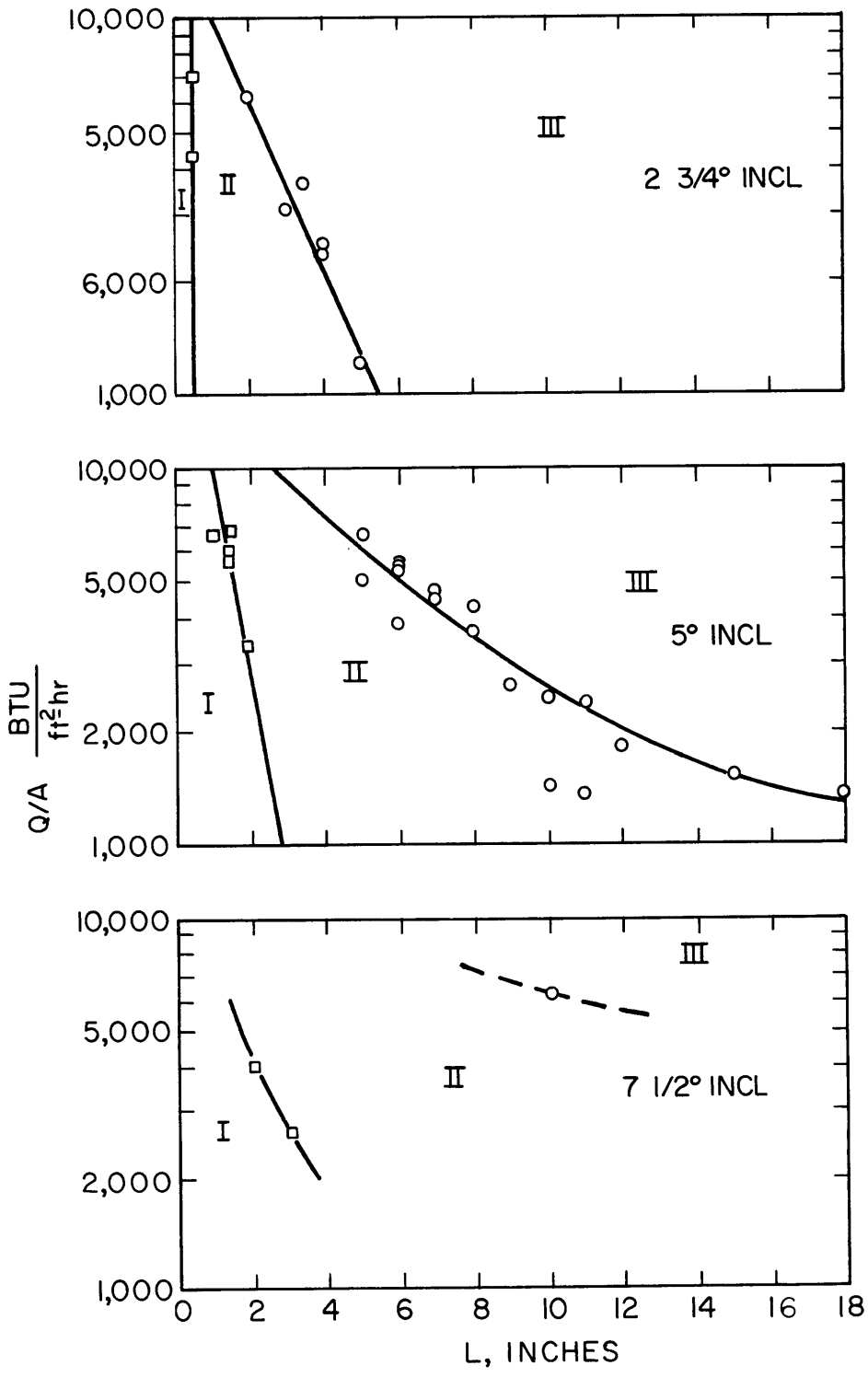

FIGURE 15. FLOW REGIME VERSUS HEAT TRANSFER RATE, I: WAVELESS FLOW; II: DEVELOPING FLOW; III: FULLY DEVELOPED RIDGE FLOW.

Freon-air interface to retreat from the secondary condenser to the primary, thus allowing the possibility of dissolved air entering the test chamber via the returning condensate. There was an almost immediate effect on the condensation on the test surface. If the surface was horizontal, patches of film which had previously been covered with drops became drop-free. Instead, the patches would have a random, ripply motion at the interface. There was also a considerable decrease in heat transfer rate.

The reason for the above behavior can be explained as follows. Because of the bulk motion of vapor towards the interface, a concentration gradient of the non-condensable gas is set up with a maximum concentration at the interface. The concentration at the interface is highest where the local heat transfer rate is highest, i. e. where the condensate film is thinnest. If we perturb the film at a point so that it starts to grow in thickness, the heat transfer rate, hence the concentration, will diminish at that point. Since the concentration is in direct proportion to the partial pressure and the total pressure remains constant, the partial pressure of the condensing vapor will increase, as will the saturation temperature. The rise in temperature of the interface will result in a lowering of the surface tension. The resulting surface tension gradient gives rise to a flow of condensate away from the point under consideration, thus diminishing the rate of growth of the

perturbation. In this respect, it is seen that non-condensables have a stabilizing effect on the interface [19].

Because of the drastic difference in the appearance of the interface in the presence of non-condensable gases, we feel quite certain that the results presented in this work are free of the effects of non-condensable gases.

CHAPTER III

ANALYTICAL PROGRAM

3.1 General Approach

As the phenomenon under consideration is fundamentally an instability, a logical approach might be an examination of the changes brought about when an initially unperturbed, laminar flow becomes unstable. The normal procedure in this case has been to linearize the equations of motion about the unperturbed state and from the resulting equations, determine the characteristics of the new flow. Certain information, such as the wavelength, wave velocity, etc., is then used to provide quantitative information for the formulation of an idealized model of the ultimate stages of the instability. Such a procedure has been used successfully for phenomena in which the perturbations maintain their form as they grow. An example is film boiling, where the arrangement of vapor bubbles at the liquid-vapor interface is quite similar to the wave pattern predicted by the Taylor Instability analysis, and the wavelength suggested by the analysis correlates quite well with bubble size. This situation is in contrast with the subject of this study, as is illustrated by Figure 14. A first order, linearized analysis such as Brooke Benjamin's correctly predicts the shallow, transversely oriented waves that appear near the leading edge of the inclined surface. However, these shallow waves undergo drastic changes as they move down the surface. The transverse wave crests themselves become wavelike, until a region is reached in which the wave crests are now oriented in the longitudinal direction. The prediction of these non-

linear effects would require the inclusion of higher order terms in the perturbation analysis, and the added difficulty of a three-dimensional, as opposed to two-dimensional analysis. The solution to such a problem has yet to be attempted. It is clear that the previously applied procedures would have poor results in predicting heat transfer rates for the phenomena that we are considering.

We shall show that, if the ultimate state of the instability is non-chaotic, there is an approach that eliminates the necessity of a stability analysis. Whereas previous procedures required the formulation of an idealized model of the shape of the interface and the empirical evaluation of certain geometric variables, the proposed analysis yields the shape of the interface as one of its results. Furthermore, the only geometric condition that must be prescribed is one which indicates the mean amplitude of the interfacial waves.

The main aspect of the phenomena under consideration that suggests that a stability analysis might be unnecessary is that, until the rupturing of the interface, all the instabilities at small angles of inclination are bounded. None of the amplitudes of the drops or of the ridges are greater than about one half of the wavelength. Also, the photographs show that all of the drops or ridges have about the same amplitude. This suggests that an equilibrium-type analysis might be sufficient to describe the interface. In this case, all but one of the necessary boundary conditions can be obtained from symmetry consider-

ations. The remaining boundary condition would be the value of the average maximum film thickness. Thus, the information necessary for the prediction of the heat transfer rate can be obtained from an experimental observation of the type of symmetry of the waves. As this information need be only of a qualitative nature, a stability analysis is unnecessary.

There are several advantages to the above approach. Unlike previous techniques, the only geometrical assumption is that of the value of the maximum film thickness. It will be shown that the final result is extremely insensitive to the exact value of this thickness. In addition to determining the shape of the interface, the analysis yields the wavelength of the disturbances and the non-linear relationship between the film thickness and the wavelength.

It should be emphasized that the elimination of the stability analysis is not without penalty. With a stability analysis, one could predict the type of symmetry of the interface. Without a stability analysis, one must obtain this information from experimental observation.

3.2 Inclined Surfaces

In this section we shall analyze the wave state that exists on the underside of slightly inclined surfaces and shall restrict ourselves to the so-called "fully developed state" which occurs after the drops have

begun to fall from the crests of the ridges. In order to make the equations independent of time, we neglect the presence of moving drops on the crests of the ridges and replace their function of condensate removal by the artifice of a plane sink located along the center-line of the ridges (See Figure 16). It will be shown that, in the region of the thin film, momentum fluxes are negligible when compared to viscous stresses, the flow in the y-direction (downstream) is small compared to the flow in the x-direction (transverse), and that in the region of thicker film where there is considerable downstream flow, the film thickness is fixed by a balance of surface and gravity forces, hence is unaffected by the flow. We furthermore make the assumption that the pressure in the film is hydrostatic, and that the heat transfer in the thin film is by conduction only.

Under the above conditions, the governing equations are (See Appendix D for a detailed derivation):

Momentum: (3-1)

$$\frac{\partial p}{\partial x} = \mu \frac{\partial^2 V_x}{\partial z^2}$$

$$\frac{\partial p}{\partial y} = \mu \frac{\partial^2 V_y}{\partial z^2} + \rho g \sin\theta$$

Pressure: (3-2)

$$p = p_{SAT} - (\rho - \rho_v) g \cos\theta (\delta - z) - \sigma \frac{\partial^2 \delta}{\partial x^2}$$

Continuity: (3-3)

$$\frac{\partial V_x}{\partial x} + \frac{\partial V_y}{\partial y} + \frac{\partial V_z}{\partial z} = 0$$

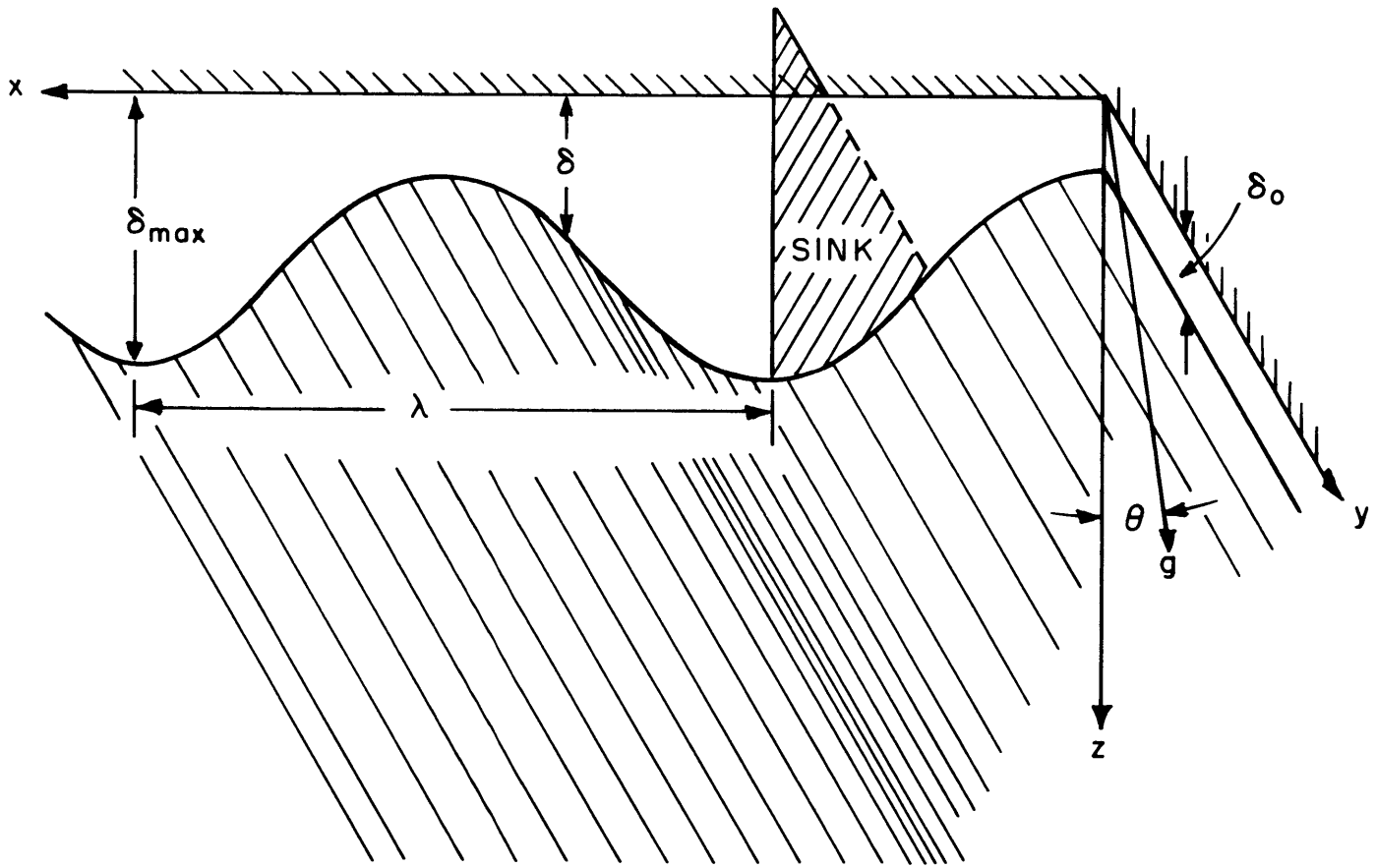

FIGURE 16. RIDGE MODEL

Conduction: $$\frac{Q}{A} = \frac{K\Delta T}{\delta} \qquad (3\text{-}4)$$

By differentiating equation (3-2) and substituting into (3-1) we get

$$-(\rho-\rho_v)g\cos\theta\frac{\partial\delta}{\partial x} - \sigma\frac{\partial^3\delta}{\partial x^3} = \mu\frac{\partial^2 V_x}{\partial z^2}$$

$$-(\rho-\rho_v)g\cos\theta\frac{\partial\delta}{\partial y} - \sigma\frac{\partial^3\delta}{\partial x^2\partial y} = \mu\frac{\partial^2 V_y}{\partial z^2} + \rho g\sin\theta \qquad (3\text{-}5)$$

If $\frac{\partial\delta}{\partial y} << \tan\theta$, and if we neglect the effect of curvature in the y-direction, then the left hand side of the y-direction momentum equation may be neglected compared to the gravity term. Equation (3-5) may now be integrated over the film thickness using the boundary conditions of zero velocity at the wall and zero shear at the interface, to obtain

$$V_x = \frac{\delta^2}{2\mu}\left[(\rho-\rho_v)g\cos\theta\frac{\partial\delta}{\partial x} + \sigma\frac{\partial^3\delta}{\partial x^3}\right]\cdot\left[2\frac{z}{\delta} - \frac{z^2}{\delta^2}\right]$$

$$V_y = \frac{\rho g\sin\theta\,\delta^2}{2\mu}\left[2\frac{z}{\delta} - \frac{z^2}{\delta^2}\right] \qquad (3\text{-}6)$$

By integrating the continuity equation over the film thickness, δ, (3-3), and making use of the relationship between the condensation rate and the velocities at the interface, namely

$$\left[V_x\,d\delta\,dy + V_y\,d\delta\,dx - V_z\,dx\,dy = \frac{Q/A}{\rho h'_{fg}}\,dx\,dy\right]_{z=\delta} \qquad (3\text{-}7)$$

we arrive at

$$\frac{\partial}{\partial x}\int_0^\delta V_x\,dz + \frac{\partial}{\partial y}\int_0^\delta V_y\,dz = \frac{Q/A}{\rho h'_{fg}} \qquad (3\text{-}8)$$

We may now use (3-6) to evaluate the above integrals to get

$$\frac{\partial}{\partial x}\left[\left((\rho-\rho_v)g\cos\theta\frac{\partial\delta}{\partial x}+\sigma\frac{\partial^3\delta}{\partial x^3}\right)\frac{\delta^3}{3\mu}\right]+\frac{\partial}{\partial y}\left[\frac{\rho g\sin\theta\,\delta^3}{3\mu}\right]=\frac{Q/A}{\rho h'_{fg}}=\frac{K\Delta T}{\delta\rho h'_{fg}} \qquad (3\text{-}9)$$

We have retained the y-dependent term up to this point to show that there is no coupling in the momentum equations. However, as this term is of order tan θ compared to the other terms, it will now be dropped. Equation (3-9) can be made dimensionless by defining the following new variables:

$$x' = \frac{x}{\sqrt{\frac{\sigma}{g(\rho-\rho_v)\cos\theta}}} \qquad \delta' = \frac{\delta}{\sqrt{\frac{\sigma}{g(\rho-\rho_v)\cos\theta}}}$$

$$T = K\mu\Delta T/\rho(\rho-\rho_v)g\cos\theta\, h'_{fg}\left(\frac{\sigma}{g(\rho-\rho_v)\cos\theta}\right)^{3/2} \qquad (3\text{-}10)$$

The lengths also could have been made dimensionless by division by $\sqrt[3]{\frac{\mu^2}{\rho(\rho-\rho_v)g\cos\theta}}$ or by $\frac{K\mu\Delta T}{\sigma\rho h'_{fg}}$. Thus in (3-10) we are implying that the characteristic dimension is determined by the ratio, $\frac{\sigma}{g(\rho-\rho_v)\cos\theta}$, of surface to gravitational forces. Upon substitution of (3-10) into (3-9) and dropping the primes, the equation describing the interface becomes

$$\frac{\delta^4}{3}\frac{\partial^4\delta}{\partial x^4}+\frac{\delta^4}{3}\frac{\partial^2\delta}{\partial x^2}+\delta^3\frac{\partial\delta}{\partial x}\frac{\partial^3\delta}{\partial x^3}+\delta^3\left(\frac{\partial\delta}{\partial x}\right)^2=T \qquad (3\text{-}11)$$

It should be noted that this equation is strictly valid only in the region of thin film. As the film becomes thicker, momentum fluxes

become larger than the viscous stresses. However, it will be shown below that in the region of thick film the shape of the interface is controlled by hydrostatics alone, and both viscous and momentum effects may be neglected.

From the symmetry of the longitudinal ridges, it is easy to deduce the boundary conditions of zero slope and zero third derivative at the point of minimum film thickness. Ordinarily the same conditions would hold at the point of maximum film thickness. However, the plane sink located at the crest of the ridge requires a discontinuity in either the first or third derivatives. It will be seen below that either choice gives essentially the same result. The remaining condition is somewhat more difficult to arrive at. Observation shows that the maximum film thickness is of the order of one half the wavelength, which is as yet undetermined. We shall arbitrarily select the value of the maximum (dimensionless) film thickness to be unity. At this stage of the analysis it is premature to discuss the reasons for this apparently arbitrary choice. In section 3.5, the reasons behind this assumption are explained. The four boundary conditions necessary to complete the solution of (3-11) are

$$\text{at } x=0: \quad \frac{\partial \delta}{\partial x} = 0 \qquad \frac{\partial^3 \delta}{\partial x^3} = 0$$

$$\text{at } x=\frac{\lambda}{2}: \quad \frac{\partial \delta}{\partial x} = 0 = \frac{\partial^3 \delta}{\partial x^3} \qquad \delta = 1 \tag{3-12}$$

An attempt was made to solve equation (3-11) by a finite difference

Since λ is as yet unknown the condn of zero slope at $\lambda/2$ serves as a def. of $\lambda/2$. Plus although 5 condns appear in Eq 3-12 only 4 are actually B.C. $_{47}$

procedure using relaxation techniques. However, no converging solution could be obtained. To overcome the problem of diverging solutions, it was decided to try to solve the equation as an initial value problem instead of a boundary value problem. To do this, of course, would require two more conditions at x = 0, namely the values of the film thickness and of the curvature. The first of these initial conditions could be obtained by dividing equation (3-11) by δ_o^5, (the dimensionless film thickness at x = 0), which results in the following equation.

$$\frac{\eta^4}{3}\frac{\partial^4\eta}{\partial x^4} + \frac{\eta^4}{3}\frac{\partial^2\eta}{\partial x^2} + \eta^3\frac{\partial\eta}{\partial x}\frac{\partial^3\eta}{\partial x^3} + \eta^3\left(\frac{\partial\eta}{\partial x}\right)^2 = \frac{T}{\delta_o^5} \qquad (3\text{-}13)$$

$$\eta = \delta/\delta_o$$

After the solution had been obtained, the value of δ_o could be found from the relation

$$\eta = 1/\delta_o \quad \text{at} \quad x = \lambda/2 \qquad (3\text{-}14)$$

The condition on the curvature at x = 0 could be found by guessing a value at x = 0 and adjusting this value until the actual boundary conditions at x = $\lambda/2$ were satisfied. As it turned out, the solution was insensitive to the choice of the value of the curvature. A change in curvature by a factor of one hundred affected the results by less than 0.001%. The reason for this is that the dominant term in the equation

at x = 0 is the one containing the fourth derivative. Regardless of the value chosen for the second derivative at x = 0, it very rapidly changes to reflect the value of the fourth derivative. The value actually used at x = 0 was $\frac{\partial^2 \eta}{\partial x^2} = 0.000001$*. Thus the new initial conditions were

at x = 0

$$\eta = 1.0$$

$$\frac{\partial \eta}{\partial x} = 0$$

$$\frac{\partial^2 \eta}{\partial x^2} = 0.000001 \qquad (3\text{-}15)$$

$$\frac{\partial^3 \eta}{\partial x^3} = 0$$

The equation was solved at the Computation Center at M. I. T. using the AIDE program which integrates non-linear ordinary differential equations. Solutions were obtained for values of T/δ_0^5 ranging from 200 to 6400. While solving the equation, the program also calculated the average reciprocal film thickness defined as

$$Nu \equiv \frac{h}{k}\sqrt{\frac{\sigma}{g(\rho-\rho_v)\cos\theta}} \qquad (3\text{-}16)$$

$$= \frac{2(\eta)_{x=\lambda/2}}{\lambda}\int_0^{\lambda/2}\frac{dx}{\eta}$$

---

* This value was used to fix x = 0 in the trough of the ridge rather than at the crest. It should be emphasized that the reformulation of the problem as an initial value problem is a computational technique and does not reflect any change in the nature of the problem being solved. For finite δ the condition that $\partial^3\eta/\partial x^3 = 0$ at $\lambda/2$ cannot be satisfied exactly. By reformulating the problem as an initial value problem with initial conditions given in Eq 3-15 the 3rd derivative is found to be extremely small at $x = \lambda/2$

The computer results may be summarized as follows:

T/δ_o^5	$\lambda/2$	$(\eta)_{x=\lambda/2}$	Nu	T
200	3.40	73.66	12.62	9.21×10^{-8}
400	3.375	103.7	15.01	3.34×10^{-8}
800	3.336	146.2	17.95	1.20×10^{-8}
1600	3.305	206.4	21.45	4.32×10^{-9}
3200	3.279	291.0	25.45	1.54×10^{-9}
6400	3.255	410.0	30.25	5.51×10^{-10}

As a first approximation, the relationship between Nu and T may be given as

$$\mathrm{Nu} = 0.822 \ (T)^{-0.169} \qquad (3\text{-}17)$$

From this expression and from the definition of the Nusselt number in equation (3-16) it can be shown that an error in the assigned value of δ_{max} (the maximum film thickness), of 100% results in an error of only 11% in the prediction of the heat transfer coefficient. Thus it is felt that the assumption that the maximum dimensionless film thickness is of the order unity (fourth boundary condition in equation (3-12)) introduces an uncertainty which is within the accuracy obtainable from an

analysis of this type.

As will be seen in the next chapter, a more definite knowledge of the value of the maximum film thickness could result in a much closer agreement between the theoretical and experimental results. However, as we have modeled the interface as a system of uniform ridges, while in reality the amplitude of a ridge varies periodically in time and space, to be more definite in fixing the value of the maximum film thickness, (perhaps at a value which would enhance the agreement between theory and experiment) would be highly imprudent unless there were a theoretical basis for determining the actual average maximum film thickness. This entire problem could be avoided if, instead of treating the system as being in a steady state, the transient nature were taken into account. Unfortunately, such a treatment would require knowledge of the initial state of the system, i. e. the condition of the interface immediately after a drop has fallen from the crest of a ridge. The determination of this state would bring us back to the very problem we are trying to avoid, that of determining the non-linear behavior of an unstable system.

3. 2. 1 Linearized Solutions

One can gain some insight into the form of an analytical solution of equation (3-11) by considering the similar problem of a static ridge, i. e. a ridge on the underside of a horizontal surface with no condensation

taking place. This corresponds to the limiting case of the ridge model at zero inclination and zero heat transfer rate (or zero temperature difference). In this case the governing equation is simply

$$\frac{dp}{dx} = 0 \tag{3-18}$$

where $p = p_{SAT} - g(\rho - \rho_v)(\delta - z) - \sigma \frac{d^2\delta}{dx^2}$

which may be integrated to give

$$\delta = A \cos\left(\frac{x}{\sqrt{\frac{\sigma}{g(\rho-\rho_v)}}}\right) + B \sin\left(\frac{x}{\sqrt{\frac{\sigma}{g(\rho-\rho_v)}}}\right) + C \tag{3-19}$$

Applying the boundary conditions of zero thickness and zero slope at x = 0, and zero slope at $x = \frac{\lambda}{2}$, we find that

$$\delta = A\left(1 - \cos\left(x/\sqrt{\frac{\sigma}{g(\rho-\rho_v)}}\right)\right)$$

$$\frac{\lambda}{2} = \pi\sqrt{\frac{\sigma}{g(\rho-\rho_v)}} \tag{3-20}$$

where the constant A determines the volume of the ridge. Solving for the pressure at the wall, z = 0, we find

$$p_{WALL} - p_{SAT} = -A\, g(\rho - \rho_v) \tag{3-21}$$

$$= -\frac{g(\rho-\rho_v)\delta_{max}}{2}$$

Thus, if we were to join such a ridge to a region of film with zero curvature, i. e. a region of film essentially at saturation pressure, the resulting pressure difference would cause a flow into the ridge. This is the basic mechanism of the condensation phenomenon. If we now assume that equation (3-20) is a solution to equation (3-11) we see that the terms on the left hand side of (3-11) are several orders of magnitude larger than the right hand term in the region of thick film. If the right hand side is equated to zero, (3-20)(and (3-19))is indeed an exact solution to (3-11) and satisfies the boundary conditions (3-12) at $x = \lambda/2$. If this solution can be joined to a solution which is valid in the thin film region and which satisfies the boundary conditions at $x = 0$, then the resulting expression might be a good representation of the shape of the interface.

3.2.2 Linearized Thin-Film Equations

In the preceding section we have shown that equation (3-20) satisfies equation (3-11) in the region of thick film. As equation (3-19) expresses a balance of surface and gravitational forces, this means that, in the thick film, the viscous stresses must be negligible compared to surface and gravitational forces. By definition, in the thin film region the viscous stresses are dominant. Therefore, to effect a complete solution, the viscous terms must be taken into account by joining the interface as described by equation (3-19) to a region of the

interface dominated by viscous stresses, that is, a "thin film" region.

Referring to the conditions (3-15), we see that, at the point of minimum film thickness, the slope of the interface is zero. Thus it is reasonable to expect that a linearization of the film thickness about a constant value should be valid about the point of minimum film thickness.

If η is expressed as

$$\eta = 1 + \psi \tag{3-22}$$

equation (3-13) may be linearized by retaining only terms which are of first order in ψ, to give the following equation

$$\frac{\partial^4 \psi}{\partial x^4} + \frac{\partial^2 \psi}{\partial x^2} = 3T/\delta_0^5 \tag{3-23}$$

This equation has the solution

$$\psi = A \sin x + B \cos x + \frac{3T x^2}{2\delta_0^5} + Cx + D \tag{3-24}$$

If we now apply the initial conditions

at x = 0

$$\psi = 0$$

$$\frac{\partial \psi}{\partial x} = 0 \tag{3-25}$$

$$\frac{\partial^2 \psi}{\partial x^2} = 0$$

$$\frac{\partial^3 \psi}{\partial x^3} = 0$$

we obtain the solution

$$\psi = \frac{3T}{\delta_0^5}\left(\cos x + \frac{x^2}{2} - 1\right) \simeq \frac{T}{\delta_0^5}\cdot\frac{x^4}{8} \qquad (3\text{-}26)$$

The complete solution may be obtained by solving the following set of equations:

$$\psi = \frac{T}{\delta_0^5}\cdot\frac{x^4}{8} \qquad x \le \epsilon \qquad (3\text{-}27a)$$

$$\psi = A\left(1 - \cos(x-\phi)\right) + C \qquad x \ge \epsilon \qquad (3\text{-}27b)$$

$$\left.\begin{aligned}\psi = \frac{T}{\delta_0^5}\cdot\frac{\epsilon^4}{8} &= A\left(1-\cos(\epsilon-\phi)\right)+C\\ &= \beta\end{aligned}\right\} \quad x = \epsilon \qquad (3\text{-}27c)$$

$$\frac{d\psi}{dx} = \frac{T}{\delta_0^5}\cdot\frac{\epsilon^3}{2} = A\sin(\epsilon-\phi) \qquad x = \epsilon \qquad (3\text{-}27d)$$

$$\frac{d^2\psi}{dx^2} = \frac{T}{\delta_0^5}\cdot\frac{3\epsilon^2}{2} = A\cos(\epsilon-\phi) \qquad x = \epsilon \qquad (3\text{-}27e)$$

Here equation (3-19) has been put into dimensionless form and modified to allow for a shift of the origin. The solution of equation (3-27) requires the determination of the four quantities, A, ϕ, C and ϵ. Ordinarily, this would be done by solving (3-27c, d and e) and an equation matching the third derivative of the two expressions at $x = \epsilon$. This procedure leads to imaginary solutions. Evidently the linearization is not

exact enough to satisfy such a high order derivative. This complication was circumvented by fixing the value of β at which the two solutions are joined. It was found that a value of $\beta = 10/27$ gave the best results when compared to the computer solution. Solution of (3-27) gives the following result, which is compared to the more exact solution from the computer in Figure 17.

$$\epsilon = \left(\frac{80\,\delta_0^5}{27\,T}\right)^{1/4} \qquad \phi = \frac{2\epsilon}{3} \qquad c = \frac{10}{\delta_1}$$

$$A = \left(\frac{20\,T}{3\,\delta_0^5}\right)^{1/2} \qquad \lambda = 2\pi + \frac{4\epsilon}{3} \qquad (3\text{-}28)$$

With these results it is now possible to be more definite in the classification of "thick" and "thin" films. As the difference between thick and thin films is the relative importance of viscous stresses, and this difference is represented by equations (3-27 a and b), it is obvious that ϵ is the dividing point between the two regions. Note, however, that ϵ is not proportional to $T^{-1/4}$, but because of the dependence of δ_0 on T, ϵ is proportional to $T^{1/6}$. Thus, in the limit as T goes to zero, ϵ goes to zero, and the film thickness is given by equation (3-20).

Using the relationship (3-14) and the above equations, equation (3-16) may be integrated to yield

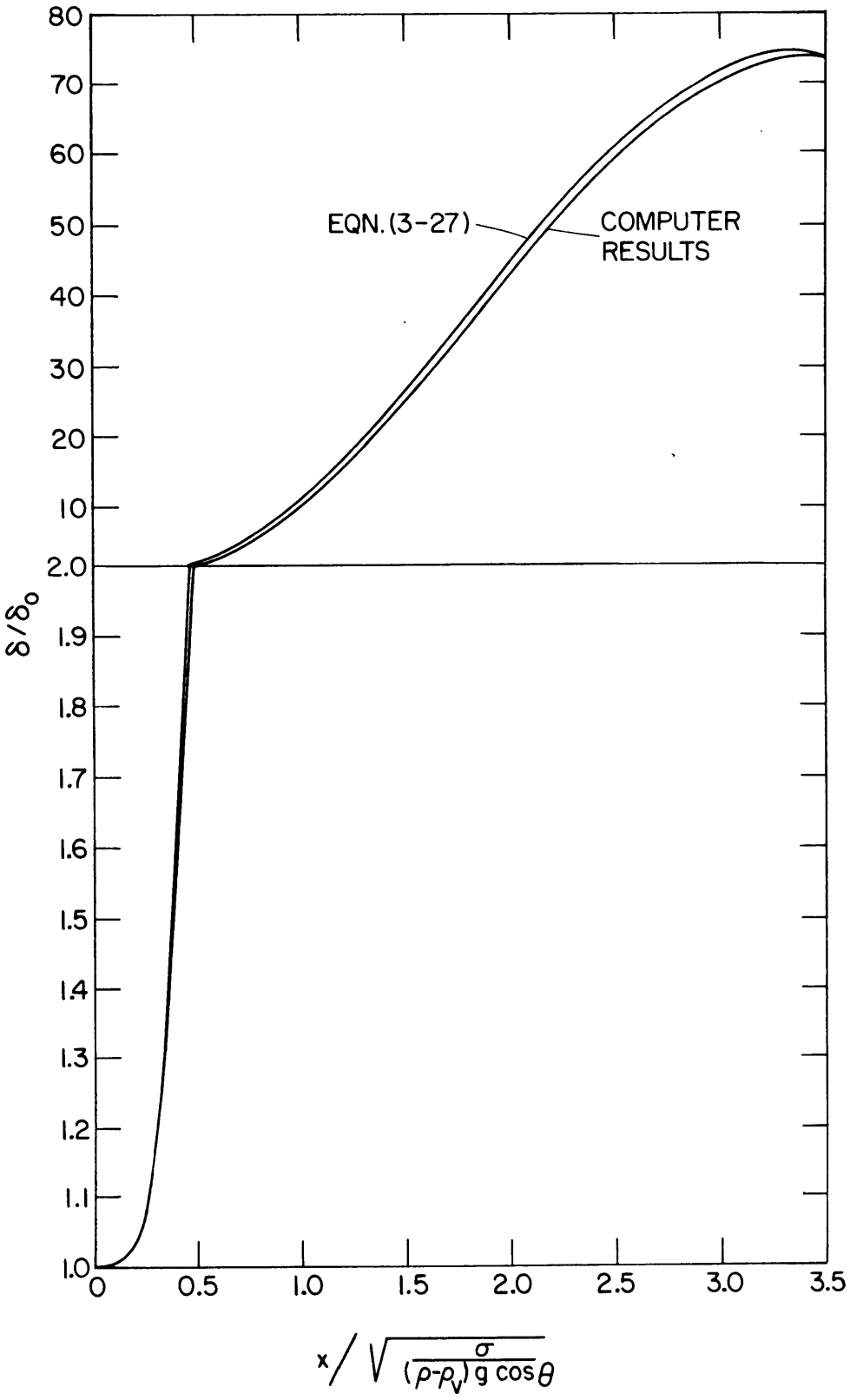

FIGURE 17. RIDGE PROFILE AT $T/\delta_0^5 = 200$

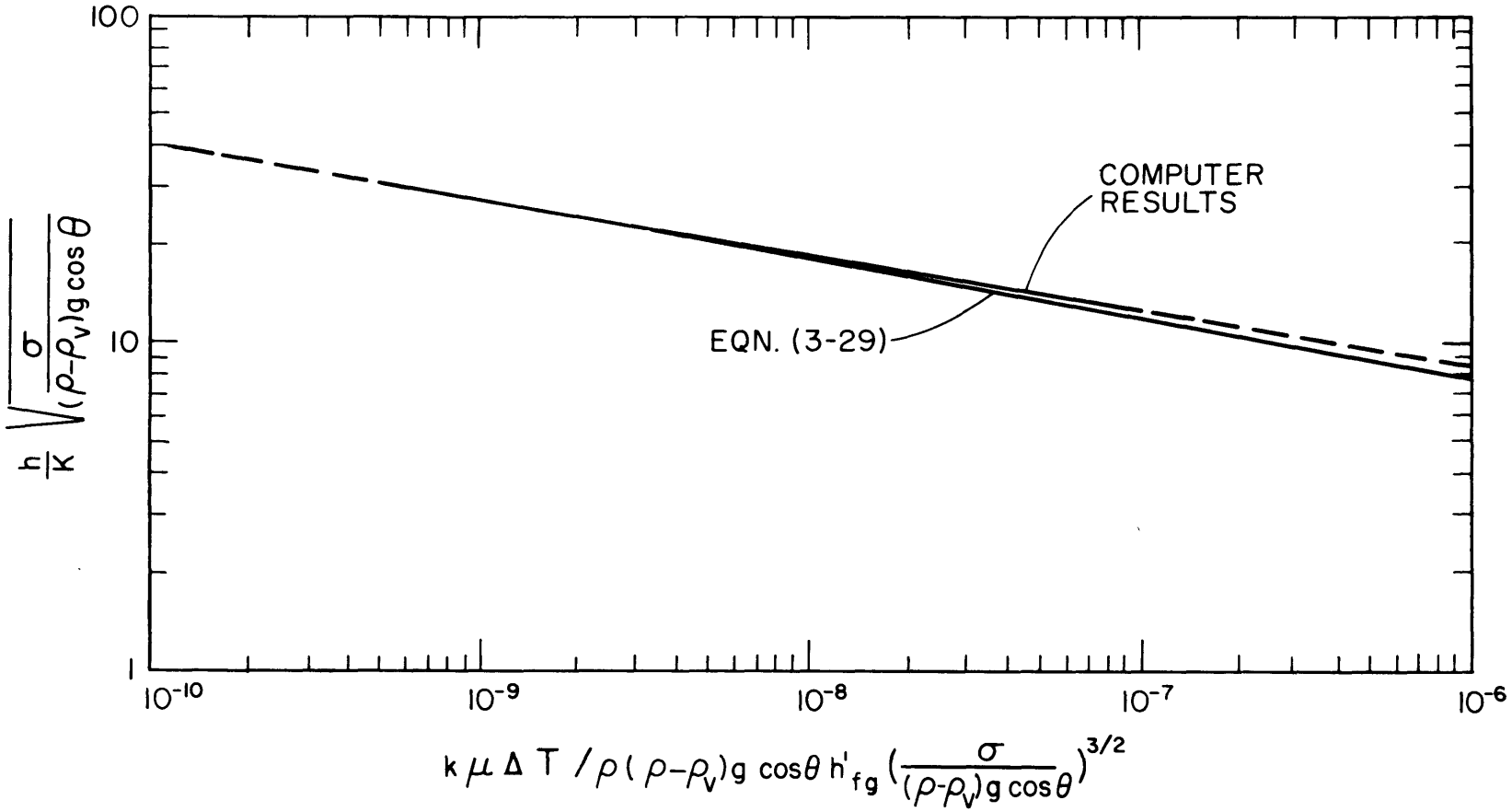

FIGURE 18. HEAT TRANSFER COEFFICIENT AS A FUNCTION OF TEMPERATURE DIFFERENCE FOR RIDGE MODEL

$$Nu = \frac{0.90\, T^{-1/6}}{1 + 1.1\, T^{1/6}} \qquad (3\text{-}29)$$

This equation is plotted in Figure 18 along with the results from the computer.

3.3 Horizontal Surfaces

The basic difference between the ridge state and state of the interface on the underside of inclined surfaces is that the former state is characterized by a parallel flow, whereas the latter exhibits an essentially radial flow into the pendent drops. In the analysis below we have neglected the transient nature of the drops. In order to satisfy continuity requirements, we have once again used the artifice of a line sink located at the center of the drop (See Figure 19). The assumptions made are basically the same as were made for the ridge model, the only real difference between the two analyses being the difference between line and cylindrical symmetry.

The equations governing the motion are:

$$\frac{\partial p}{\partial r} = \mu \frac{\partial^2 V_r}{\partial z^2} \qquad (3\text{-}30)$$

$$p = p_{SAT} - g(\rho - \rho_v)(\delta - z) - \sigma\left(\frac{\partial^2 \delta}{\partial r^2} + \frac{1}{r}\frac{\partial \delta}{\partial r}\right) \qquad (3\text{-}31)$$

$$\frac{\partial V_r}{\partial r} + \frac{V_r}{r} + \frac{\partial V_z}{\partial z} = 0 \qquad (3\text{-}32)$$

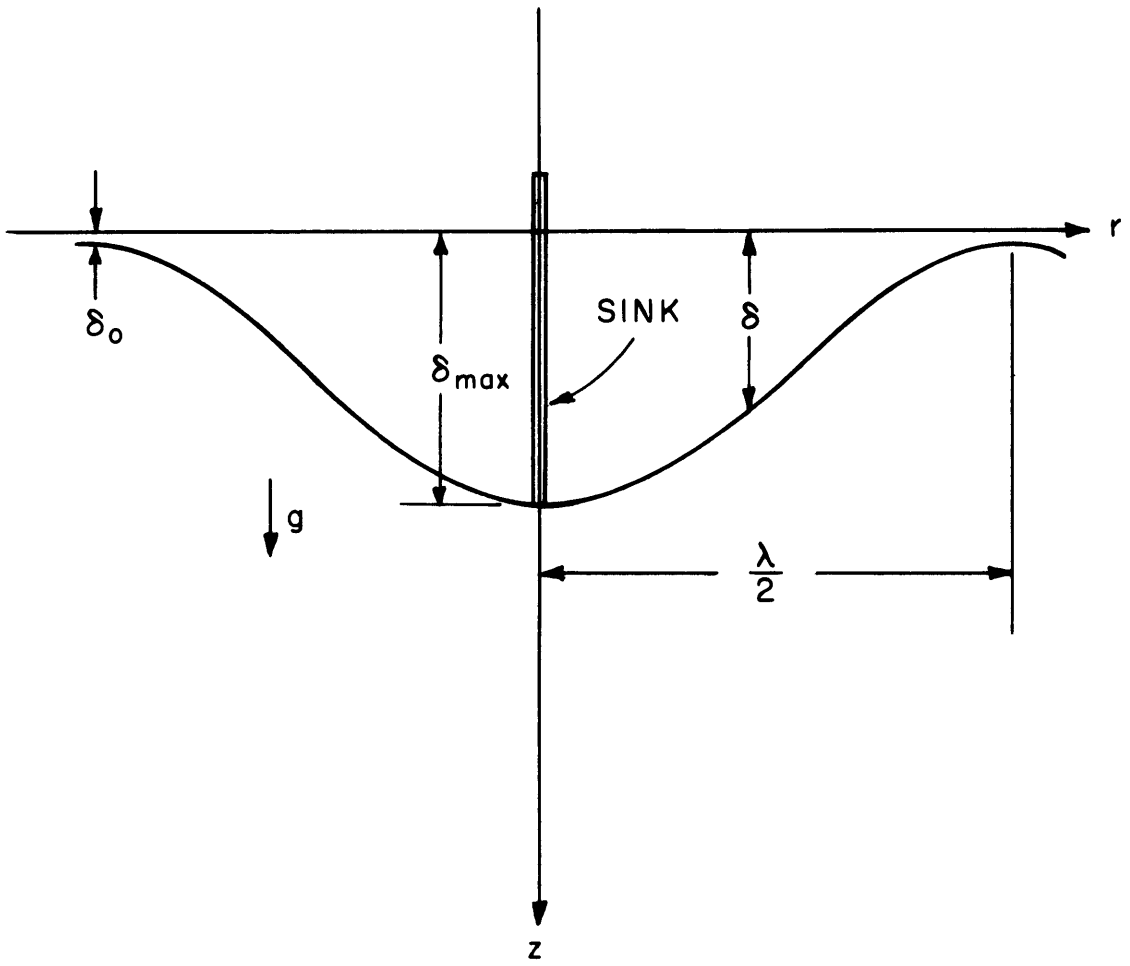

FIGURE 19. DROP MODEL

$$\frac{Q}{A} = \frac{K\Delta T}{\delta} \tag{3-33}$$

Following the same methods as were used in Section 3.2, these equations are used to determine the following equation describing the interface of the film:*

$$\eta^4 \frac{\partial^4 \eta}{\partial r^4} + \eta^4 \frac{\partial^2 \eta}{\partial r^2} + 3\eta^3 \frac{\partial \eta}{\partial r} \frac{\partial^3 \eta}{\partial r^3} + 3\eta^3 \left(\frac{\partial \eta}{\partial r}\right)^2 + \frac{\eta^4}{r} \frac{\partial \eta}{\partial r}$$

$$+ \frac{2\eta^4}{r} \frac{\partial^3 \eta}{\partial r^3} + \frac{3\eta^3}{r} \frac{\partial \eta}{\partial r} \frac{\partial^2 \eta}{\partial r^2} - \frac{\eta^4}{r^2} \frac{\partial^2 \eta}{\partial r^2} - \frac{3\eta^3}{r^2} \left(\frac{\partial \eta}{\partial r}\right)^2 + \frac{\eta^4}{r^3} \frac{\partial \eta}{\partial r} = \frac{3\Gamma}{\delta_0^5} \tag{3-34}$$

The initial conditions needed to integrate this equation are:

at $r = \frac{\lambda}{2}$

$$\eta = 1$$

$$\frac{\partial \eta}{\partial r} = 0$$

$$\frac{\partial^2 \eta}{\partial r^2} = 0.000001 \tag{3-35}$$

$$\frac{\partial^3 \eta}{\partial r^3} = 0$$

As, in this equation the radius appears explicitly, the value of the wavelength is needed in order to apply the initial conditions. This

---

*This equation has been made dimensionless according to equations (3-10) and (3-13).

problem was circumvented by guessing a value of the wavelength, integrating (3-40), and retaining only those wavelengths which give zero slope at or near r = 0. The integration could not be carried out all the way to r = 0 since the left hand side of (3-34) becomes infinite at that point. This is because the pretense of the line sink at r = 0 requires either infinite film thickness or infinite velocity at r = 0. However, a very short distance away from the origin, the velocities are extremely small, and the shape of the interface is controlled solely by the balance of surface and gravity forces. Equation (3-34) was integrated on the computer and the results of the integration are summarized below.

$\lambda/2$	R^*	$3T/\delta_0^5$	$(\eta)_{r=R^*}$	Nu	T
4.0	0.2	7812.5	449.6	62.4	1.43×10^{-10}
4.05	--	1562.5	206.4	41.3	1.40×10^{-9}
4.05	0.3	7812.5	435.6	59.8	1.68×10^{-10}
4.1	0.3	1562.5	198.6	39.3	1.69×10^{-9}
4.15	--	312.5	94.0	26.4	1.42×10^{-8}
4.2	0.3	312.5	90.0	25.1	1.76×10^{-8}
4.3	--	62.5	43.2	16.5	1.38×10^{-7}

In the table above, R^* refers to the radius at which the interface has zero slope. The Nusselt number was calculated according to the formula

$$Nu = \frac{4(\eta)_{r=R^*}}{\pi \lambda^2} \int_0^{\lambda/2} \frac{2\pi r\, dr}{\eta} \qquad (3\text{-}36)$$

where it has been assumed that the value of the film thickness at $r = 0$ is equal to $\sqrt{\frac{\sigma}{g(\rho-\rho_v)}}$. A plot of Nusselt number as a function of the dimensionless temperature difference is shown in Figure 20, where it is seen that the relationship can be accurately represented by

$$Nu = 0.81\ T^{-0.193} \qquad T < 10^{-8} \tag{3-37a}$$

$$Nu = 0.69\ T^{-0.20} \qquad 10^{-8} < T < 10^{-6} \tag{3-37b}$$

A linearization of equation (3-34) may be carried out using the methods of Section 3. 2. 1 and 3. 2. 2. Using the result of the linearization in equation (3-36) still requires a numerical integration, so that little is gained by this procedure.

3. 4 Maximum Film Thickness

Aside from experimental observation, there is some theoretical justification for the assumption that the maximum film thickness is of the order $\sqrt{\frac{\sigma}{g(\rho-\rho_v)\cos\theta}}$. Bashforth and Adams[20] calculated the exact shapes of sessile and pendent drops. They show that the volume of a stable pendent drop reaches a maximum when $\delta_{max} = 2.24\sqrt{\frac{\sigma}{g(\rho-\rho_v)}}$.

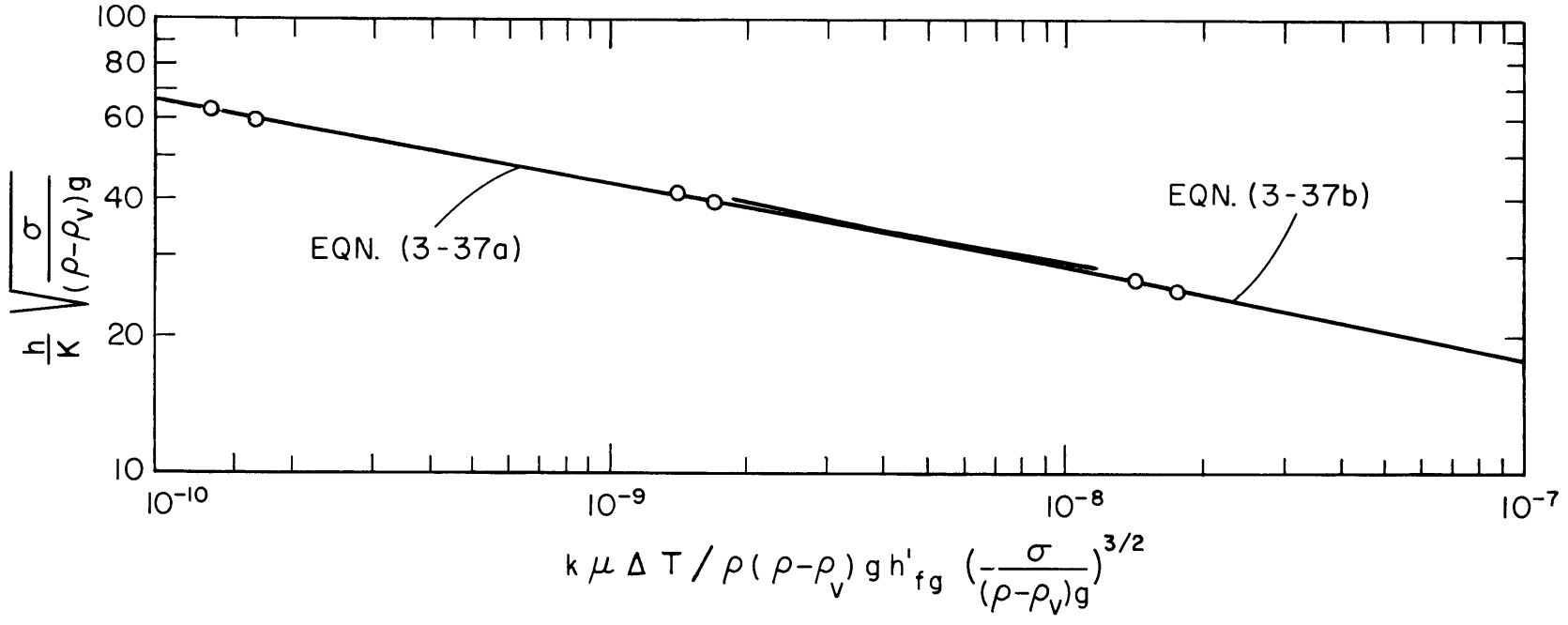

FIGURE 20. HEAT TRANSFER COEFFICIENT AS A FUNCTION OF TEMPERATURE DIFFERENCE FOR DROP MODEL

If we interpret this to mean that a further increase in amplitude (or volume) renders the drop unstable, then the average drop (or ridge) found on the condensing surface will have a height somewhat less than $2.24\sqrt{\frac{\sigma}{g(\rho-\rho_v)\cos\theta}}$. Thus we are somewhat justified in assuming the average maximum film thickness of the ridge and drop model to be of the order $\sqrt{\frac{\sigma}{g(\rho-\rho_v)\cos\theta}}$.

Assuming that the value of the maximum film thickness is unknown, then one can show that the Nusselt number, $h\sqrt{\frac{\sigma}{g(\rho-\rho_v)\cos\theta}}/k$ can be expressed as

$$Nu = C_1\left(\delta_{max}/\sqrt{\frac{\sigma}{g(\rho-\rho_v)\cos\theta}}\right)^{5C_2-1} \cdot T^{-C_2} \qquad (3\text{-}38)$$

Thus, if the assumed value of $\delta_{max}/\sqrt{\frac{\sigma}{g(\rho-\rho_v)\cos\theta}}$ is in error by a factor of M, the predicted value of the Nusselt number will be in error by a factor of $(M)^{5C_2-1}$. For the ridge model, C_2 equals 1/6. Therefore an error of 100% in the value of δ_{max} results in an error of 11.3% in the Nusselt number. Likewise, for the drop model, an error of 100% in the value of δ_{max} results in an error of 0 to 2.5% in the value of the Nusselt number.

Using the expression for the wavelength given in equation (3-28),

one can show that

$$\lambda = 2\pi + 6.88\, T^{1/6} \left(\delta_{max} / \sqrt{\frac{\sigma}{g(\rho-\rho_v)\cos\theta}} \right)^{-5/6} \qquad (3\text{-}39)$$

Therefore if $\delta_{max} / \sqrt{\frac{\sigma}{g(\rho-\rho_v)\cos\theta}}$ is actually equal to 0.5 instead of 1.0, then the value of the wavelength will be in error by 7.6% at $T = 10^{-6}$. For later reference, we note that, at a value of $T = 10^{-7}$, in order for λ to equal 8.72, $\delta_{max} / \sqrt{\frac{\sigma}{g(\rho-\rho_v)\cos\theta}}$ must equal 0.138*.

In regard to the Nusselt number and the wavelength, the examples above illustrate that the uncertainty in the value of the maximum film thickness has little effect.

3.5 Summary

In this section we have formulated two models for flows on the underside of horizontal surfaces and slightly inclined surfaces. The horizontal state is characterized by a radial flow of condensate into pendent drops. For inclined surfaces, only the flows which are charac-

---

*The linearization enabling us to derive equation (3-39) is not strictly valid at this wavelength. However, the orders of magnitude of these quantities is correct.

terized by longitudinal ridges have been analyzed. Furthermore, the analysis applies only for the quasi-fully developed state which occurs after drops have begun to fall from the crests of the ridges. In this state, the flow is predominantly transverse in the troughs of the ridges, while in the crests the direction of flow is downstream.

It should be emphasized that the two-dimensional, linearized analysis of Section 3.2.2 is not meant to be represented as an analysis independent of the computer results. The point at which the two equations describing the interface were joined was chosen so that there would be agreement between the two analyses. This dependence could be eliminated if a third solution to equation (3-13) could be found which is valid in the transition region between the viscous region and the hydrostatic region.

The basic assumptions which were made in all the preceding analyses were as follows:

The flow in the region of the thin film is dominated by viscous stresses and the flow is laminar.

This requires that $\frac{k\Delta T}{\mu h'_{fg}}$ be much less than unity.

The downstream flow may be neglected in comparison to the transverse flow in the region of thin film. This requires

that tan $\theta << 1$, and that the flow is quasi-fully developed.

The shape of the central portion of the ridge or drop is fixed by a balance of surface and gravity forces. As this will be the case if $\delta_{max} \gg \delta_o$, T must be smaller than 10^{-6}.

The maximum film thickness is of the order $\sqrt{\frac{\sigma}{g(\rho-\rho_v)\cos\theta}}$. In the preceding section, this assumption is shown to have but slight effect on the heat transfer results.

CHAPTER IV

DISCUSSION

4.1 Interpretation of Results

Before comparing the experimental results with the different analytical models it will be helpful to examine the manner in which the heat transfer data reflect the presence of the various regimes of flow described in Section 2.6.4. If more than one regime exists on the test surface simultaneously, the total measured heat transfer rate will be a weighted average of the heat transfer rates of the individual regimes. In order to isolate the heat transfer rate in the regime of interest, we must account for the heat transferred in the other regimes. Thus, if L is the total lenght of the test surface, and L_n is the length of the surface occupied by the n^{th} regime

$$(L)(Q/A)_{total} = (L_1)(Q/A)_1 + (L_2)(Q/A)_2 + \ldots + (L_m)(Q/A)_m \qquad (4\text{-}1)$$

It is evident from the photographs of the test surface that in the bulk of the experiments that the measured heat transfer rates are averages including more than one regime. However, we can use the maps of the various regimes in Figure 15 to solve equation (4-1) and

account for this complication. To simplify matters, we shall use a two-regime model having waveless flow from the leading edge to L_1, and fully-developed ridge type flow from L_1 to L. For waveless flow, the Nusselt theory predicts[21]

$$\frac{(Q/A)_\theta}{(Q/A)_{VERTICAL}} = \left[\frac{L \sin\theta}{L_1}\right]^{1/4} \qquad (4\text{-}2)$$

This equation is not valid as sin θ approaches zero, however, its use at small angles of inclination is sufficient for our purposes. Equation (4-2) is plotted versus angle of inclination in Figure 21 as curve CD. Here the length L_1 equals L as there is no ridge type flow. On curve FC, L_1 is less than L. Using equation (3-17) to determine the heat transfer rate in the ridge type flow, the heat transfer rate from L_1 to L is

$$\frac{Q}{A} = 0.822\left[\frac{k\mu\Delta T\left(\sqrt{\frac{g(\rho-\rho_v)\cos\theta}{\sigma}}\right)^3}{\rho(\rho-\rho_v)g\cos\theta\, h'_{fg}}\right]^{-.169}\left[\frac{K\Delta T}{\sqrt{\frac{\sigma}{g(\rho-\rho_v)\cos\theta}}}\right] \qquad (4\text{-}3)$$

If the two heat transfer rates, weighted by their respective lengths, are summed, the resultant curve is EBCD. At point B, the wave state changes from a ridge type flow to one which is more aptly described as a flow of individual drops. Assuming a smooth transition

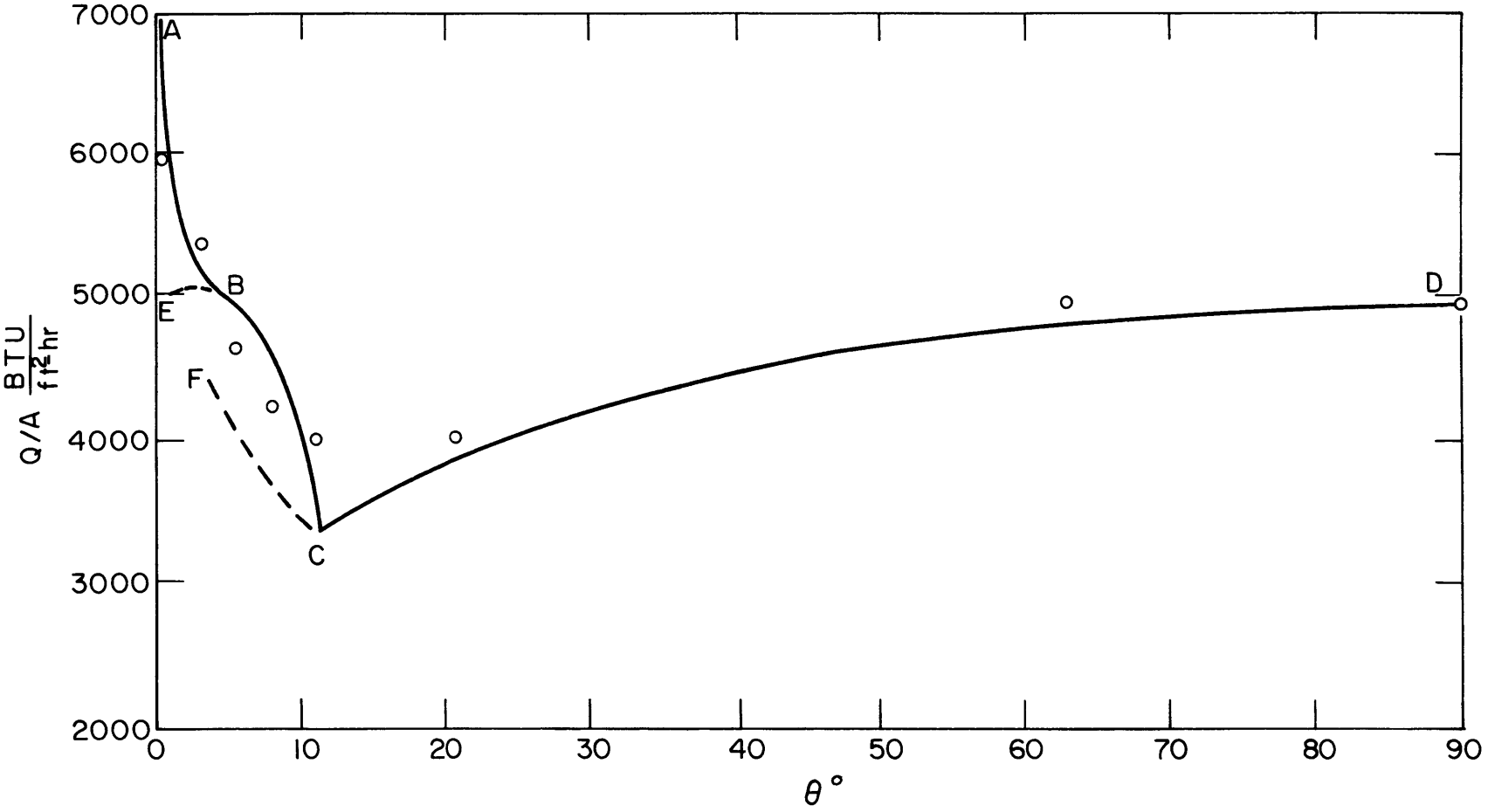

FIGURE 21. HEAT TRANSFER RATE AS A FUNCTION OF ANGLE AT A TEMPERATURE DIFFERENCE OF 40° F

from the ridge to the drop model, the actual curve should follow ABCD. In determining this curve, L_1 was taken to be one half the actual distance to the point at which drops first fall from the crests of the ridges. This assumption neglects the existence of the transition region between the smooth, waveless flow and the fully developed ridge state. One result of this assumption is that a discontinuity in slope occurs at the minimum point C, while there should actually be smooth curve at the minimum.

Due to the approximate nature of the above treatment, it is not expected that it will yield exact agreement with the experimental results. The several data points in Figure 21 show that, although the agreement is not exact, the data follow the trend of the curve ABCD and do not exhibit severe deviations from it.

Figure 21 illustrates several important points concerning the interpretation of the results. Although the analysis indicates that, at small angles of inclination, the heat transfer rate should be almost independent of angle, (proportional to $(\cos \theta)^{5/12}$) due to the transition from the drop to the ridge type flow and due to the effects of the undeveloped length, no region of constant heat transfer rate will be observed as the angle of inclination is varied. Secondly, between the angles of

20 to 90 degrees, the apparently naive assumption that the heat transfer rate varies as $((\sin \theta)/L)^{1/4}$ appears to be an excellent approximation. This would suggest that the effects of interfacial waves in the undeveloped region of flow are about the same for moderately inclined surfaces as for vertical surfaces.

4.2 Inclined Surfaces

The data for surfaces inclined at angles of 2 3/4 and 5 degrees are compared with equation (3-29) in Figure 22. No correction has been made for the undeveloped length. In reducing the data to the form of (3-29) all fluid properties were evaluated at the film temperature, $T_{wall} + \Delta T/2$, except for the surface tension and h'_{fg} which were evaluated at the saturation temperature.

Although at these angles the flow is not fully developed over the entire length of the test surface, Figure 21 indicates that the effects of the undeveloped region are small. As in Figure 21, the heat transfer rates at 2 3/4 degrees are seen to be consistently higher than those at 5 degrees. Overall, it is seen that the data agree with the theory to within an error of less than 10%.

One area of disagreement between the theory and the experiment lies in the wavelength of the ridges. The theory predicts a wavelength of about 0.275 inches. The measurements indicate a wavelength of 0.353 inches and sometimes 0.333 inches, about 21 to 28% higher.

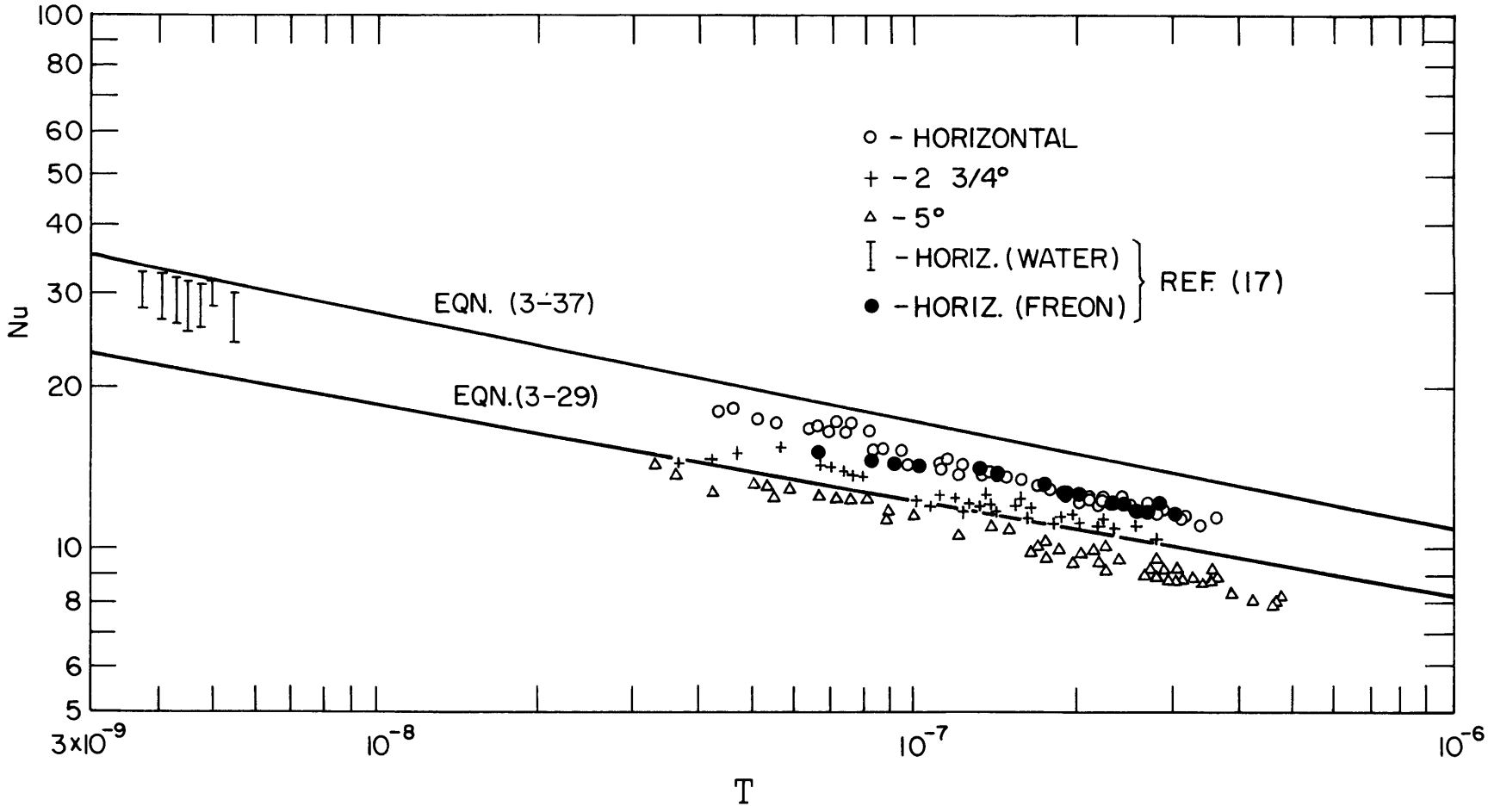

FIGURE 22. COMPARISON OF DATA WITH THEORY

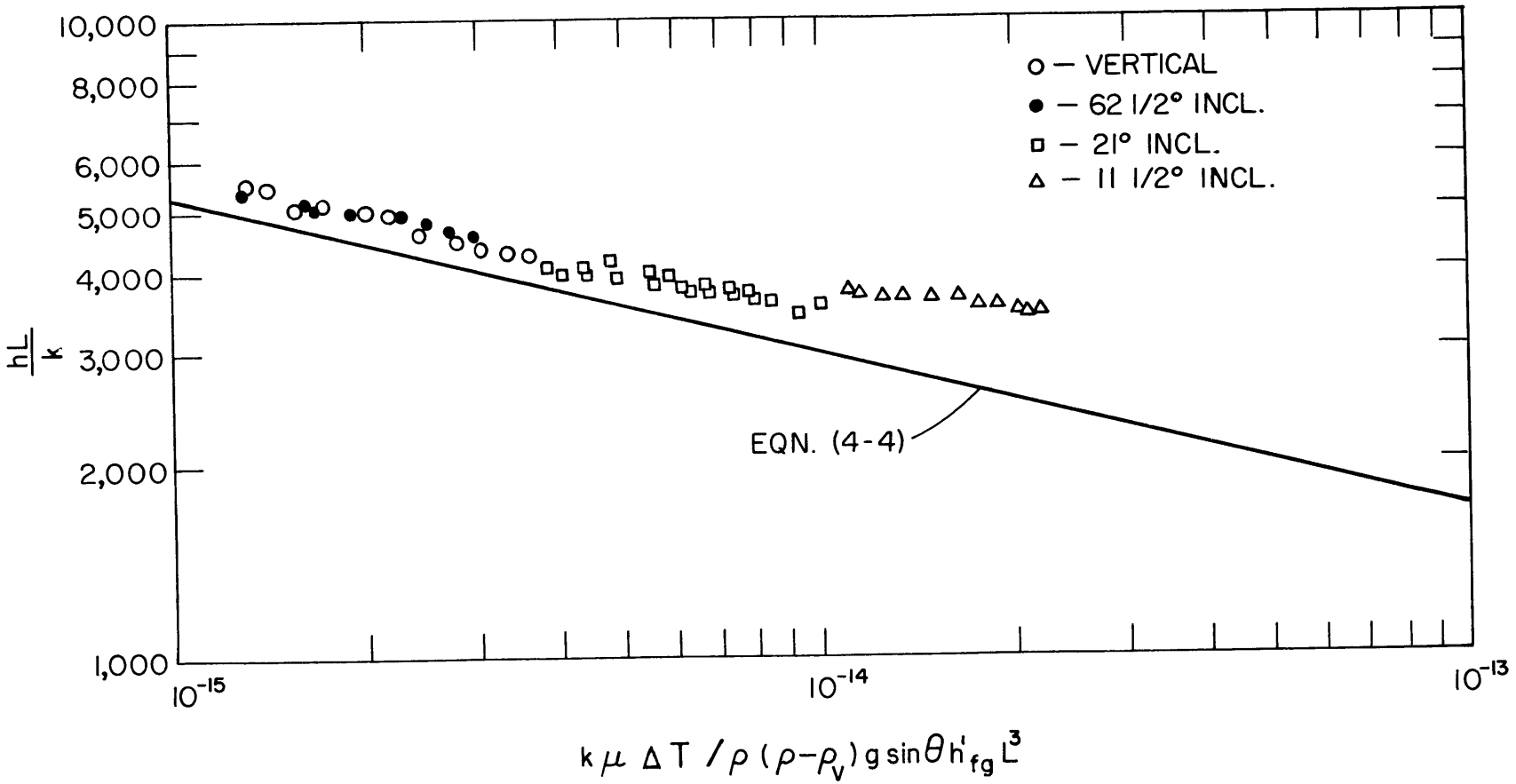

FIGURE 23. HEAT TRANSFER COEFFICIENT AS A FUNCTION OF TEMPERATURE DIFFERENCE

There are several possible reasons for this discrepancy which will be discussed in Section 4. 5.

4. 3 Horizontal Surfaces

In addition to the data from inclined surfaces, Figure 22 also includes the data from the horizontal tests and a plot of equation (3-37). It is seen that the data fall from 10 to 15% below the theoretical curve. From the observation that the average drop density is about 6. 5 drops per square inch, we can calculate the wavelength on the basis that each drop subtends an area of $\pi \lambda^2 /4$. This results in a wavelength of 0. 443 inches as compared to the predicted value of 0. 35 inches, or an error of 26%.

Although no water data were taken, we have plotted some water data from reference 17. There is some question as to the validity of this data, as the apparatus used for the experiments was later found to be defective. However, the Freon-113 data from the same apparatus is found to agree with the data obtained in this investigation, so there is some justification for its acceptance.

4. 4 Vertical Surfaces

In Figure 23 we have plotted the vertical test data along with the theoretical curve based on Nusselt's analysis (21).

$$\frac{hL}{k} = 0.943\left[\frac{k\mu\Delta T}{\rho(\rho-\rho_v)g\sin\theta\, h'_{fg} L^3}\right]^{-1/4} \qquad (4\text{-}4)$$

For comparison, the data for angles of inclination of 21 and 62 1/2 degrees are also included. It is apparent that,at these angles, the effects of the interfacial waves are about the same as at an inclination of 90 degrees. The net effect of the waves is an increase in the heat transfer rate of about 10% above the Nusselt theory.

4.5 Wavelengths of Drops and Ridges

Previously we indicated that, for inclined surfaces, the observed wavelength was about 21 to 28% higher than predicted. For horizontal surfaces, the wavelength of the drops, based on drop density, was also 26% higher than predicted. There are several possible explanations for these increased wavelengths.

Perhaps an obvious explanation is that, due to the dependence of the wavelength on maximum film thickness, as shown in equation (3-39), an incorrect value of the maximum film thickness has led to the error in wavelength. However, we showed in Section 3.4 that, in order for $\lambda / \sqrt{\frac{\sigma}{g(\rho-\rho_v)\cos\theta}}$ to equal 8.72 (the observed value), $\delta_{max} / \sqrt{\frac{\sigma}{g(\rho-\rho_v)\cos\theta}}$ would have to be 0.138. For Freon-113, this corresponds to a maximum film thickness of 0.0056 inches, an absurd value.

Another possible reason is that the value of the surface tension

used in computing the wavelength is incorrect. If this is so, then the actual value would have to be about 50% higher than the published value. However, the published values are well documented [22], and an error of as much as 50% is inconceivable. Another possibility is that the surface tension during condensation is different from the "static" surface tension due to thermodynamic non-equilibrium at the interface. One result of this is that the liquid at the interface is not at the saturation temperature. Using Umur's [23] results to determine the surface temperature variation one can show that the effects of surface tension variation due to a variation in the surface temperature are four orders of magnitude smaller than the viscous stresses in the thin film. Furthermore, a lowering of the interfacial temperature sufficient to account for a 50% increase in the surface tension would require an interfacial temperature below the wall temperature. Still another possibility is that, due to continual transformation from vapor to liquid at the interface, the surface tension is not at its equilibrium value. However, Levich [24] discounts this possibility.

Although no data were obtained for condensation of steam, an observation of the number of ridges at 8 degrees inclination was made. Seven well defined ridges were observed, making the wavelength 0.857 inches. This value is also about 28% higher than predicted. The fact that both water and Freon-113 exhibit the same difference leads one to

suspect an error in formulation rather than an error in fluid properties. It is possible that the linearization of the curvature in the expressions describing the interface is the cause of the error. On the contrary, comparison with the exact results of Bashforth and Adams shows that the linearization results in a slight overestimation of the wavelength of the pendent drop and, by inference, the ridge also. Another possibility is that the longitudinal component of flow that was neglected in comparison to the transverse component in the thin film region is responsible for this discrepancy. This explanation, though, would not explain the similar error in the horizontal case, where there is no longitudinal flow.

The most likely explanation is that given by Lienhard and Wong (25). They analyzed the dominant unstable wavelength during film boiling on a horizontal cylinder and found that the experimentally observed wavelengths were about 25% higher than the predicted wavelength. From photographs of the liquid vapor interface, they observed that neighboring vapor bubbles frequently coalesced. Thus, a count of the number of bubbles per unit length would indicate a wavelength somewhat higher than would be indicated were there no bubble mergers. Examination of high speed motion pictures of the horizontal condensing surface shows that neighboring drops do coalesce, and that the rate of coalescence

increases with decreasing heat flux.

Although the explanation given by Lienhard and Wong appears to be confirmed for the horizontal case, it does not seem to apply to the case of condensation of the underside on an inclined surface. For, although it is entirely possible for two neighboring ridges to coalesce, no instances were observed for small angles of inclination. What was observed, however, was that the ridges did not run straight downstream, but had a sinuous motion. The wavelength of the sinuosity was of the order of the distance between the drops running along the crests of the ridges. The amplitude of the sinuosity increased with increasing angle of inclination. Although at small angles the sinuous motion did not cause any outright coalescence of the ridges, it undoubtedly did alter the symmetry of the ridges, hence the boundary conditions (3-12). Thus a ridge would alternately gain and lose condensate during each cycle of sinuosity. Although we can only speculate that the sinuous motion results in a net increase in wavelength, this is the most likely mechanism for altering the wavelength.

Throughout this report, we have stressed the similarity between film boiling on a horizontal surface and film condensation on the underside of a horizontal surface. Because of this similarity, one may question the fact that, whereas investigators of film boiling have assumed that the dominant wavelength is the fastest growing wave-

length of a Taylor Instability, the wavelength that we have derived does not correspond to this wavelength. In fact, the wavelength given in equation (3-20) corresponds to the critical wavelength of a Taylor Instability, i. e. the wavelength that is neutrally stable. This is not surprising, as the steady state analysis requires the system to be in equilibrium, hence a disturbance can neither grow nor decay.

This basic difference in formulation may be justified by the fact that condensing systems are dominated by viscous stresses far more than are boiling systems. This is evidenced by the fact that the term $\frac{K\Delta T}{\mu h'_{fg}}$, which expresses the ratio of inertial to viscous forces, is about an order of magnitude larger for film boiling than for film condensation. Thus, for a large part of the growth time of a vapor bubble, the growth is limited solely by inertial forces, hence its growth rate and wavelength are closely approximated by the inviscid Taylor Instability formulation. On the other hand, the growth of a liquid drop (or ridge) is very quickly limited by viscosity and its wavelength corresponds to a less unstable wavelength, or one that is closer to the neutrally stable wavelength.

4.6 Conclusions

As a result of this study, we may draw the following con-

clusions:

1. If the ultimate state of a bounded instability is quasi-stationary and non-chaotic, then this state may be analyzed under the assumption that a steady state exists. A qualitative description of the configuration of the interface obtained from experimental observation eliminates the necessity of investigating the stability of the unperturbed system. This procedure is most applicable when the instability is highly non-linear and a non-linear stability analysis would be impractical.

For the particular subject of this investigation, the only geometric assumption that was made was that the value of the maximum dimensionless film thickness is of order unity. We were fortunate that the heat transfer results were highly insensitive to this assumption. If the techniques used in this study are applied to other phenomena, it is possible that this assumption may not yield conclusive results.

2. An estimate of the accuracy with which the hydrodynamics were modeled may be inferred from the predicted values of the wavelengths. For horizontal surfaces, the theoretical value is

in error by 26%. This error is probably due to coalescence of neighboring drops. For inclined surfaces, the error lies between 21% and 28%. Of the several possible sources of this error, it is believed that the sinuous motion of the ridges is the most likely.

3. Experimentally observed heat transfer rates for laminar film condensation on the underside of a horizontal surface are from 10% to 15% below those predicted by equation (3-37). This error remains about the same for values of the dimensionless temperature difference, T , ranging from 4×10^{-9} to 5×10^{-7}. Equation (3-37) is expected to maintain this accuracy for values of T less than 10^{-6} and values of $\frac{K \Delta T}{\mu h'_{fg}}$ much less than unity.

4. Experimentally observed heat transfer rates for film condensation on the underside of slightly inclined surfaces agree with equation (3-29) to within an error of 10%. In addition to the above restrictions, this equation should be valid if tan θ is small and if the flow is in the quasi-fully developed state.

5. All of the heat transfer data from 20 to 90 degrees incli-

nation fall from 10% to 15% above the theoretical curve based upon the Nusselt theory. This suggests that, beyond 20 degrees, the net effect of interfacial waves is to increase the heat transfer rate by a roughly constant amount.

4.7 Suggestions for Further Investigation

Some idea of the areas that require further study may be gained from deficiencies in the results of this investigation. The most immediate improvement in the results presented here would be a more accurate prediction of the wavelength of the disturbances. It would also be of interest to take into account the momentum fluxes in the film so that the region of validity of the analysis could be extended. This would be of use for the prediction of film boiling heat transfer rates.

We have made no attempt to correlate heat transfer rates at angles for which equation (3-29) is no longer valid. However, before such a study is undertaken, it would be advisable to map the various regimes of flow and to identify the parameters which determine the various regimes. We should point out that, because of the non-linearity of the surface waves, we do not expect that a linearized analysis such as Brooke Benjamin's will yield meaningful results in this area of investigation. The most likely approach appears to be a non-linear formulation which treats the phenomenon as a convective instability.

Another area which is worthy of further investigation is the effect of non-condensable gases on the interfacial instability. We have shown that, in addition to lowering the interfacial temperature, hence the temperature difference available for conduction through the film, non-condensable gases have a stabilizing effect on the hydrodynamics by causing variations in the interfacial tension. Although these effects are detrimental to heat transfer, there may be cases where it is beneficial to dampen an instability in this manner.

BIBLIOGRAPHY

1. Nusselt, W., Zeit. Ver. Deut. Ing., Vol. 60, 1916, pp. 541, 569.

2. Bromley, L. A., Ind. & Eng. Chem., Vol. 44, 1952, pp. 2966-2969.

3. Rohsenow, W. M., Trans. A. S. M. E., Vol. 78, 1956, pp. 1645-1648.

4. Sparrow, E. M. and J. L. Gregg, J. Heat Transfer, Trans. A. S. M. E., Series C, Vol. 81, 1959, pp. 13-18.

5. Rohsenow, W. M., Webber, J. H. and A. T. Ling, Trans. A. S. M. E., Vol. 78, 1956, pp. 1637-1643.

6. Koh, J. C. Y., Sparrow, E. M. and J. P. Hartnett, Int. J. Heat Mass Transfer, Vol. 2, 1961, pp. 69-82.

7. Chen, M. M., J. Heat Transfer, Trans. A. S. M. E., Series C, Vol. 83, 1961, pp. 48-60.

8. Hanratty, T. J., and A. Hershman, A. I. Ch. E. Journal, Vol. 7, 1961, pp. 488-497.

9. Kapitza, P. L., J. Exp. Theor. Phys., U. S. S. R., Vol. 18, 1948, pp. 3-12.

10. Dukler, A. E. and O. P. Bergelin, Chem. Eng. Prog., Vol. 48, 1952, pp. 557-563.

11. Brooke Benjamin, T., J. Fluid Mech., Vol. 2, 1957, pp. 554-574.

12. Binnie, A. M., J. Fluid Mech., Vol. 2, 1957, pp. 551-570.

13. Gaster, M., J. Fluid Mech., Vol. 14, 1962, pp. 222-224.

14. Watson, J., J. Fluid Mech., Vol. 14, 1962, pp. 211-221.

15. Taylor, G. I., Proc. Roy. Soc., Vol. A201, 1950, pp. 192-196.

16. Popov, V. D., Trudy KTIPP im A. I. Mikoyana, Vol. 11, 1951, pp. 87-97.

17. Gerstmann, J., S. M. Thesis, Dept. Mech. Eng., M. I. T., 1964.

18. Berenson, P. J., Report No. 17, Heat Transfer Laboratory, Dept. Mech. Eng., M. I. T., 1960.

19. Trefethen, L. M., personal communication, Medford, Mass., 1963.

20. Bashforth, F. and J. Adams, Capillary Action, Cambridge, England, 1883.

21. Rohsenow, W. M., and H. Y. Choi, Heat Mass and Momentum Transfer, Prentice Hall, Englewood Cliffs, New Jersey, 1961, pp. 237-240.

22. Surface Tension of the "Freon" Compounds, Freon Technical Bulletin No. D-27, E. I. Du Pont De Nemours & Co., Wilmington, Delaware, 1964.

23. Umur, A., Report No. 9041-25, Dept. Mech. Eng., M. I. T., 1963.

24. Levich, V. G., Physicochemical Hydrodynamics, Prentice-Hall, Englewood Cliffs, New Jersey, 1962, p. 403.

25. Lienhard, J. H. and P. T. Y. Wong, A. S. M. E. Paper No. 63-HT-3, 1963.

APPENDIX A

Calculation of Heat Losses Through Insulation

A conservative estimate of the heat losses through the insulation may be determined by assuming one-dimensional heat flux through the insulation and adding to this the two-dimensional heat flux in the corner regions where the insulation is joined to the copper condenser block. We shall assume the following conditions exist:

1. The temperature is uniform throughout the copper block.
2. The surface heat transfer coefficient is 100 BTU/ft^2-hr-^oF.
3. The insulation is two inches thick.
4. The thermal conductivity of the insulation is 0.015 BTU/ft-hr-^oF.
5. The area of the uninsulated surface of the copper block is 108 in^2.
6. The area of the insulated surface of the copper block is 192 in^2.
7. The perimeter of the test surface is 48 inches.

Assuming one-dimensional heat flux through the insulation, the percentage heat loss is

$$Q_{loss} / Q_{test\ surf.} = (192/108) \times 1/(1+hL/k) \qquad (A-1)$$

$$= (192/108 \times 1/(1+100 \times 0.167/0.015)$$

$$= 0.0016$$

or 0.16%

The heat flux through the corner regions may be determined by evaluating the series solution to the problem of two-dimensional heat flow from a surface at constant temperature to an adjacent surface exposed to a fluid at a different temperature. However, for the particular conditions that we are dealing with, the series converges very slowly. As an alternative, we may estimate the corner heat losses by considering the insulation to be a semi-infinite slab with the following boundary conditions:

$$\text{at } x = 0,\ T = T_{sat}; \qquad \text{at } x = L, \qquad \frac{\partial T}{\partial x} = 0 \qquad \text{(A-2)}$$

$$\text{at } y = 0,\ T = T_{\text{test surf.}}; \text{ at } y = \infty,\ T = T_{sat}$$

The advantage of this approximation of the true boundary conditions is that this formulation has a closed-form solution. Unfortunately, it results in an infinite heat flux due to the temperature discontinuity at (0, 0). This difficulty may be overcome by determining the value of y on the x = 0 face at which the heat transfer rate is equal to h ΔT, and limiting the heat transfer rate up to this point to the amount h ΔT. Schneider* shows that, for the case of the semi-infinite slab with the boundary conditions (A-2), the temperature distribution is

$$\theta \equiv \frac{T - T_{SAT}}{T_{TEST\ SURF.} - T_{SAT}} = \frac{2}{\pi} \tan^{-1}\left[\frac{\sin(\pi x/2L)}{\sinh(\pi y/2L)}\right] \qquad \text{(A-3)}$$

*Schneider, P. J., "Conduction Heat Transfer", Addison-Wesley Publishing Co., Reading, Mass., (1955) Page 127.

Differentiating with respect to x to find the heat flux at x = 0, we find

$$\left(\frac{\partial\theta}{\partial x}\right)_{x=0} = \frac{\operatorname{csch}(\pi y/2L)}{L} \qquad \text{(A-4)}$$

Thus the point at which the heat transfer rate is equal to $h(T_{sat} - T_{test\ surf.})$ is given by

$$\operatorname{csch}(\pi y/2L) = hL/k \qquad \text{(A-5)}$$

or $y/L \simeq \pi k/2hL$

With this result, we may determine the percentage corner heat loss by the relationship

$$Q_{loss}/Q_{test\ surf.} = \pi kP/2hA + (kP/hA)\int_{\frac{\pi k}{2hL}}^{\infty} \operatorname{csch}(\pi y/2L)\,d(y/L) \qquad \text{(A-6)}$$

$$= \pi kP/2hA - (\pi kP/2hA)x(\ln \tanh(\pi k/2hL))$$

where P is the perimeter of the test surface and A is the area of the test surface. Numerically the result of (A-6) is

$$Q_{loss}/Q_{test\ surf.} = 0.00125 + 0.0082 = 0.945\% \qquad \text{(A-7)}$$

The formulation leading to (A-7) is by no means exact. Inexact

as it is, it does however illustrate the fact that the region of insulation where the conductance is large compared to the surface heat transfer coefficient (i. e. the region between y = 0 and y = π k/2hL) contributes very little to the total heat loss. On the other hand, the magnitude of the second term in (A-6) indicates that the bulk of the losses occurs near the corner regions where the heat flux is predominantly two dimensional.

Summing the results of equations (A-1) and (A-7), the maximum error in the measurements of the condensation rate is estimated to be about 1%.

APPENDIX B

Test Data

This section contains the raw test data upon which this report is based. We have listed the results of 22 of the 31 tests actually run. Tests performed for checking out the system and those tests which were obviously invalid due to equipment failure, leaks, impure test fluid or observable non-condensable gases have been omitted. In addition, if during a test there was an interruption in recording the data, or if the system was not operating at a steady state, then those data have been omitted. The 31 tests performed with the copper test section are numbered 26 to 56. Tests #1 through #25 were performed on an earlier brass test section which was discarded due to unsatisfactory performance.

The column labeled Q(0-9)/Q(9-18) is the ratio of the heat flux over the first half of the test section to that over the second half. This was obtained from the measurements of the coolant temperature rise over the first 8 1/4 inches and over the second 9 3/4 inches which were corrected to represent the heat transfer rates over equal areas. This measurement is a useful indicator of the accuracy of the measurement of the overall heat transfer rate. In the case of horizontal surfaces, neglecting the effect of the slight non-uniformity of the surface temperature, the ratio Q(0-9)/Q(9-18) should be unity. Thus, any data in which

this ratio differs significantly from unity should be suspect.

The method of data reduction is presented in Appendix C.

TABLE 1

Test No. 30
Date: 3/30/65
Test: Calibration-Horizontal
Flow Rate: 1.8 - 3.65 gpm

Point #	T. C. #1 μv	T. C. #2 μv	T. C. #3 μv	T. C. #4 μv	ΔT_{io} °F	Q/A $\frac{BTU}{ft^2\text{-hr}}$	Flow gpm
1.	6	6	6	6	.0674	3	3.38
2.	0	0	0	0	.069	7	3.38
3.	1.5	1.5	1.5	1.5	.0715	13	3.38
4.	-1	-1	-1	-1	.038	-92	3.65
5.	0	0	0	0	.055	-50	3.65
6.	0	0	0	0	.063	-31	3.65
7.	-3	-	-	-3	.058	73	2.85
8.	-2.5	-	-	-2.5	.0565	16	2.85
9.	1	-	-	1	.059	20	2.85
10.	-3	-	-	-3	.034	-51	1.80
11.	-3	-	-	-3	.03	10	1.80
12.	-	-	-	-	-	-	1.80
13.	-5	-	-	-4.5	.039	21	1.80
14.	3.5	-	-	-3	.016	-7	1.80
15.	1	-	-	1	.00	-26	2.35
16.	2	-	-	2	.030	-7	2.35
17.	3	-	-	3	.039	7	2.35
18.	4	-	-	4.5	.042	12	2.35

TABLE 2

Test No. 32
Date 4/2/65
Test: Horizontal
Flow Rate: 3.67 - 3.83 gpm

Point #	T. C. #1 μv	T. C. #2 μv	T. C. #3 μv	T. C. #4 μv	ΔT_{avg} °F	ΔT_{io} °F	Q/A $\frac{BTU}{ft^2\text{-hr}}$	h $\frac{BTU}{ft^2\text{-hr-}^\circ F}$	$\frac{Q(0\text{-}9)}{Q(9\text{-}18)}$	Flow gpm
1.	1191	1195	1162	1134	50.4	2.88	7150	142	1.01	3.83
2.	1025	1025	1004	978	43.2	2.61	6390	147	1.02	3.80
3.	914	919	902	885	38.8	2.40	5860	151	1.02	3.80
4.	845	845	823	800	35.7	2.21	5200	146	1.02	3.68
5.	711	712	691	672	29.7	1.98	4640	156	1.03	3.67
6.	632	637	617	598	26.3	1.79	4160	158	1.07	3.67

TABLE 3

Test No. 33
Date: 4/2/65
Test: Horizontal
Flow Rate: 2.09 - 2.48 gpm

Point #	T. C. #1 μv	T. C. #2 μv	T. C. #3 μv	T. C. #4 μv	ΔT_{avg} °F	ΔT_{io} °F	Q/A $\frac{BTU}{ft^2\text{-hr}}$	h $\frac{BTU}{ft^2\text{-hr-}^\circ F}$	$\frac{Q(0\text{-}9)}{Q(9\text{-}18)}$	Flow gpm
1.	520	511	494	478	21.2	2.25	3610	170	1.18	2.48
2.	490	484	471	458	20.1	2.20	3480	173	1.16	2.25
3.	385	378	365	352	15.4	1.91	2810	182	1.14	2.28
4.	367	359	349	336	14.7	1.96	2880	198	1.12	2.28
5.	-	-	-	-	-	-	-	-	-	2.22
6.	334	326	315	302	13.25	1.81	2590	195	1.04	2.22
7.	299	292	281	269	11.85	1.70	2380	201	1.04	2.18
8.	269	262	253	241	10.65	1.56	2150	202	1.06	2.15
9.	252	245	235	225	9.95	1.48	2000	201	1.05	2.12
10.	210	205	197	188	8.3	1.29	1725	211	1.06	2.11
11.	199	194	185.5	178	7.85	1.24	1640	209	1.06	2.09

TABLE 4

Test No. 45
Date: 5/25/65
Test: Horizontal
Flow Rate: 2.15 - 2.64 gpm

Point #	T. C. #1 μv	T. C. #4 μv	ΔT_{avg} °F	ΔT_{io} °F	Q/A BTU/ft²-hr	h BTU/ft²-hr-°F	Q(0-9)/Q(9-18)	Flow gpm
1.	1344	1265	56.5	5.26	8030	142	1.04	2.32
2.	1277	1193	53.5	5.17	7410	138	1.05	2.18
3.	1201	1122	50.1	5.01	7070	141	1.02	2.15
4.	1132	1054	47.1	4.89	6920	147	1.03	2.15
5.	1095	1031	45.6	3.82	6630	145	1.02	2.64
6.	1032	971.5	43.0	3.70	6200	144	1.02	2.56
7.	954	893.5	38.6	3.48	5780	149	1.02	2.54
8.	848	791	35.2	3.18	5240	147	1.03	2.53
9.	806	756	33.4	3.03	4910	146	1.01	2.49
10	769	719	31.7	2.99	4790	150	1.06	2.45

TABLE 5

Test No. 46
Date: 5/25/65
Test: Horizontal
Flow Rate: 2.24 - 2.65 gpm

Point #	T. C. #1 μv	T. C. #4 μv	ΔT_{avg} °F	ΔT_{io} °F	Q/A BTU/ft²-hr	h BTU/ft²-hr-°F	Q(0-9)/Q(9-18)	Flow gpm
1.	1000	936	41.5	3.88	6140	148	1.05	2.41
2.	919	863	38.2	3.33	5740	150	1.02	2.65
3.	878	821	36.4	3.25	5560	153	1.05	2.62
4.	781	728	32.2	3.07	5010	155.5	1.03	2.50
5.	715	665	29.4	2.94	4690	159	1.03	2.45
6.	666	619	27.2	2.79	4410	162	1.05	2.43
7.	608	564	24.8	2.62	4050	163	1.07	2.37
8.	556	511	22.5	2.43	3720	165	1.10	2.36
9.	519	477	21.0	2.33	3470	165	1.13	2.30
10.	476	437	19.3	2.20	3270	169	1.23	2.30
11.	422	384	16.8	2.05	3030	180	1.19	2.29
12.	341	309	13.5	1.885	2750	204	1.18	2.27
13.	292	264	11.6	1.60	2300	198	1.05	2.25
14.	287	259.5	11.4	1.565	2260	198	1.05	2.26
15.	234	211	9.27	1.33	1880	203	1.08	2.24

TABLE 6

Test No. 47
Date: 5/26/65
Test: Horizontal
Flow Rate: 3.62 - 3.70 gpm

Point #	T. C. #1 μv	T. C. #4 μv	ΔT_{avg} °F	ΔT_{io} °F	Q/A BTU/ft²-hr	h BTU/ft²-hr-°F	Q(0-9)/Q(9-18)	Flow gpm
1.	887	849	37.2	2.34	5560	149	1.04	3.70
2.	823	792	34.6	2.25	5330	154	1.03	3.70
3.	761	727	31.8	2.09	4930	156	1.04	3.70
4.	690	659	28.8	1.94	4580	159	1.05	3.71
5.	612	587	25.4	1.75	4110	162	1.07	3.71
6.	564	539	22.3	1.59	3710	166	1.13	3.71
7.	510	486	21.0	1.47	3420	163	1.19	3.72
8.	475	452	19.6	1.40	3250	166	1.23	3.72
9.	424	404	17.5	1.32	3050	174	1.27	3.72
10.	366	347	14.8	1.185	2720	183	1.16	3.72
11.	317	301	12.85	1.17	2600	202	1.07	3.62
12.	291	273	11.7	1.05	2320	207	1.00	3.63
13.	266	252	10.8	.985	2170	200	.98	3.63

TABLE 7

Test No. 36
Date: 4/11/65
Test: Inclined - 2 3/4°
Flow Rate: 2.0 - 3.8 gpm

Point #	T. C. #1 μv	T. C. #2 μv	T. C. #3 μv	T. C. #4 μv	ΔT_{avg} °F	ΔT_{io} °F	Q/A BTU/ft²-hr	h BTU/ft²-hr-°F	Q(0-9)/Q(9-18)	Flow gpm
1.	1076	1067	1048	1025	45.6	2.40	5870	128.6	1.08	3.80
2.	943	936	918	896	39.9	2.21	5340	134	1.05	3.78
3.	878	871	855	836	37.1	2.10	5070	137	1.03	3.78
4.	827	821	807	789	35.0	1.995	4830	138	1.05	3.79
5.	672	659	638	619	27.7	3.050	4110	148	1.08	2.06
6.	580	567	548	530	23.8	2.66	3480	150	1.07	2.01
7.	534	524	510	498	22.1	2.39	3100	140	1.14	2.0
8.	756	744	726	700	31.4	2.74	4250	135	1.07	2.38
9.	695	683	664	646	28.9	2.78	4180	145	1.06	2.31
10.	656	645	624	606	27.1	2.71	3980	147	1.05	2.26
11.	596	586	569	554	24.6	2.23	3650	148	1.05	2.53
12.	567	556	543	527	23.4	2.11	3390	145	1.06	2.49
13.	546	535	522	506	22.5	2.07	3270	145	1.13	2.45
14.	517	505	490	475	21.2	2.01	3160	149	1.08	2.44
15.	485	476	461	448	20.0	1.94	3040	152	1.12	2.83
16.	464	456	444	430	19.2	1.89	2960	154	1.15	2.43

TABLE 8

Test No. 37
Date. 4/20/65
Test: Inclined 2 3/4 °
Flow Rate: 2.03 - 2.26 gpm

Point #	T. C. #1 μv	T. C. #2 μv	T. C. #3 μv	T. C. #4 μv	ΔT_{avg} °F	ΔT_{io} °F	Q/A BTU/ft²-hr	h BTU/ft²-hr-°F	Q(0-9)/Q(9-18)	Flow gpm
1.	1020	1006	975	948	42.6	3.95	5710	134	1.06	2.2
2.	960	943	914	886	40.0	3.80	5340	133.5	1.05	2.14
3.	902	887	857	832	37.2	3.76	5170	139	1.05	2.09
4.	817	804	779	757	33.9	3.22	4780	141	1.06	2.26
5.	776	763	741	720	32.1	3.09	4530	141	1.07	2.24
6.	693	681	658	640	28.7	2.84	3990	139	1.05	2.15
7.	613	602	583	564	25.3	2.61	3610	143	1.06	2.12
8.	568	553	537	519	23.2	2.43	3340	144	1.12	2.11
9.	519	509	491	473	21.3	2.27	3080	144	1.15	2.09
10.	480	468	454	439	19.7	2.11	2840	144	1.18	2.07
11.	449	440	425	409	18.4	2.01	2700	147	1.18	2.07
12.	408	398	383	369	16.6	1.89	2540	153	1.18	2.07
13.	355	346	334	321	14.45	1.79	2360	163	1.12	2.05
14.	320	312	300	284	13.0	1.65	2180	168	1.06	2.03
15.	288	--	--	261	10.6	1.475	1930	183	1.09	2.04
16.	246	--	--	224	9.3	1.31	1700	183	1.05	2.03

TABLE 9

Test No. 38
Date: 4/20/65
Test: Inclined 2 3/4°
Flow Rate: 1.98 - 2.08 gpm

Point #	T. C. #1 μv	T. C. #4 μv	ΔT_{avg} °F	ΔT_{io} °F	Q/A BTU/ft²-hr	h BTU/ft²-hr-°F	Q(0-9)/Q(9-18)	Flow gpm
1.	361	331	14.7	1.78	2380	162	1.12	2.08
2.	334	304	13.6	1.89	2250	165	1.09	2.07
3.	305	277	12.4	1.60	2100	169	1.06	2.04
4.	261	236	10.5	1.31	1680	160	1.09	2.01
5.	225	203	8.7	1.22	1560	179	1.04	2.01
6.	201.5	180.5	7.8	1.07	1340	172	1.06	1.99
7.	175	152.5	6.8	.94	1160	171	1.06	1.98

TABLE 10

Test No. 34
Date: 4/6/65
Test: Inclined 5°
Flow Rate: 2.51 - 3.80 gpm

Point #	T. C. #1 μv	T. C. #2 μv	T. C. #3 μv	T. C. #4 μv	ΔT_{avg} °F	ΔT_{io} °F	Q/A $\frac{BTU}{ft^2\text{-hr}}$	h $\frac{BTU}{ft^2\text{-hr-}^\circ F}$	$\frac{Q(0\text{-}9)}{Q(9\text{-}18)}$	Flow gpm
1.	1296	1285	1269	1243	55	2.59	6330	115	1.05	3.80
2.	1210	1202	1185	1161	51.5	2.43	5930	115	1.04	3.80
3.	1092	1083	1067	1045	46.1	2.26	5480	118.5	1.03	3.79
4.	9845	974	956	939	41.3	2.11	4810	116.5	1.05	3.57
5.	872	--	--	833	36.6	1.97	4470	122	1.00	3.57
6.	711	--	--	678	29.7	1.66	3750	126	1.06	3.58
7.	642.5	633	625	611	26.6	1.55	3540	133	1.04	3.63
8.	577.5	--	--	550	23.8	1.35	3180	134	1.12	3.65
9.	524.5	--	--	499	21.7	1.23	2800	129	1.14	3.67
10.	449	--	--	421	18.2	1.56	2540	139.5	1.14	2.55
11.	408	--	--	384	16.5	1.42	2290	139	1.10	2.53
12.	375	--	--	351	15.1	1.42	2270	150	1.10	2.51
13.	350	--	--	327	14.1	1.31	2090	148	1.04	2.52

TABLE 11

Test No. 35
Date: 4/6/65
Test: Inclined 5°
Flow Rate 2.34-2.47 gpm

Point #	T. C. #1 μv	T. C. #4 μv	ΔT_{avg} °F	ΔT_{io} °F	Q/A $\frac{BTU}{ft^2\text{-hr}}$	h $\frac{BTU}{ft^2\text{-hr-}^\circ F}$	$\frac{Q(0\text{-}9)}{Q(9\text{-}18)}$	Flow gpm
1.	414	385	16.5	1.475	2330	141	1.10	2.47
2.	333	309	13.35	1.29	1980	148	1.08	2.41
3.	310	287	12.4	1.22	1850	149	1.04	2.40
4.	283	261	11.1	1.14	1710	154	1.04	2.38
5.	260.5	240	10.4	1.055	1550	149	1.11	2.35
6.	254.5	234.5	10.15	1.068	1580	155	1.02	2.36
7.	240	221	9.6	1.01	1495	156	1.08	2.37
8.	201.5	185	8.03	.84	1210	151	1.07	2.34
9.	174.5	159.5	6.95	.778	1120	161	1.11	2.35
10.	158	146	6.3	.75	1075	170	1.06	2.35

TABLE 12

Test No. 48
Date: 5/28/65
Test: Inclined 5°
Flow Rate 1.99 - 3.66 gpm

Point #	T. C. #1 μv	T. C. #4 μv	ΔT_{avg} °F	ΔT_{io} °F	Q/A $\frac{BTU}{ft^2\text{-hr}}$	h $\frac{BTU}{ft^2\text{-hr-}^\circ F}$	$\frac{Q(0\text{-}9)}{Q(9\text{-}18)}$	Flow gpm
1.	1212	1174	51.6	2.40	5630	109	1.09	3.66
2.	1176	1138	49.8	2.31	5420	109	1.09	3.66
3.	1132	1094	48.0	2.23	5220	109	1.07	3.66
4.	1050	1015	44.3	2.11	4930	111	1.09	3.66
5.	966	933	40.7	1.97	4790	117	1.06	3.66
6.	887	256	37.4	1.86	4300	115	1.02	3.65
7.	809	777	33.9	1.76	3940	116	1.03	3.53
8.	740	693	30.6	2.65	3630	118	1.04	2.1
9.	709	662	29.2	2.7	3510	120	1.05	1.99

TABLE 13

Test No. 49
Date: 5/28/65
Test: Inclined 5°
Flow Rate. 3.53 - 3.58 gpm

Point #	T. C. #1 μv	T. C. #4 μv	ΔT_{avg} °F	ΔT_{io} °F	Q/A $\frac{BTU}{ft^2\text{-}hr}$	h $\frac{BTU}{ft^2\text{-}hr\text{-}^\circ F}$	$\frac{Q(0\text{-}9)}{Q(9\text{-}18)}$	Flow gpm
1.	1645	1603	71.5	3.25	7480	104.5	.97	3.55
2.	1645	1600	71.4	3.20	7350	103	1.01	3.54
3.	1641	1598	71.3	3.18	7300	102	.99	3.54
4.	1625	1583	70.6	3.10	7110	101	1.02	3.54
5.	1592.5	1547	69.0	3.02	6900	100	1.03	3.53
6.	1510	1464	65.1	2.87	6560	101	1.06	3.53
7.	1408	1363	60.5	2.715	6200	103	1.06	3.54
8.	1276	1234	54.5	2.57	5900	108	1.04	3.56
9.	1194	1152	51.0	2.425	5590	109	1.03	3.58
10.	1102	1062	47.0	2.27	5220	111	1.04	3.58

TABLE 14

Test No. 50
Date 6/1/65
Test Inclined 5°
Flow Rate 3.46 - 3.50 gpm

Point #	T. C. #1 μv	T. C. #4 μv	ΔT_{avg} °F	ΔT_{io} °F	Q/A $\frac{BTU}{ft^2\text{-}hr}$	h $\frac{BTU}{ft^2\text{-}hr\text{-}^\circ F}$	$\frac{Q(0\text{-}9)}{Q(9\text{-}18)}$	Flow gpm
1.	1381	1337	57.8	2.83	6400	111	1.08	3.50
2.	1310	1268	56.0	2.715	6140	109.5	1.07	3.50
3.	1227	1184	52.5	2.58	5800	110	1.05	3.49
4.	1108	1070	47.3	2.39	5350	113	1.02	3.48
5.	1052	1013	44.7	2.29	5100	114	1.04	3.47
6.	918	883	38.8	2.05	4770	123	1.00	3.46
7.	827	792	34.8	1.89	4160	119	1.03	3.46
8.	773	741	32.5	1.80	3960	122	1.06	3.46

TABLE 15

Test No. 51
Date: 6/1/65
Test Inclined (Sideways) 5°
Flow Rate 3.29 - 3.40 gpm

Point #	T. C. #1 μv	T. C. #4 μv	ΔT_{avg} °F	ΔT_{io} °F	Q/A $\frac{BTU}{ft^2\text{-}hr}$	h $\frac{BTU}{ft^2\text{-}hr\text{-}^\circ F}$	$\frac{Q(0\text{-}9)}{Q(9\text{-}18)}$	Flow gpm
1.	1263	1225	53.9	2.63	5870	105.5	1.08	3.36
2.	1225	1182	51.9	2.54	5720	107.0	1.06	3.39
3.	1142	1107	48.2	2.4	5360	108.3	1.04	3.36
4.	1068	1032	45.1	2.27	4960	106	1.11	3.29
5.	924	890	38.6	1.99	4500	112	1.03	3.40
6.	857	828	36.1	1.85	4170	111	1.06	3.39

TABLE 16

Test No. 40
Date 4/22/65
Test: Inclined 7.5°
Flow Rate: 1.72 - 2.38 gpm

Point #	T. C. #1 μv	T. C. #4 μv	ΔT_{avg} °F	ΔT_{io} °F	Q/A BTU/ft²-hr	h BTU/ft²-hr-°F	Q(0-9)/Q(9-18)	Flow gpm
1.	589	557	24.5	1.765	2700	110	1.17	2.38
2.	537	509	22.3	1.66	2530	113.5	1.29	2.37
3.	485	457	20.1	1.52	2270	113	1.26	2.34
4.	416	393	17.2	1.34	1980	115	1.22	2.32
5.	366.5	344	14.9	1.34	1980	133	1.12	2.32
6.	349.5	330.5	14.5	1.27	1860	128	1.10	2.31
7.	292	275	12.3	1.04	1500	122	1.06	2.31
8.	246	231	10.1	.905	1295	128	1.07	2.31
9.	222	195	8.8	1.01	1125	128	1.03	1.76
10.	194	179	7.9	.955	1050	133	1.10	1.73
11.	173.4	158	7.0	.87	950	136	1.14	1.73
12.	156.5	143.5	6.15	.81	880	143	1.12	1.72

TABLE 17

Test No. 41
Date: 4/22/65
Test: Inclined 7.5°
Flow Rate: 2.34 - 3.80 gpm

Point #	T. C. #1 μv	T. C. #4 μv	ΔT_{avg} °F	ΔT_{io} °F	Q/A BTU/ft²-hr	h BTU/ft²-hr-°F	Q(0-9)/Q(9-18)	Flow gpm
1.	1294	1262	55.6	2.42	5900	106	1.10	3.8
2.	1262	1230	54.2	2.32	5650	104	1.08	3.8
3.	1222	1190	52.4	2.26	5500	105	1.07	3.8
4.	1156	1126	49.5	2.15	5230	105.5	1.06	3.8
5.	1050	1020	45.1	1.99	4710	104.5	1.06	3.72
6.	963	935	41.0	1.87	4430	106	1.06	3.73
7.	814	780	34.3	1.62	3810	111	1.01	3.73
8.	730	694	30.7	2.20	3390	110	1.07	2.38
9.	641	609	26.8	1.97	3000	112	1.08	2.36
10.	581	547	24.1	1.77	2670	111	1.18	2.35
11.	540	512	22.5	1.66	2490	111	1.26	2.34

TABLE 18

Test No. 52
Date: 6/23/65
Test: Inclined 11.5°
Flow Rate: 3.66 - 3.70 gpm

Point #	T. C. #1 μv	T. C. #2 μv	T. C. #3 μv	T. C. #4 μv	ΔT_{avg} °F	ΔT_{io} °F	Q/A BTU/ft²-hr	h BTU/ft²-hr-°F	Q(0-9)/Q(9-18)	Flow gpm
1.	1347	--	--	1328	58.3	2.38	5590	96	1.10	3.66
2.	1310	--	--	1293	56.7	2.32	5450	96	1.11	3.66
3.	1274	1288	1268	1255	55.4	2.27	5330	96	1.07	3.66
4.	1195	1209	1187	1173	51.8	2.15	5020	97	1.08	3.66
5.	1129	1142	1121	1106	48.9	2.04	4780	98	1.07	3.67
6.	1070	1084	1063	1044	46.2	1.97	4600	100	1.08	3.67
7.	990	1003	985	971	42.7	1.82	4260	100	1.07	3.68
8.	890	902	884.5	871	38.2	1.66	3880	101	1.06	3.69
9.	840	851	835	823	36.0	1.59	3610	101	1.05	3.69
10.	787	796	782	769	33.6	1.48	3440	102	1.03	3.70
11.	750	761	746	736	32.2	1.43	3310	103	1.03	3.69

TABLE 19

Test No. 53
Date: 6/23/65
Test: Inclined 21°
Flow Rate: 3.49 - 3.60 gpm

Point #	T. C. #1 μv	T. C. #2 μv	T. C. #3 μv	T. C. #4 μv	ΔT_{avg} °F	ΔT_{io} °F	Q/A $\frac{BTU}{ft^2\text{-}hr}$	h $\frac{BTU}{ft^2\text{-}hr\text{-}°F}$	$\frac{Q(0\text{-}9)}{Q(9\text{-}18)}$	Flow gpm
1.	1130	1150	1140	1124	49.3	2.08	4790	97	1.33	3.60
2.	1077	1095	1086	1074	47.0	2.01	4490	95.5	1.29	3.50
3.	993	1011	1001	989	43.2	1.93	4300	99.5	1.29	3.50
4.	923	940	980	918	40.1	1.81	4010	100	1.29	3.49
5.	857	874	865	856	37.2	1.72	3800	102	1.28	3.49
6.	806	821	814	805	34.9	1.64	3600	103	1.30	3.48
7.	742	756	748	740	32.1	1.53	3360	105	1.28	3.49
8.	677	690	683	676	29.2	1.42	3110	100	1.29	3.50

TABLE 20

Test No. 54
Date: 6/24/65
Test: Inclined 21°
Flow Rate: 1.95 - 3.75

Point #	T. C. #1 μv	T. C. #2 μv	T. C. #3 μv	T. C. #4 μv	ΔT_{avg} °F	ΔT_{io} °F	Q/A $\frac{BTU}{ft^2\text{-}hr}$	h $\frac{BTU}{ft^2\text{-}hr\text{-}°F}$	$\frac{Q(0\text{-}9)}{Q(9\text{-}18)}$	Flow gpm
1.	931	950	942	930	40.2	1.74	4130	103	1.27	3.75
2.	868	883	874	864	37.2	1.62	3830	103	1.25	3.75
3.	811	826	818	809	34.8	1.56	3670	105	1.24	3.74
4.	760	773	766	758	33.7	1.49	3500	104	1.25	3.75
5.	717	732	723	716	30.8	1.42	3340	108	1.23	3.76
6.	666.5	678.5	672	665	28.7	1.33	3110	109	1.25	3.75
7.	606	617	610	605	26.0	1.22	2820	108	1.26	3.74
8.	547	558	552	545	23.3	1.10	2530	109	1.41	3.74
9.	505	515	509.5	504	21.4	1.03	2350	110	1.38	3.75
10.	605	613	601	583	25.3	2.24	2920	115	1.27	2.0
11.	550	557	547	536	23.0	1.97	2550	111	1.35	1.99
12.	494	501	490	481	20.6	1.82	2300	111.5	1.40	1.95
13.	461	467.5	457.5	449	19.2	1.74	2200	114.5	1.42	1.96

TABLE 21

Test No. 55
Date: 6/25/65
Test: Inclined 62.5°
Flow Rate: 1.81 - 1.90

Point #	T. C. #1 μv	T. C. #2 μv	T. C. #3 μv	T. C. #4 μv	ΔT_{avg} °F	ΔT_{io} °F	Q/A $\frac{BTU}{ft^2\text{-}hr}$	h $\frac{BTU}{ft^2\text{-}hr\text{-}°F}$	$\frac{Q(0\text{-}9)}{Q(9\text{-}18)}$	Flow gpm
1.	867	879	864	845	37.2	3.78	4720	127	1.33	1.90
2.	810	821	809	793	34.8	3.67	4450	128	1.35	1.85
3.	745	754	742	729	31.9	3.46	4170	131	1.32	1.84
4.	667	676	664	653	28.5	3.24	3860	135	1.34	1.82
5.	577	586	575	564	24.6	2.79	3360	137	1.35	1.84
6.	527	535	523	514	22.4	2.64	3140	140	1.39	1.82
7.	498	507	494	486	21.2	2.52	2990	141	1.42	1.82
8.	410	418	407	399	17.4	2.21	2610	150	1.41	1.81

TABLE 22

Test No. 56
Date: 6/28/65
Test: Vertical
Flow Rate: 1.9 - 3.74

Point #	T. C. #1 μv	T. C. #2 μv	T. C. #3 μv	T. C. #4 μv	ΔT_{avg} °F	ΔT_{io} °F	Q/A BTU/ft²-hr	h BTU/ft²-hr-°F	$\frac{Q(0-9)}{Q(9-18)}$	Flow gpm
1.	1132	1155	1150	1141	49.7	2.46	5880	118	1.39	3.72
2.	1065	1086	1080	1071	46.7	2.36	5640	120	1.33	3.73
3.	985	1004	999	992	43.1	2.23	5290	122	1.31	3.71
4.	905	918	911	905	39.3	2.09	4950	126	1.30	3.71
5.	796	810	805	798	34.6	1.91	4550	128	1.29	3.74
6.	724	737	731	726	31.4	1.78	4230	135	1.32	3.74
7.	672	683	679	674	29.1	1.68	3990	137	1.32	3.74
8.	588	595	583	574	25.1	2.81	3490	139	1.39	1.9
9.	542	548	537	528	23.0	2.69	3190	139	1.37	1.81
10.	489	496	482	474	20.7	2.69	3060	148	1.39	1.74
11.	460	467	457	451	19.6	2.18	2920	149	1.41	2.06
12.	370	378	368	362	15.75	1.96	2510	159	1.38	1.97
13.	347	355	346	339	14.75	1.92	2430	165	1.41	1.95

APPENDIX C

Method of Data Reduction

In this section we shall illustrate the method of data reduction by performing a sample calculation of point #5, test No. 45. For the sake of brevity, some of the raw data are not included in the tables of Appendix B as they were either redundant or could be determined by a simple calculation. These were:

Vapor temperature; this was maintained at $118.5 \pm .5^{\circ}F$.

Surface temperature; this is simply the vapor temperature minus the temperature difference.

Coolant temperature; this was always within $10^{\circ}F$ less than the surface temperature.

Thermopile emf; this is reported as the actual temperature rise of the coolant, ΔT_{io}.

Thermocouple emf between the inlet and a point 8 1/4 inches from the leading edge and emf between a point 8 1/4 inches from the leading edge and the outlet; instead, this is represented in the form Q(0-9)/Q(9-18).

In addition to the data reported in Table 4 of Appendix B, the following data were obtained for point 45-5:

Vapor temperature emf	1946 microvolts

Thermopile emf	423 microvolts
Thermocouple emf, 0"-8 3/4"	40.0 microvolts
Thermocouple emf, 8 3/4"- 18"	46.1 microvolts

Temperature

Calculation of the temperature indicated by a thermocouple necessitates knowledge of the temperature of the reference junction and the thermoelectric power of the thermocouple* at the average temperature of the two junctions. As the reference junction of the vapor temperature thermocouple was at the ice point, $32^{o}F$, the vapor temperature for point 45-5 is

$$T_{vapor} = (1946 \text{ microvolts}) \times (.0441\ ^{o}F \text{ per microvolt}) + 32\ ^{o}F$$
$$= 118^{o}F \qquad \text{(C-1)}$$

In calculating the temperature difference, one needs to know only the thermoelectric power at the average temperature of the two junctions. Thus,

$$\Delta T_{avg} = (1093 + 1031) \times (.0429)/2 = 45.6\ ^{o}F \qquad \text{(C-2)}$$

and since there are five pairs of junctions in the thermopile,

$$\Delta T_{io} = (423) \times (.0451)/5 = 3.82\ ^{o}F \qquad \text{(C-3)}$$

---

*See, for example, Handbook of Chemistry and Physics, The Chemical Rubber Publishing Co., Cleveland, Ohio, 1962, Page 2669.

Heat Transfer Rate

The ratio of the amount of heat transferred over the first half of the test surface to that over the second half is given approximately by

$$Q(0\text{-}9)/Q(9\text{-}18) = \left(\Delta T_{(0\text{-}8\ 1/4)} / \Delta T_{(8\ 1/4\text{-}18)} \right) \times ((9\ 3/4)/(8\ 1/4))$$

$$= (40/46.1) \times 1.18 \qquad \text{(C-4)}$$

$$= 1.02$$

The overall heat transfer rate is determined by the steady flow energy equation, which relates the enthalpy change of the coolant to the heat that is transferred to it.

$$Q = \omega \Delta h \qquad \text{(C-5)}$$

where Δh may be determined from the relation

$$\Delta h = \left(\frac{\partial h}{\partial p}\right) \Delta p + \left(\frac{\partial h}{\partial T}\right) \Delta T \qquad \text{(C-6)}$$

$$= \left(\frac{\partial h}{\partial p}\right) \Delta p + C_p \Delta T$$

The pressure drop, Δp, which is due to turbulent losses in the coolant channels, is assumed to vary as the flow rate, ω, to the 1.8 power. Thus,

$$\Delta p = -C \omega^{1.8} \qquad \text{(C-7)}$$

where the value of C was found to be 2.75 psi/gpm$^{1.8}$. For water at 100°F and atmospheric pressure, $\left(\frac{\partial h}{\partial p}\right)_T$ is equal to 0.0027 (BTU/lbm)/(lbf/in^2)*. As the area of the test surface was 3/4 ft^2, and using a value of 62.0 lbm/ft^3 for the density of water and 1.0 BTU/lbm -°F for the specific heat, the formula for the heat transfer rate may be written as

$$Q/A = \frac{(62.0)(60)(\text{Flow})}{(3/4)(7.48)} \left((1.0)\ \Delta T_{io} - (C)(\text{Flow})^{1.8}(0.0027)\right) \qquad \text{(C-8)}$$

$$= 663\ (\text{Flow})(\ \Delta T_{io}\ ) - 4.92(\text{Flow})^{2.8}$$

where (Flow) is expressed in gpm and ΔT_{io} in degrees F and Q/A in BTU/ft^2-hr.

For point 45-5, ΔT_{io} was found to be 3.82 °F and the flow rate 2.64 gpm. Substituting these values into (C-8), we find the heat transfer rate to be 6630 BTU/ft^2-hr.

---

* Keenan, J. H., and F. G. Keyes, "Thermodynamic Properties of Steam", John Wiley & Sons, New York, 1936.

APPENDIX D

Derivation of Governing Equations

In this section we shall list the basic assumptions made in analyzing the flow of the condensate film. Using the basic assumptions to eliminate the effects which are negligible, we shall reduce the energy, momentum and continuity equations to the forms presented in Chapter III. In general the basic assumptions are that the flow is two-dimensional, and the pressure hydrostatic, and that the heat transfer is one-dimensional. The specific assumptions are as follows:

1. In the thin film, the characteristic dimension normal to the condensing surface is the film thickness, δ .
2. The characteristic transverse dimension is the wavelength, λ .
3. The characteristic longitudinal dimension is the distance between the drops on the crests of the ridges, designated as L.
4. The order of the characteristic dimensions is $L \gg \lambda \gg \delta$.
5. The maximum ridge height is of order λ .
6. The angle of inclination, θ, is small.
7. The pressure in the film is hydrostatic.
8. The characteristic time is the period with which drops fall from the interface.

9. The vapor exerts negligible shear on the interface.

10. The wall temperature and the vapor temperature are uniform.

11. The velocity normal to the condensing surface, v_z, may be neglected in comparison to the other velocities. This condition results from assumptions 4 and 7.

12. The group $k \Delta T/\mu h'_{fg}$ is much less than unity.

13. The group $C_p \Delta T/h_{fg}$ is much less than unity. Therefore h'_{fg} is approximately equal to h_{fg}.

14. The magnitude of the transverse velocity in the thin film, v_x, is governed by the flow of condensate into the ridges. This of course assumes that there is no net downstream (longitudinal) flow in the thin film. In section 3.2 this assumption is shown to be consistent if tan θ is small.

Before examining the governing equations, we shall determine the order of magnitude of the characteristic transverse velocity and the characteristic time. Assumption 14 requires that the condensate formed in the thin film flows transversely into the adjacent ridges. Thus

$$\text{flow rate} = (\text{heat transfer rate}) \times (\text{area})/\rho\, h'_{fg}$$

$$v_x\, \delta\, L \simeq (k \Delta T/\delta) \times (\lambda L)/\rho\, h'_{fg} \qquad \text{(D-1)}$$

$$v_x = 0(\lambda k \Delta T/\delta^2 h'_{fg})$$

Similarly, the characteristic time is given by

$$\text{time} = \frac{(\text{volume of drop}) \times (\text{drops per unit area}) \times (\rho h'_{fg})}{\text{heat transfer rate}}$$

or

$$\text{time} \simeq (\lambda^3) \times (1/\lambda L) \times (\rho h'_{fg}) \times (\delta / k \Delta T) \qquad \text{(D-2)}$$

$$\text{time} = 0 (\lambda^2 \delta \rho h'_{fg} / Lk \Delta T)$$

Utilizing the basic assumptions, the governing equations may be written as

Momentum:

$$\frac{\partial V_x}{\partial t} + V_x \frac{\partial V_x}{\partial x} + V_y \frac{\partial V_x}{\partial y} = -\frac{1}{\rho}\frac{\partial p}{\partial x} + \frac{\mu}{\rho}\frac{\partial^2 V_x}{\partial z^2} \qquad \text{(D-3)}$$

$$\frac{\partial V_y}{\partial t} + V_x \frac{\partial V_y}{\partial x} + V_y \frac{\partial V_y}{\partial y} = -\frac{1}{\rho}\frac{\partial p}{\partial y} + \frac{\mu}{\rho}\frac{\partial^2 V_y}{\partial z^2} + g \sin\theta$$

$$0 = -\frac{1}{\rho}\frac{\partial p}{\partial z} + g \cos\theta$$

Continuity:

$$\frac{\partial V_x}{\partial x} + \frac{\partial V_y}{\partial y} + \frac{\partial V_z}{\partial z} = 0 \qquad \text{(D-4)}$$

Energy:

$$\frac{\partial T}{\partial t} + V_x \frac{\partial T}{\partial x} + V_y \frac{\partial T}{\partial y} = \frac{k}{\rho C_p}\frac{\partial^2 T}{\partial z^2} \qquad \text{(D-5)}$$

Substituting the result of (D-1) into (D-4) we see that the order of magnitude of the characteristic longitudinal velocity is

$$v_y = O(Lk\,\Delta T/\delta^2 \rho\, h'_{fg}) \qquad \text{(D-6)}$$

Replacing the terms in equations (D-3) and (D-5) by their respective orders of magnitude results in the following equations

$$O\left(\frac{\delta L\, k\Delta T}{\lambda^2 \mu\, h'_{fg}}\right) + O\left(\frac{k\Delta T}{\mu h'_{fg}}\right) + O\left(\frac{k\Delta T}{\mu h'_{fg}}\right) = \frac{-\delta^4 \rho h'_{fg}}{\lambda\, k \mu \Delta T}\frac{\partial p}{\partial x} + O(1) \qquad \text{(D-7)}$$

$$O\left(\frac{\delta L\, k\Delta T}{\lambda^2 \mu\, h'_{fg}}\right) + O\left(\frac{k\Delta T}{\mu h'_{fg}}\right) + O\left(\frac{k\Delta T}{\mu h'_{fg}}\right) = \frac{-\delta^4 \rho h'_{fg}}{L k \mu \Delta T}\left[\frac{\partial p}{\partial y} - \rho g \sin\theta\right] + O(1)$$

$$O\left(\frac{\delta L\, C_p \Delta T}{\lambda^2\, h'_{fg}}\right) + O\left(\frac{C_p \Delta T}{h'_{fg}}\right) + O\left(\frac{C_p \Delta T}{h'_{fg}}\right) = O(1) \qquad \text{(D-8)}$$

It is evident from equation (D-7), that if the time dependent term in the momentum equation is to be negligible, we must further qualify assumption 4 to require $\delta/\lambda < \lambda/L$.

Dropping the terms in equations (D-7) and (D-8) which are small compared to unity, the momentum and energy equations may be written as

Momentum:

$$\frac{\partial p}{\partial x} = \mu \frac{\partial^2 V_x}{\partial z^2}$$

$$\frac{\partial p}{\partial y} = \mu \frac{\partial^2 V_y}{\partial z^2} + \rho g \sin\theta \qquad \text{(D-9)}$$

$$\frac{\partial p}{\partial z} = \rho g \cos\theta$$

Energy:

$$\frac{\partial^2 T}{\partial z^2} = 0 \qquad \text{(D-10)}$$

Equation (D-10) requires that the temperature profile in the film be linear. As the boundary conditions are

$$\begin{aligned} &\text{at } z = 0, \quad T = T_{wall} \\ &\text{at } z = \delta, \quad T = T_{sat} \end{aligned} \qquad \text{(D-11)}$$

the heat transfer rate may be expressed as

$$Q/A = k \frac{\partial T}{\partial z} = k \Delta T/\delta \qquad \text{(D-12)}$$

The z-direction momentum equation in (D-9), which is the result of the pressure being hydrostatic, may be solved by making use of the fact that the vapor pressure is p_{sat}, and that the pressures on either side of the interface differ by an amount $\sigma / R_1 + R_2$, where R_1 and R_2 are two orthogonal radii of curvature of the interface. In Cartesian coordinates, the radii of curvature are given by

$$1/R_1 + 1/R_2 = \frac{\partial^2 \delta}{\partial x^2} \Big/ \left(1 + \left(\frac{\partial \delta}{\partial x}\right)^2\right)^{3/2} + \frac{\partial^2 \delta}{\partial y^2} \Big/ \left(1 + \left(\frac{\partial \delta}{\partial y}\right)^2\right)^{3/2} \qquad \text{(D-13)}$$

If the slopes of the interface are small, this expression may be approximated by

$$1/R_1 + 1/R_2 = \frac{\partial^2 \delta}{\partial x^2} + \frac{\partial^2 \delta}{\partial y^2} \qquad \text{(D-14)}$$

Thus the pressure in the film is

$$p = p_{sat} - (\rho - \rho_v)\, g \cos\theta\, (\delta - z) - \sigma\left(\frac{\partial^2 \delta}{\partial x^2} + \frac{\partial^2 \delta}{\partial y^2}\right) \quad \text{(D-15)}$$

The curvature in the y-direction is of order λ^2/L^2 compared to the x-direction curvature, so the y-dependent term may be neglected.

The above equation, together with equations (D-12) and (D-9) are now in a form suitable for determining the shape of the interface. This analysis is presented in Section 3.2. The order of magnitude analysis is similar for the case of a horizontal surface, i. e. the drop model presented in Section 3.4. The only basic difference is that instead of $\lambda \ll L$, now $\lambda = L$.

APPENDIX E

Properties of Freon-113

The Freon-113 used in all the tests was the commercial grade refrigerant supplied by E. I. DuPont De Nemours & Co., designated as F-113. The properties listed here were obtained from the manufacturer.

Thermodynamic Properties*

Vapor Pressure (psia):

$$\log_{10} p = 33.0655 - \frac{4330.98}{T} - 9.2635 \log_{10} T + 0.0020539T.$$

(T = temperature ^{o}R.)

Equation of State:

$$p = (0.0000500T-0.0214)\rho_v^3 + (0.002618T-4.035)\rho_v^2 + 0.05728T\rho_v$$

(ρ_v = vapor density lbm/ft^3)

Liquid Density (lbm/ft^3)

$$= 103.555-0.07126t - 0.0000636t^2$$

(t = temperature ^{o}F.)

Specific Heat of Vapor at 1 atm. (BTU/lbm-^{o}F)

$$C_p = 0.1455 + 0.000111t$$

---

*Source: Freon Technical Bulletin T-113A

Specific Heat of Liquid (BTU/lbm-^{o}F)

(a) Determined from table of saturated properties.

0.203 @ 11^{o}F 0.214 @ 73^{o}F 0.233 @ 146^{o}F

(b) Determined by calorimetric measurement

0.212 @ 11^{o}F 0.220 @ 73^{o}F 0.228 @ 146^{o}F

Physical Properties

Molecular Weight:* 187.39

Boiling Point at 1 atm. (^{o}F):* 117.6

Liquid Viscosity(Centipoises):*

0.747 @ 60^{o}F 0.646 @ 80^{o}F 0.564 @ 100^{o}F 0.497 @ 120^{o}F

Heat of Vaporization at 1 atm. (BTU/lbm):** 63.12

Density Difference, $\rho - \rho_v$ (gm/cc)†

1.60991 @ 40^{o}F 1.55731 @ 80^{o}F 1.49942 @ 120^{o}F

Surface Tension (dynes/cm)†

21.14 @ 40^{o}F 18.51 @ 80^{o}F 15.91 @ 120^{o}F

Liquid Thermal Conductivity (BTU/ft-hr-^{o}F)††

0.048 @ -4^{o}F 0.0435 @ 68^{o}F

---

* Source: Freon Technical Bulletin T-113A

** Source: Freon Technical Bulletin B-2

† Source: Freon Technical Bulletin D-27

†† Source: Freon Technical Bulletin X-78. There is only fair agreement among the various values reported. We have reported those designated as the "most probable values". They may be in error by as much as 10%. The value of the thermal conductivity given in Bulletin B-2 as 0.0521 @ 86^{o}F is incorrect.

APPENDIX F

Estimate of Experimental Errors

Surface Temperature

The main error in surface temperature measurement resulted from the fact that the thermocouples used for the measurements reached only to within 1/8 inch of the surface of the test section. Assuming a linear temperature profile in the copper test section, the error in the measurement of surface temperature is

$$\frac{(\text{actual} \quad \Delta T) - (\text{measured} \quad \Delta T)}{(\text{actual} \quad \Delta T)} = -\frac{hL}{k} \qquad \text{(F-1)}$$

where h is the surface heat transfer coefficient, L is the separation between the thermocouple and the surface, and k is the thermal conductivity of the test section. Using a value of 220 BTU/ft-hr-^{o}F for the conductivity of copper, and 200 BTU/ft^{2}-hr-^{o}F for the heat transfer coefficient, the error in temperature difference is -0.95%

Heat Transfer Rate

Errors in the measured heat transfer rate result from heat leaks through the insulation, errors in measurement of the flow rate, errors in the thermopile, errors in accounting for the pressure drop of the coolant, and error due to the thermal capacity of the thermopile

wells. Of these, the first is calculated in Appendix A, and is found to be about 1%. A good estimate of the remaining sources of error may be deduced from the results of Test #30 shown in Table 1 of Appendix B. Assuming the nominal temperature difference available for condensation to be zero, there should be no net heat transfer. The measured heat transfer rates were all less than 100 BTU/ft^2-hr. Thus, for horizontal and slightly inclined surfaces, if the ratio Q(0-9)/Q(9-18) does not differ significantly from unity, the overall error in the heat transfer rate is estimated to be a constant error of $\pm$ 100 BTU/ft^2-hr and an error due to heat losses through the insulation of -1%.

In the context of errors in the heat transfer rate, we should add the uncertainty in the value of the thermal conductivity of Freon-113. As Explained in Appendix E, there is poor agreement in the several published values of the thermal conductivity of Freon-113. We estimate that the value used in computing the dimensionless temperature difference and the Nusselt number may be in error by as much as 10%.